January 2020

Durability Performance Of Geopolymer Concrete Beams And Columns Exposed To Hygrothermal Environment

Najeb Hasen Sh Sawsi
Wayne State University

DURABILITY PERFORMANCE OF GEOPOLYMER CONCRETE BEAMS AND COLUMNS EXPOSED TO HYGROTHERMAL ENVIRONMENT

by

NAJEB HASEN SH.SAWSI

DISSERTATION

Submitted to the Graduate School

of Wayne State University,

Detroit, Michigan

in partial fulfillment of the requirements

for the degree of

DOCTOR OF PHILOSOPHY

2020

MAJOR: CIVIL ENGINEERING

Approved by

_____

Advisor Date

_____

_____

_____

_____

DEDICATION

To: my wife Enas

my father, my mother,

my sons: Mohamed, Motasem, Moin, Hasan

my daughter Mafaz,

my brothers and sisters

also,

To: my teachers

ACKNOWLEDGMENTS

I would like to express my grateful thanks to ALLAH for all his bounties, particularly health, knowledge and patience.

Then; I wish to thank the following people for their help:

Dr. Hwai-Chung Wu, my committee chair, academic advisor and mentor during my study at Wayne State University. I want to express my heartfelt appreciation. for his continuous help, advice, interest, guidance, and patience. He provided valuable time and knowledge of the subject making this dissertation successful. It has been a great pleasure working with Dr.Wu over the past 5 years in the PhD period and 3 years in the masters before that.

Dr. Usmen Mumtaz, Civil and Environmental Engineering Department Chair, and my committee member, for his assistance during my PhD study at Wayne State University. He was my support at all the time, and he always encourage me to continue to finish.

Dr. Christopher Eamon, my committee member, for the help he provided during my study.

Dr. Alper Murat, my committee member.

Many thanks to **(Headwaters Resources, lnc**) for donating Fly ash material.

Furthermore, thanks are extended to all the staff members of the Civil and Environmental Engineering Department at Wayne State Univers

TABLE OF CONTENTS

LIST OF FIGURES

LIST OF TABLES

CHAPTER ONE INTRODUCTION

1.1 Overview

Many high temperature conditions are becoming more common. Based on to US Environmental Protection Agency data (EPA, 2016), since the 1970s, In the United States, unusuale hot summer days (highs) have become more common in recent decades.Un normal hot summer nights have become more common at an even faster rate. This phenomenon indicates less nocturnal "cooling down." After experiencing many winters with unusually low temperatures in the United States, unusually cold winter temperatures have become less common particularly very cold nights. It has become more normal to record daily high temperatures than record lows. Between 2000 to 2009, the record highs are twice as high as record low (EPA, 2016).

Figure 1. 1 Displays U.S. annual values From 1895 to 2015, the Heat Wave Index. The contiguous 48 states are protected by these results. Interpretation: An index value of 0.2 (for example) might mean that 20% of the country experienced one heat wave, 10% of the country experienced two heat waves, or some other frequency and area combination resulted in this value. (EPA, 2016).

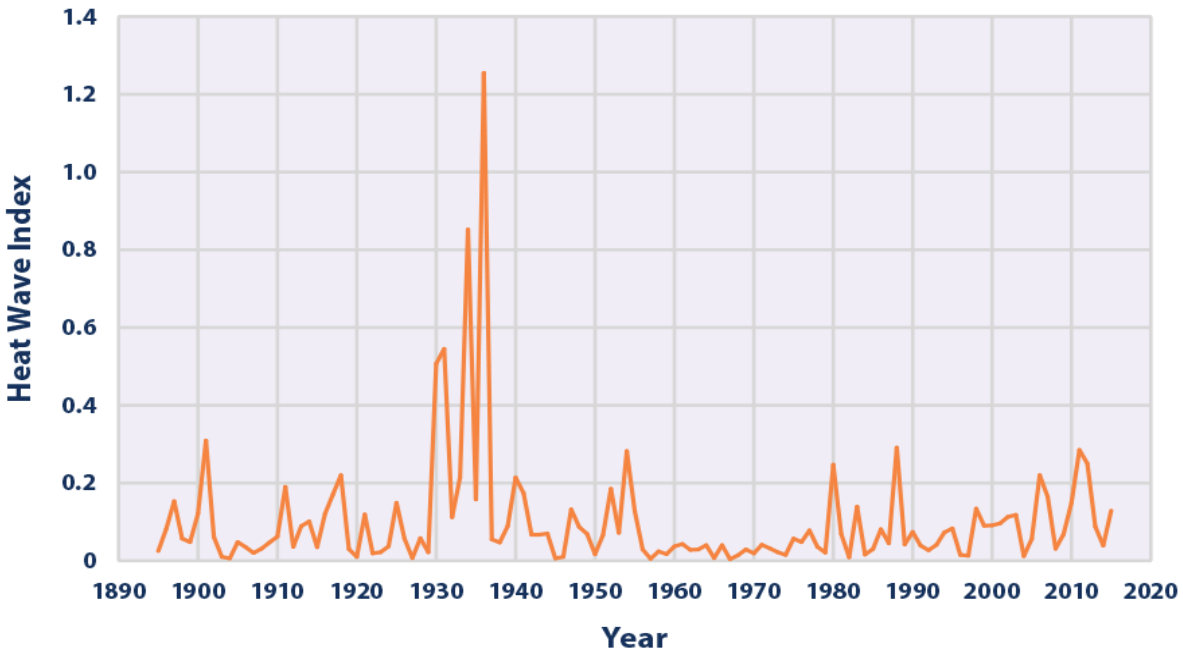

Figure 1.1 U.S. Annual Heat Wave Index, 1895–2015(EPA, 2016).

These conditions of weather change have to be considered on concrete structure construction. Hot weather climate may cause problems in concrete. Concrete properties and serviceability are adversely affected. Most of these issues have to do with the higher rate of hydration of cement at higher temperatures and increased rate of moisture evaporation from fresh ly mixed concrete.. The rate of cement hydration is dependent on concrete temperature, cement composition and fineness, and admixtures used (Noori 2005). Many organization including ACI have recommended hot weather concreting practices to minimize the adverse effects of hot weather conditions on concrete properties (Naik and Singh, 1990). However, Such practices are rarely followed. As a result, properties of concrete strength are adversely affected by hot weather. Adding fly ash to concrete may help alleviate some of the problems associated with hot weather concreting, as the presence of Class F fly ash in concrete mixtures contributes to a reduction in water demand and a reduction in hydration level and heat. (Naik and Singh, 1990), however, little data exist

concerning actual performance of geopolymer concrete manufactured, placed, and cured under such conditions.

1.2 Hot weather environmental

Hot weather, as described in ACI 305R, is any combination of the following conditions that tends to impair the quality of freshly mixed or hardened concrete by accelerating the rate of moisture loss and hydration of cement or otherwise resulting in adverse effects (Noori 2005):

-High ambient temperature

-High concrete temperature

-Low relative humidity

-High wind speed, and solar radiation

Hot weather issues are most severe in the summer, but the related climatic elements of excessive winds, low relative humidity and photo voltaic radiation can occur at any time, especially in arid or tropical climates. Hot weather prerequisites can produce a rapid charge of evaporation of moisture from the floor of the newly positioned concrete and accelerated setting time, amongst other.

1.2.1 Potential problems in hot weather

Potential problems for concrete in the freshly mixed state are likely to include:

-Increased water demand.

-Increased rate of slump loss and corresponding tendency to add water at the job site.

-Increased rate of setting, resulting in greater difficulty with handling, compacting, and finishing, and a greater risk of cold joints.

-Increased tendency for plastic-shrinkage cracking; and

-Increased difficulty in controlling entrained air content.

Potential deficiencies to concrete in the hardened state may include**:**

-Decreased 28-day and later strengths resulting from either higher water demand, higher concrete temperature, or both at time of placement or during the first several days.

Increased drying tendency and differential thermal cracking either from cooling of the overall structure or from temperature differentials within the member's cross section.

-Decreased durability resulting from cracking.

-Greater variability of surface appearance, such as cold joints or color difference, because of specific hydration levels and liquid cement ratios (w / cm).

-Increased potential for reinforcing steel corrosion—making possible the ingress of corrosive solutions.

-Increased permeability as a result of high water content, inadequate curing, carbonation, lightweight aggregates, or improper matrix-aggregate proportions.

1.2.2 Effects of hot weather on concrete properties

Properties of concrete that make it a notable development material can be affected adversely through warm weather. Strength, impermeability, dimensional stability, and resistance of the concrete to weathering, wear, and chemical attack all depend on the following factors: determination and acceptable control of substances and mixture proportioning; initial co ncrete temperature; wind speed; photo voltaic radiation; ambient temperature; and humidity condition at some point of the setting and curing period.

Hot weather can also create troubles in mixing, placing, and curing hydraulic cement concrete. These problems can adversely affect the behavior and serviceability of the concrete. Most of these issues relate to the increase rate of cement hydration at higher temperature and accelerated evaporation rate of moisture from the freshly combined concrete. The rate of

cement hydration is established on concrete temperature, cement composition and fineness, and admixtures used.

According to ASTM C 31/C 31M, concrete test specimens made in the field used to check the laboratory's adequacy mixture proportions for strength or as a basis for acceptance or quality control should be cured initially at 60 to 80 F (16 to 27 C) (Suyun Ham, and Taekeun, 2013). If the initial 24 h curing is at 100 F (38 C), the 28-day compressive strength of the test specimens may be 10 to 15% lower than if curing temperature with the required ASTM C 31/C 31M (Suyun Ham, and Taekeun, 2013). If the cylinders are allowed to dry at early ages, strengths will be reduced even further (Cebeci 1987). Therefore, proper fabrication, curing, and testing of the test specimens during hot weather is critical, and steps should be taken to ensure that the specified procedures are followed.

Fly ash is commonly used in Portland as a partial substitute cement, it might impart a slower rate of setting and of early strength gain to the concrete (Kapoor, Shruti, 2014), in hot weather concreting, which is attractive. Faster setting cements or cements causing a rapid slump loss in hot weather may successfully work in conjunction with this product. The use of fly ash may reduce the rate of slump loss of concrete under hot conditions (Ravina 1984; Gaynor et al 1985).

1.3 Fly Ash (green materials)

The subject of research these days is to improve and produce a sustainable material that have manufacturing manner with a low power requirement and minimum feasible environmental cost. Since the demand for Portland cement is increasing day by day, and the cement enterprise is held accountable for some of the CO2 emissions (Sun 2009, Motorwala, Shah, Kammula, Nannapaneni 2013). An increasing interest in environmental issues has pressured the industries

to develop products and materials that are more environmentally friendly such as the industrial wastes like fly ash – Greener materials.

1.3.1 Definition of fly ash

Fly ash is solid, fine-grained powdery materials resulting from the combustion of pulverized coal in power station furnaces, Figure 1.1(Kapoor, Shruti, 2014).

Figure 1.2 Fly ash, a powder resembling cement, has been used in concrete since the 1930s. (IMG12190) (Kapoor, Shruti, 2014).

Fly ash is the main waste generated in the coal-fired power stations.

1.3.2 Properties of Fly Ash

Properties of fly ash particles are generally spherical in shape and range in size from 0.5 µm to 300 µm (Motorwala, Shah, Kammula, Nannapaneni 2013). The chemical composition is mainly composed of the oxides of silicon (SiO_2), aluminium (Al_2O_3), iron (Fe_2O_3), and calcium (CaO), whereas magnesium, potassium, sodium, titanium, and sulphur are also present in a lesser amount (Motorwala, Shah, Kammula, Nannapaneni 2013).

Two classes of fly ash are defined by ASTM C618: Class F fly ash and Class C fly ash (Table 1.1). The burning of harder, older anthracite and bituminous coal typically produces Class F fly ash.

This fly ash is pozzolanic in nature, and contains less than 20% lime (CaO) (https://en.wikipedia.org/wiki/Fly_ash). Possessing pozzolanic properties, the glassy silica and alumina of Class F fly ash requires a cementing agent, such as Portland cement, quicklime, or hydrated lime—mixed with water to react and produce cementitious compounds. Alternatively, adding a chemical activator such as sodium silicate (water glass) to a Class F ash can form a polymeric binder, also called geopolymer (https://en.wikipedia.org/wiki/Fly_ash).

Class C fly ash is produced from the burning of younger lignite or sub-bituminous coal, in addition to having pozzolanic properties, also has some self-cementing properties. In the presence of water, Class C fly ash hardens and gets stronger over time. Class C fly ash generally contains more than 20% lime (CaO). Unlike Class F, self-cementing Class C fly ash does not require an activator. Alkali and sulfate (SO_4) contents are generally higher in Class C fly ashes (https://en.wikipedia.org/wiki/Fly_ash).

Table1.1. Chemical requirements for fly ash classes (from ASTM C618) (Sun 2005).

Chemical difference	Class F	Class C
Silicon dioxide (SiO2) + aluminum oxide (Al2O3) + iron oxide (Fe2O3), min. %	70.0	50.0
Sulfur trioxide (SO3), max. %	5.0	5.0
Moisture content, max. %	3.0	3.0
Loss on ignition, max. %	6.0	6.0
Available alkalis (as Na2O), max. %	1.5	1.5

The chief difference between these classes is the amount of calcium, silica, alumina, and iron content in the ash. The chemical properties of the fly ash are largely influenced by the chemical content of the coal burned (https://en.wikipedia.org/wiki/Fly_ash).

1.3.3 The Use of Fly Ash

Fly ash is presently used in cement, concrete, structural fill, waste stabilization, flowable fill for mining, soil amendment and stabilization, mineral filler, paving; and so on (Sun 2005). Among the modern-day restricted use of fly ash, utility in the discipline of cement and concrete accounts for a large component of about 50% (Sun 2005). Fly ash has been used round the world as an ingredient in concrete for greater than 60 years. When fly ash is added to the concrete mix, some of the cement can be replaced, and the concrete with fly ash is more long lasting and more suitable than concrete made with cement alone (Sun 2005). The benefits of the use of fly ash in concrete include: 1) lowered permeability;

2) Expanded lengthy time period strength; 3) decreased cracks from warmness of hydration; and 4) improved resistance to sulfate and different chemical assault.

1.4 Alkali Activated Cement (Geopolymers)

Among the most necessary advances of research and technological improvement for possible applications of Coal-fired fly ash, the improvement of new inorganic polymeric materials, named alkali activated cement or "Geopolymers", looks to obtain increasing attention at some stage in the last twenty years. Geopolymers are inorganic polymeric materials.

Chemically, geopolymers consist of three-dimensionally cross-linked units of AlO_4^- and SiO_4 tetrahedra, where positive ions (Na^+, K^+, Li^+, Ca^{2+}, Ba^{2+}, H_3O^+, et al.) must be present to balance the negative charges of the framework (Sun, Wu 2013). It was Davidovits (1989, 1991,

1994a) who first examined the chemistry of such material in details and coined the term "geopolymer" in the 1980's (Sun 2005). Structural units such as siliate (-Si -O-Al -), sialate-siloxo (-Si -O-Al -O-Si -O-) and sialatedisiloxo (-Si -O-Al -O-Si -O-Si -O-) were proposed by Davidovits to envisage the chemical structure of geopolymers. Geopolymerization process is based on a complicate heterogeneous reaction that takes place between a solid material rich in alumina-silicate oxides and an alkali metal silicate solution under highly alkaline conditions. The geopolymerization reaction is exothermic and carried out under atmospheric pressure at temperatures below 100^{o}C (Panias D., Giannopoulou I. P. 2006). The most proposed mechanism for geo-polymerization process includes the following four stages , which proceed in parallel and thus, it is impossible to be distinguished : (i) dissolution of Si and Al from the solid alumina silicate materials in the strong alkaline aqueous solution. (ii) formation of Si and / or Si-Al oligomers in the aqueous phase, (iii) poly condensation of oligomers to form a three-dimensional alumina silicate framework and (iv) bonding of the undissolved solid particles into the geopolymeric framework and hardening of the whole geo polymeric system (Panias D., Giannopoulou I. P. 2006).

Geopolymers possess outstanding physic-chemical and mechanical properties, which include low density, micro- or Nano- porosity, negligible shrinkage, high strength, terrific surface hardness and full-size thermal stability, hearth and chemical resistance. Due to these properties, these substances are seen as alternative materials for certain industrial functions in the areas of construction, transportation, road building, aerospace, mining and metallurgy. The utilization of coal-fired fly ash in the improvement of geopolymers for building functions has been and continues to be problem of many research studies.

According to previous studies (Hua et al., 1999 ; Swanepoel et al., 2002), geopolymerisation involves a chemical reaction between various aluminosilicate oxides with silicates under highly alkaline conditions, which can be presented schematically as follow:

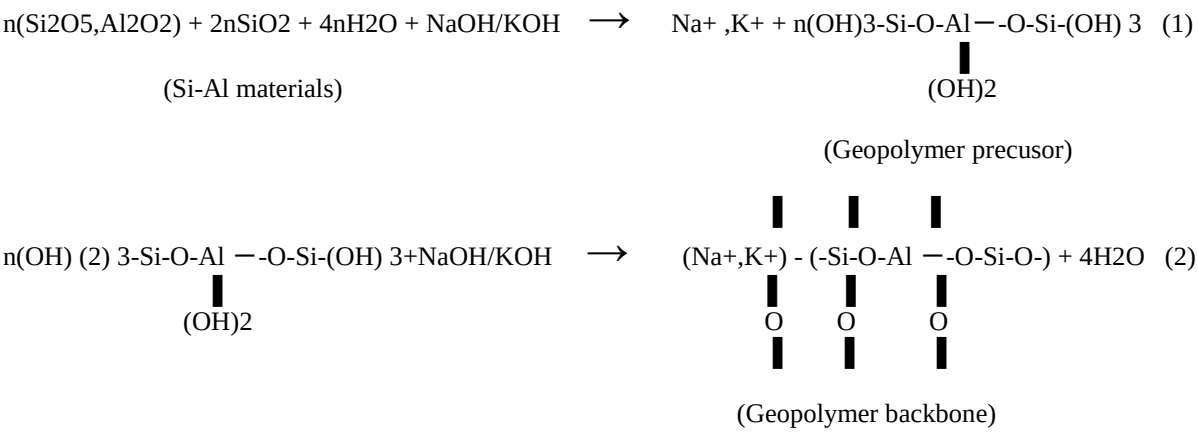

1.4.1 Fields of Applications

According to Davidovits (1988b), geopolymeric materials have a wide range of applications in the industry sector such as the automotive sector and aerospace, nonferrous foundries and metallurgy, civil engineering and plastic industries (Wallah and Rangan 2006). The type of application of geopolymeric materials is determined by the chemical structure in terms of the atomic ratio Si:Al in the polysialate. Davidovits (1999) classified the type of application according to the Si:Al ratio as presented in Table 1.2. A low ratio of Si:Al of 1, 2, or 3 initiates a 3D-Network that is very rigid, while Si:Al ratio higher than 15 provides a polymeric character to the geopolymeric material. It can be seen from Table 1.2 that for many applications in the civil engineering field a low Si:Al ratio is suitable (Wallah and Rangan 2006).

One of the potential fields of application of geopolymeric materials is in toxic waste management, because geopolymers are similar to zeolitical materials that have been known for their ability to

absorb the toxic chemical wastes (Davidovits, 1988b). Comrie et. al., (1988) also provided an overview and relevant test results of the potential of the use of geopolymer technology in toxic waste management (Wallah and Rangan 2006). Based on tests using geopolymite 50, they recommend that geopolymeric materials could be used in waste containment. Geopolymite 50 is a registered trademark of Cordi-Geopolymere SA, a type of geopolymeric binder prepared by mixing various alumina-silicates with alkali hardeners (Davidovits, 1988b).

Table 1.2 Applications of Geopolymeric Materials Based on Si:Al Atomic Ratio (Wallah and Rangan 2006)

Si:Al ratio	Applications
1	- Bricks - Ceramics - Fire protection
2	- Low CO_2 cements and concretes - Radioactive and toxic waste encapsulation
3	- Fire protection fibre glass composite - Foundry equipments - Heat resistant composites, 200°C to 1000°C - Tooling for aeronautics titanium process
>3	- Sealants for industry, 200°C to 600°C - Tooling for aeronautics SPF aluminium
20 - 35	- Fire resistant and heat resistant fibre composites

Another application of geopolymer is in the strengthening of concrete structural elements (Wallah and Rangan 2006). Balaguru et. al. (1997) reported the results of the investigation on using geopolymers, instead of organic polymers, for fastening carbon fabrics to surfaces of reinforced concrete beams. Geopolymer was found to have great adhesion both to the concrete surface and in the cloth interl aminar. In addition, the researchers observed that geopolymer was fire resistant, did not degrade under UV light, and was chemically compatible with concrete (Wallah and Rangan 2006).

1.4.2 Properties of Geopolymers

The geopolymeric materials are "polymers", thus they transform, polycondense, and adopt a shape swiftly at near room temperature, like natural polymers; however also "geo-materials", as a result they are minerals which are hard, weather resistant and can face up to higher temperature than organic polymers. Geopolymers have the properties as follows:

1- Low-energy consumption and environmental friendly.

2- Good mechanical property and excessive early-age strength.

Geopolymers have splendid mechanical properties. The compressive power of greater than 60MPa was reached by means of Rahier et al. (1996a). The energy of geopolymer depends on the nature of supply substances. Geopolymers made from calcined supply materials, such as metakaolin, fly ash, slag, etc., yield greater compressive energy in contrast to these made from non-calcined materials, such as kaolin clay. Geopolymers set and enhance strength quickly. In most cases, 70% of the ultimate compressive power can be developed in the first 4 hours of setting (Van Jaarsveld et al, 1997).

3-Superior chemical resistance. Geopolymers made from metakaolin possesses proper chemical resistance. The values in Table 1.3 show their finest acid resistance over other cement systems. Palomo additionally studied the steadiness of geopolymers made from metakaolin when uncovered to aggressive options (Palomo et al, 1999a). Prisms of mortar made from sand and alkali-activated metakaolin had been immersed in deionized water, sea water, sodium sulfate solution (4.4% wt), and sulfuric acid answer (0.001M) for up to 270 days (Sun 2005). It was observed that the nature of the aggressive solution had little negative effect on the evolution of microstructure and strength of these materials (Sun 2005). It was also found that the samples exposed to the aggressive solutions for more than 90 days experienced a slight increase in their

flexural strength with time, which was related to the microstructure change of the paste material (Sun 2005). Sun and Wu (2013) have studied the chemical and freeze–thaw resistance of fly ash-based inorganic mortars, they found that: (i) fly ash specimens have no deterioration in 5% Na_2SO_4 solutions up to 24 weeks, and fly ash shows continuous increases in mass, dynamic modulus, and compressive strength with time.(ii) The resistance of fly ash mortars to 5% Na_2SO_4 solutions was better than OPC, at least for the time period (24 weeks) investigated in their study; (iii) Fly ash mortars deteriorated in strong H_2SO_4 solutions. The higher was the concentration, the faster was the deterioration rate; (iiii) Fly ash mortars showed superior freeze–thaw resistance to OPC.

Table 1.3. Break up in 5% acid solutions (% of matrix dissolved under identical conditions)

(Van Jaarsveld et al, 1997)

Matrix	H2SO4	HCl
Portland cement	95	78
Portland cement/slag blend	96	15
Ca-aluminate cement	30	50
Geoplymer	7	6

4-Superior freeze-thaw performance. By test, after 180 freeze-thaw cycles, geopolymer specimens made from metakaolin showed mass loss less than 0.1%, and strength loss less than 5% (Sun and Wu 2013).

5- Superior high-temperature resistance. Geopolymers of the sialatedisiloxo resins, harden like thermosetting organic resins, but have use-temperature range up to 1000°C (1830°F) (Davidovits et al, 1991). In Barbosa's study (Barbosa et al, 2003a, 2003b), geopolymers with high Al/Si ratio

have especially high thermal stability with melting points in the range of 1400°C (2550°F) (Sun 2005).

6- Low permeability. The permeability of geopolymer binders is in the order of 10^{-10} m/s (http://www.geopolymer.org), (the permeability of normal concrete is in the range of 10^{-9} to 10^{-10} m/s), which is very low and can favor the use of these materials as immobilization systems for waste materials (Sun 2005).

1.4 Objectives

The aim of this research is to study the effect of hot weather environments (either by changing relative humidity and temperature is kept constant, or by changing temperature but relative humidity is maintained same) on the durability performance of geopolymer concrete beams and columns. The study will include the long term influence of moisture, high temperature, and combined hygrothermal conditions on the mechanical properties of geopolymer beams and columns. This study will focus first on the long-term properties of geopolymer beams and columns that listed below:

Mechanical properties:

- Compressive Strength
- Tensile strength.
- Elastic modulus.
- Stress-Strain Response.

Analytical methods available for Portland cement concrete will be used to predict the test results.

In addition, finite element analysis will be used to investigate the influence of the deterioration of geopolymer on long-term structure performance of geopolymer concrete beams, and columns.

CHAPTER TWO: LITERATURE REVIEW

2.1 Hot weather environments

Hot weather, as described via ACI 305R, is any combination of the following prerequisites that tends to impair the first-rate of freshly mixed or hardened concrete via accelerating the rate of moisture loss and rate of cement hydration, or in any other case causing detrimental results:

-High ambient temperature

-High concrete temperature

-Low relative humidity

-High wind speed, and solar radiation

Hot climate issues are most regularly encountered in the summer season , but the associated climatic factors of excessive winds, low relative humidity and photo voltaic radiation can appear at any time, mainly in arid or tropical climates. Hot weather conditions can produce a fast rate of evaporation of moisture from the surface of the newly placed concrete and accelerated placing time, among different problems.

2.2 Effect of hot weather on concrete properties

Portland cement concrete can improve undesirable characteristics when the material reveals high temperatures while it is being mixed, transported, cast, finished, and cured at some stage in warm climate. High concrete temperature affect important properties of the plastic mixture: increased water demand of the mixture , accelerated slump loss, reduction in sitting times , extended tendency for plastic shrinkage cracking, finishing problems, and decreased manage of entrained air content.

High mixture temperatures additionally affect important properties of the hardened concrete such

as decreased last strength, expanded tendency for moisture and thermal shrinkage cracks, diminished material durability, and reduced uniformity of surface appearance (Samarai et al. 1983; Schindler and McCullough 2002).

ACI Committee 305 (2006) recommends keeping concrete temperatures beneath ninety five _F (35 _C) and stresses the importance of cautiously monitoring prerequisites to minimize evaporation, specially till appropriate curing strategies have been put in place. ACI Committee 305 (2006) also suggests quite a few techniques to limit the temperature of concrete, which includes ‘‘shading combination stockpiles, sprinkling water on coarse aggregate stockpiles, using chilled water for concrete production, substituting chipped or shaved ice for parts of the mixing water, and cooling concrete materials the use of liquid nitrogen’’ (ACI Committee 305 2006). Many researchers have tried to explain the detrimental results of the hot weather concreting on the concrete properties, however there nonetheless exist a number of theories such as Feret’s relation thinking about electricity and sketch factors, Arrhenius regulation associated with power and maturity and the hydration kinetics (Kayyali 1984; Mouret et al. 2003; Ortiz et al. 2005). Such researches have been performed underneath well-controlled laboratory condition, so they cannot reflect the true area situation with many variables. Furthermore, there is no clear proof for the detrimental effects beneath warm weather. Recently, some researches have pronounced unconventional outcomes on the warm weather concreting.

Mustafa and Yusof (1991) showed that the outdoor shrinkage under hot weather could be less than the controlled indoor shrinkage under same temperature condition and that the long-term effects of the hot weather might not be adverse as those usually reported in other researches. Ait-Aidera et al. (2007) found that the addition of water under hot weather can offer sufficient moisture to the

hydration process to evolve under more or less valid conditions even though an increase in W/C ratio would generally lead to a fall in the concrete strength.

Additionally, most of the associated problems cuased by placing concrete in hot weather conditions relate to the increased rate of cement hydration at higher temperatures and the increased rate of evaporation of moisture from the fresh concrete.

The properties of concrete that may be affected by hot weather conditions include:

2.2.1 Setting time

As the concrete temperature increases, the setting time, and thus the time to place, compact and finish the concrete is reduced, Figure 2.1 (Hot Weather Concreting Nov. 2004).

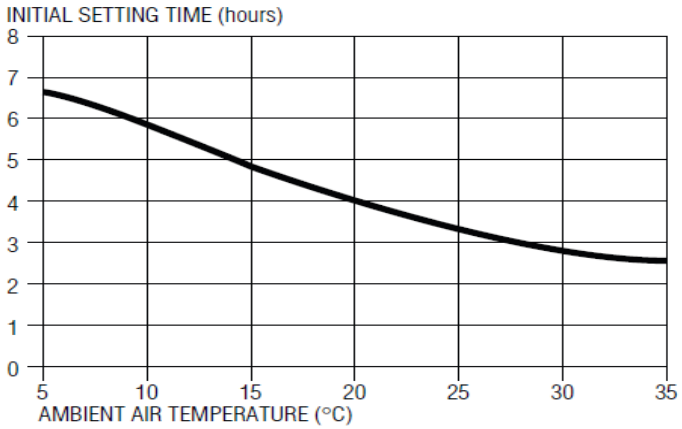

Figure 2.1 Influence of air temperature on setting
times of concrete made with Type GP cement (Hot Weather Concreting Nov. 2004).

2.2.2 Workability and slump

Higher temperatures reduce the workability (or slump) of the concrete more rapidly with time Figure 2.2. Adding more water to improve the workability of the mix decreases the strength and increases the permeability, and ultimately affects the durability of the concrete (Hot Weather Concreting Nov. 2004).

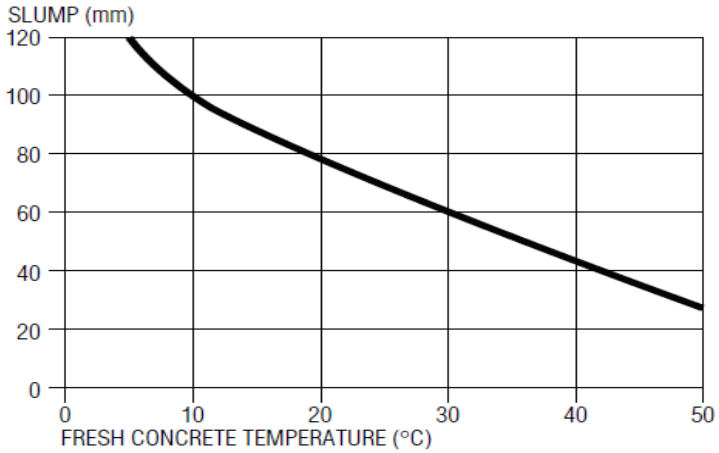

Figure 2.2 Decrease in workability of fresh concrete (as measured by slump), made with constant water content, as temperature increases

2.2.3 Compressive strength

Higher water demand and higher concrete temperature may want to lead to reduced 28-day strengths. If extra water is delivered to the concrete mix at greater temperatures to keep or restore workability, the water cement ratio will be increased, ensuing in a loss of each viable power and durability (Hot Weather Concreting Nov. 2004).

This may also increase the drying shrinkage of the hardened concrete. Where water is not added, the reduced setting time and workability increase the potential for inadequate compaction (itself of a major influence on strength), the formation of cold joints and poor finishes (Hot Weather Concreting Nov. 2004).

2.2.4 Concrete temperature

Hot weather conditions may accentuate the temperature rise in concrete caused by the heat of hydration (Hot Weather Concreting Nov. 2004). In large sections thermal gradients through the element may cause thermal cracking. Laboratory tests indicate that sustained higher tempreture have a significant impact on the gain in compressive strength of hard concrete (Figure 2.3). While increased concrete temperatures may result in an increase in the early rate of strength gain, in the

longer term, concrete cured at lower temperatures will achieve higher ultimate strength (Hot Weather Concreting Nov. 2004).

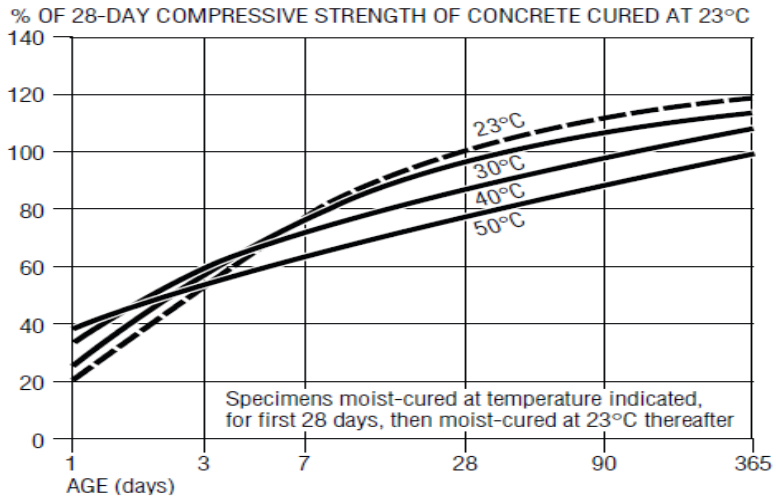

Figure 2.3: Effect of high curing temperatures on concrete compressive strength (Hot Weather Concreting Nov. 2004).

2.2.5 Poor surface appearance

With the increased rate of evaporation, the surface of the concrete will dry out and stiffen (Hot Weather Concreting Nov. 2004). In the case of flatwork this may lead to premature finishing of the surface, trapping an amount of bleed water within the mix. The compacted surface layer (from finishing) may cause the rising bleed water to be trapped below the surface, resulting in debonding of the surface layer and subsequent flaking. Also, colour differences on the surface may result from different rates of hydration and cooling effects (Hot Weather Concreting Nov. 2004).

2.2.6 Plastic shrinkage cracking

Hot weather conditions accelerate the loss of moisture from the surface (Hot Weather Concreting Nov. 2004). If the rate of evaporation is increased than the rate of bleeding (rate at which water rises to the surface), surface drying will occur, resulting in shrinkage of the concrete.

When the shrinkage stresses exceed the tensile capability of the concrete, cracking will show up. The probability of plastic shrinkage cracking is therefore larger whenever warm weather conditions expand evaporation or the concrete has a decreased bleeding rate. Plastic shrinkage cracks can be quite deep, as the plastic concrete has little capability to face up to shrinkage stresses, and cracks proceed to widen and propagate until the shrinkage stresses are relieved. Note plastic shrinkage cracks seldom prolong to free edges, as unrestrained contraction of the concrete is viable at these locations.

2.2.7 Thermal cracking

Concrete is at risk of thermal cracking when placed first, and the hydration heat increases the temperature of the concrete's interior. Rapid changes in external concrete surface temperature, such as placing concrete slabs, walls or pavements on a hot day followed by a cool night, result in thermal gradients between the warm / hot interior and the colder external surface.. The warmer interior provides a restraint to the colder external surface, which wants to contract (Hot Weather Concreting Nov. 2004). Depending on the temperature differential, cracking of the concrete may result. Massive or thick concrete elements are more at risk because of the insulating effect that the concrete provides to the interior of the element.

2.3 Effect of Fly Ash on the Properties of Fresh Concrete

Addition of fly ash to concrete ought to help alleviate some of the issues arising from warm climate concreting, as the presence of Class F fly ash in concrete combos leads to reduce in water demand, and decreased the rate and amount of heat of hydration (Tarun R. Naik, AND Shiw S. Singh 1990).

The properties of concrete that might also be affected with the aid of fly ash include

2.3.1 Workability

The use of high-quality fly ash with a high degree of fineness and low carbon content reduces the water demand for concrete and therefore the use of fly ash should allow concrete to be produ ced at a lower water content compared to portland cement concrete with the same workability (Figure 2.4 and Figure 2.5). Although the exact amount of water reduction varies widely with the nature of the fly ash and other parameters of the mix, a gross approximation is that each 10% of fly ash should allow a water reduction of at least 3% (Thomas 2007)

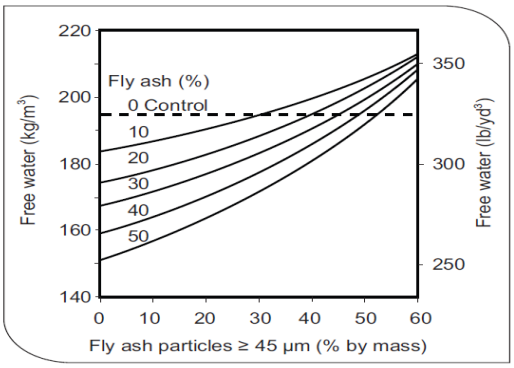

Figure 2.4 Effect of fly ash fineness on water demand of concretes proportioned for equal slump (Owens 1979).

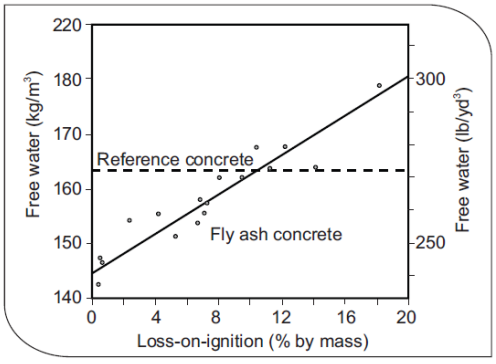

Figure 2.5 Effect of fly ash LOI on water demand of concrete proportioned for equal slump (Sturrup 1983)

A well-proportioned fly ash concrete mixture will have improved workability when compared with a portland cement concrete of the same slump. This means that, at a given slump, fly ash concrete flows and consolidates better than a conventional portland cement concrete when vibrated. The use of fly ash also improves the cohesiveness and reduces segregation of concrete. The spherical particle shape lubricates the mix rendering it easier to pump and reducing wear on equipment (Best 1980) (Figure 2.6).

It should be emphasized that these benefits will only be realized in well-proportioned concrete. The fresh concrete properties were heavily influenced by the proportions of the

mixture,including the type and quantity of cementing material, the water content, aggregate gradi ng, the presence of trained air and chemical admixtures.

Coarser fly ashes or those with high carbon levels generally reduce water demand, and some may even increase water demand (Figures 2.4 and Figure 2.5).

Before using these ashes in concrete, careful consideration should be given, especially at higher levels of replacement in structural concrete. (Thomas 2007).

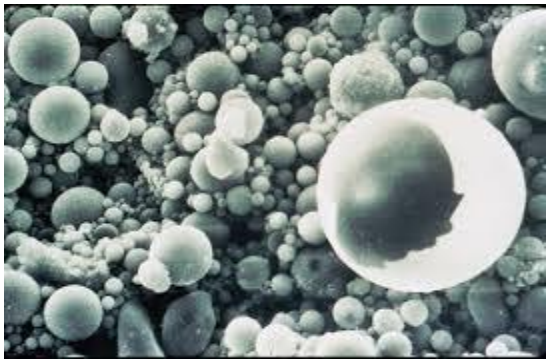

Figure 2.6. Micrograph showing spherical fly ash particles (IMG12309) (Thomas 2007).

2.3.2 Bleeding

Generally fly ash will reduce the rate and amount of bleeding primarily due to the reduced water demand (Gebler 1986).

Particular care is required to determine when the bleeding process has finished before any final finishing of exposed slabs. High levels of fly ash used in concrete with low water contents can virtually eliminate bleeding. Therefore, the freshly placed concrete should be finished as quickly as possible and immediately protected to prevent plastic shrinkage cracking when the ambient conditions are such that rapid evaporation of surface moisture is likely (Thomas 2007).

The guidance given in ACI 305, Hot Weather Concreting should be followed. An exception to this rule is the use of fly ash without adequate water control, in which case bleed ing (and segregation) would increase compared to cement concrete from portland..

2.3.3 Air Entrainment

Concrete containing low-calcium (Class F) fly ashes generally requires a higher dose of air-entraining admixture to achieve a satisfactory air-void system. This is mainly due to the presence of unburned carbon (Figure 2.7) which absorbs the admixture. Consequently, higher doses of air entraining admixture are required as either the fly ash content of the concrete increases or the carbon content of the fly ash increases. By determining its loss-on-ignition , the carbon content of fly ash is usually measured indirectly (LOI) (Thomas 2007).

The increased demand for air entraining admixture should not present a significant problem to the concrete producer provided the carbon content of the fly ash does not vary significantly between deliveries. It has been shown that as the admixture dose required for a specific air content increases, the rate of air loss also increases (Gebler 1983).

In particular, high-calcium fly ashes allow a smaller increase in air-training dose compared to low-calcium fly ashes. Some Class C fly ashes high in water soluble alkali that require even less mixing than those mixtures that do not need fly ash.(Pistilli 1983).

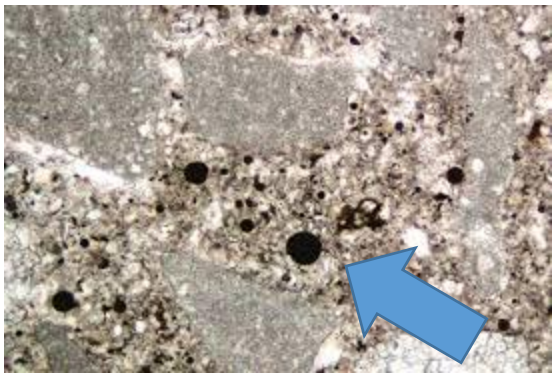

Figure 2.7 Concrete in thin-section. Fly ashes with a high content of unburnt carbon (highlighted with arrow) generally require higher doses of air-entraining admixture (Courtesy V. Jennings, CTLGroup) (Thomas 2007).

2.3.4 Setting Time

The impact of fly ash on the concrete setting behavior depends not only on the composition and quantity of used fly ash, but also on the type and quantity of cement, the ratio of water to cement materials (w / cm), type, quantity and concrete temperature of chemical admixtures (Thomas 2007). Low-calcium fly ashes are reasonably well-established to expand both the initial and final concrete array as shown in Figure 2.8.

The delay due to fly ash tends to be low during hot weather and is likely to be positive in many cases. Using fly ash, especially at high replacement levels, could lead to very significant delays in both the initial and final set during cold weather (Thomas 2007). These delays can lead to difficulties in placement, particularly with regard to the timing of finishing operations for floor slabs and floor slabs or security to prevent the freezing of plastic concrete. Practical considerations may require that the fly ash content is limited during cold-weather concreting. The use of set-accelerating admixtures can counteract the retarding effects of whole or part of fly ash. The setting time can also be shortened by using ASTM C150 Type III cement (or ASTMC1157 Type HE) or by increasing the concrete's initial temperature during processing (e.g., heating mixing water and/or aggregates).

Higher-calcium fly ashes generally delay setting to a lower degree than low-calcium fly ashes, probably because fly ash's hydraulic reactivity increases as calcium content increases. Nevertheless, the effect of high-calcium fly ashes is more difficult to predict because the use of some of these ashes with certain combinations of cement-admixture can result in either a fast (or even flash) setting or a severe delay in setting (Wang 2006, Roberts 2007, and Thomas 2007).

Testing is required with all fly ashes, but especially with higher-calcium fly ashes, before a new fly ash source is introduced into a plant. Testing can determine the effect of fly ash on other plant materials ' concrete setting behavior.

This testing should be conducted at a range of fly ash levels and at different temperatures.

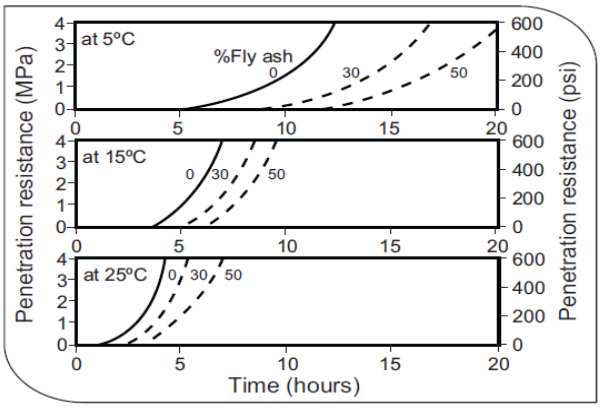

Figure 2.8 Effect of fly ash and temperature on the penetration resistance of setting concretes proportioned for equal strength at 28 days and workability (Concrete Society 1991).

2.3.5 Heat of Hydration

Reducing the rate of heat produced and hence the concrete's internal temperature rise has long been an incentive to use fly ash in the construction of mass concrete. Ontario Hydro (Mustard 1959) carried out one of the first full-scale field trials during the construction of the Otto Holden Dam in northern Ontario around 1950. Two elements of the dam, measuring 3.7 x 4.3 x 11.0 m (12 x 14 x 36 ft), were constructed with embedded temperature monitors. One element was constructed using a concrete of 305 kg / m3 (514 lb / yd3) of portland cement and the other with a concrete of the same cement content but replaced by a Class F fly ash of 30 percent of portland cement. Figure 2.9 shows the results from this study indicating that the use of fly ash reduced the maximum temperature rise over ambient from 47°C to 32°C (85°F to 58°F).

In massive concrete pours where the heat loss rate is low, the maximum temperature increase in fly ash concrete will primarily depend on the amount and composition of the used portland cement and fly ash along with the concrete temperature at the time of placement. Concrete with low portland cement content and high fly ash content is suitable to reduce autogenous temperature rises. For example, Langley and coworkers (Langley 1992) cast three 3.05 x 3.05 x 3.05 m (10 x 10 x 10 ft) blocks with embedded thermocouples, and showed that the incorporation of 55% fly ash reduced the peak temperature by 29°C (52°F) when the cementitious material content was held constant and by 53°C (95°F) when the total cementitious content was reduced (Table 2.1). The high-volume fly ash (HVFA) concrete mixes (with ~ 55% Class F fly ash) were effective in reducing both the rate of heat development and the maximum temperature reached within the concrete block.

Table 2.2 shows data from a later study (Bisaillon 1994) using large monoliths (2.5 x 4.0 x 5.0 m (8.2 x 13.1 x 16.4 ft)) cast with HVFA concrete with Type F fly ash.

These results again indicate that the autogenous temperature rise can be kept very low with high-volume fly ash when the total cementitious content is kept low (in this case 280 kg/m^3 (472 lb/yd^3)).

This property can be very advantageous if the strength of the early age is not important.

In commercial applications, HVFA concrete systems have been used successfully to regulate temperature increases in large placements (Mehta 2000, Mehta 2002, and Manmohan 2002). Most of the published work on fly ash's effects on heat development rate and concrete temperature rise has focused on low-calcium Class F fly ash. Work by the Reclamation Bureau (Dunstan 1984) showed that the rate of heat development generally increases with the ash's calcium content. When used at normal replacement levels, fly ashes high in calcium may produce little or no decrease in hydration heat (as compared to plain portland cement). Similar results have been reported in studies on insulated mortar specimens (Barrow 1989), where the use of high-calcium ash (> 30% CaO) has been found to delay the initial heat evolution but has not reduced the maximum temperature increase. However, Carrette (1993) reported no consistent trend between ash composition and rise in temperature for concrete containing high levels of fly ash (56 percent by weight of cemented material).

The ash calcium levels used in the study ranged up to 20% CaO. Studies conducted at Ontario Hydro in Canada (Thomas 1995) using a wide range of fly ashes (2.6% to 27.1% CaO) showed that the 7-day hydration heat of cement fly ash pastes was strongly correlated with the calcium content of fly ash in accordance with Dunstan (1984).However, these studies also indicated that high-calcium fly ashes could be used to meet performance criteria for ASTM C150 Type IV or ASTM C1157 Type LH cements when used at a sufficient replacement level (Figure 2.10).

High levels of fly ash of high calcium (Class C) were used to control the rise of temperature in the foundations of mass concrete. One example is the concrete raft foundation for the Windsor Courthouse (Ellis Don 1996). This concrete raft of 10,000 m3 (13,000 yd3) was 1.2 m (4 ft) thick and was mounted in volumes between 1400 m3 and 1700 m3 (1830 yd3 to 2220 yd3) with placement rates (beton pumping) up to 100 m3/h (130 yd3/h). Concrete with 50 percent Class C fly ash was used to control temperature while thermocouples were used to determine when it was possible to remove thermal blankets without causing thermal shock.

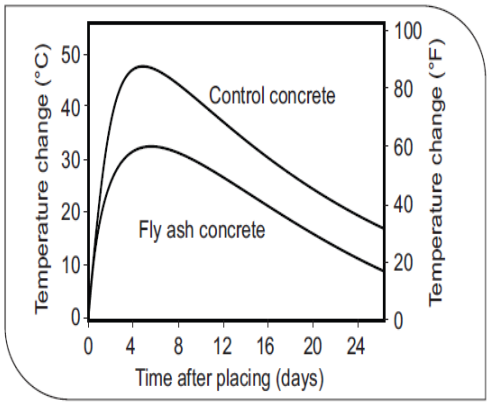

Figure 2.9 Effect of fly ash on temperature rise in concrete dams (Mustard 1959**).**

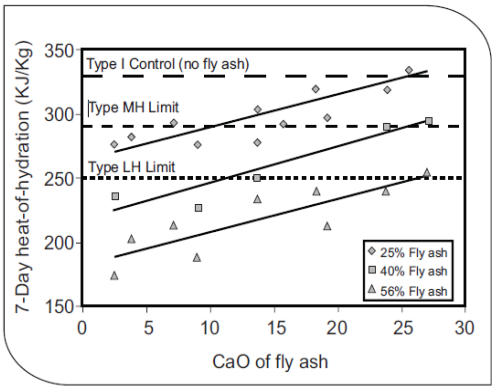

Figure 2.10 Effect of fly ash on heat of hydration using conduction (isothermal) calorimetry (Thomas 1995).

Table 2.1 Temperature Rise in Large Concrete Blocks Produced with HVFA Concrete

Mix	Cement kg/m³ (lb/yd³)	Fly ash kg/m³ (lb/yd³)	w/cm	Max. temp °C (°F)	Time to max. (h)
1	400 (674)	-	0.33	83 (181)	24
2	180 (303)	220 (370)	0.27	54 (129)	96
3	100 (168)	125 (211)	0.49	30 (86)	168

(Langley 1992)

Table 2.2 Temperature Rise in Large Concrete Monoliths Produced with HVFA Concrete

Mix	Cement kg/m³ (lb/yd³)	Fly ash kg/m³ (lb/yd³)	w/cm	Strength MPa (psi) 1-day	3-day	Max. temp °C (°F)	Time to max. (h)
1	365 (600) Type I	-	0.45	10.3 (1495)	-	68 (154)	29
2	125 (211) Type I	155 (261)	0.46	1.6 (230)	5.1 (740)	44 (111)	53
3	170 (287) Type I	220 (370)	0.29	8.4 (1220)	15.6 (2260)	54 (129)	57
4	330 (556) Type II	-	0.50	7.3 (1060)	14.0 (2030)	55 (131)	75
5	125 (211) Type I	155 (261)	0.41	2.5 (365)	8.4 (1220)	47 (117)	98

(Bisaillon 1994)

2.3.6 Finishing and Curing

The use of fly ash may result in significant delays in setting time, which may result in delays in finishing operations (Thomas 2007). The rate of pozzolanic reaction at normal temperatures is slower than the rate of cement hydration, and fly ash concrete must be properly cured if the full benefits of its incorporation are to be realized. When using high levels of fly ash, it is generally recommended that the concrete be cured moist for a minimum of 7 days. It was recommended that the curing duration be extended further (e.g. to 14 days) where possible, or that a curing membrane be placed after 7 days of moist curing (Malhotra 2005). If in practice sufficient healing is not feasible, the amount of fly ash used in the concrete should be reduced.

2.4 Effect of Fly Ash on the Properties of Hardened Concrete

2.4.1 Compressive Strength Development

Figure 2.11 shows the effect on compressive strength of replacing a certain mass of portland cement with an equal mass of low-calcium (Class F) fly ash and maintaining a constant w/cm. (Thomas 2007). As the level of replacement increases the early-age strength decreases.

However, long-term strength development is improved when fly ash is used and at some age the strength of the fly ash concrete will equal that of the plain portland cement concrete so long as sufficient curing is provided (Thomas 2007). The age at which strength parity with the control (portland cement) concrete is achieved is greater at higher levels of fly ash. The ultimate strength achieved by the concrete increases with increasing fly ash content, at least with replacement levels up to 50% (Thomas 2007).

In general, the differences in portland cement early-age strength and fly ash concrete are lower for fly ash with higher calcium levels, but this is not always the case.In many cases, concrete is proportioned at a specified age (typically 28 days) to achieve a certain minimum strength (Thomas 2007). This can be achieved by selecting the appropriate water-to-cement ratio (w / cm) for mixing cement and fly ash used. The w / cm required varies depending on the fly ash replacement level, the ash composition and the specified age and strength. If the stated strength is needed at 28 days or earlier, lower w / cm values are usually required when using higher fly ash levels. A lower w / cm can be achieved by combining I reducing the water content either by taking advantage of the lower demand in the presence of fly ash, or by using a water-reducing mixture, or both; and (ii) increasing the mix's total cement content. The use of an accelerated admixture can be considered when the intensity is needed at an early age (for example, 1 day) (Thomas 2007). Temperature strongly influences the rate of early-age strength development, and this is particularly

the case for fly ash concrete as the pozzolanic reaction is more temperature sensitive than the hydration of portland cement. Temperature-matched curing improved the strength of fly ash concrete at all ages up to 28 days, the effect being most pronounced at an early age: at 3 days the strength of the temperature-matched cured cubes was almost twice that of the cubes stored under standard conditions (Thomas 2007). Temperature-matched curing resulted in a slight increase in portland cement concrete strength at 3 days (5 percent increase over normally cured concrete), but substantially weakened the strength at later ages. The difference in the early-age in situ strength of concrete with and without fly ash can be much lower in large sections or in concrete placed at high temperatures than predicted on the basis of test specimens stored under standard laboratory conditions (Thomas 2007). As a result, the strength gain of fly ash concrete could be lower in small sections placed in cold weather than predicted based on cylinders stored under standard conditions. Given the high sensitivity of fly ash concrete to curing temperature, especially when using higher levels of fly ash, the use of methods (such as temperature-matched curing or cast-in-place cylinders) to determine the in-situ strength of the concrete may be prudent.

If relatively high strengths are needed at a very early age, it will generally be necessary to limit t he amount of fly ash used if suitable measures are taken to improve the fly ash's early strength co ntribution (e.g. heat-curing or accelerator usage or both), particularly when the concrete is put at low temperatures. In well-cured and properly-proportioned fly ash concrete, where a reduction in the mixing water content is made to take advantage of the reduced water demand resulting from the use of the fly ash, the amount of shrinkage should be equal to or less than an equivalent portland cement concrete mix. It has been reported that the drying shrinkage of high volume fly ash concrete is generally less than conventional concrete (Malhotra 2005 and Atis 2003) and this is undoubtedly due to the low amounts of water used in producing such concrete.

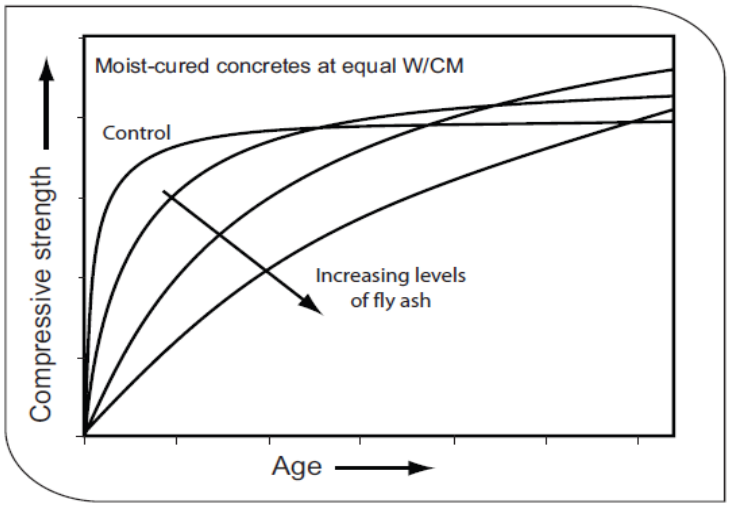

Figure 2.11. Schematic effect of fly ash on compressive strength development of concrete.

2.5 Mechanical properties of concrete as influenced by inclusion of fly ash and temperature

Numerous studies have been conducted to evaluate mechanical properties of fly ash concrete. Based on past research, Berry and Malhotra (1980) stated that the incorporation of fly ash into concrete results in improved workability, pumpability, cohesiveness, finishing ability, ultimate strength and durability. Lane and Best (1982) indicated that fly ash properties influenced the compressive strength of concrete to a greater degree compared to its influence on modulus of elasticity. They reported that the elasticity and compressive strength modulus was lower in early ages and higher in later ages compared to the non-fly ash reference concrete. Lohtia et al. (1976) indicated that 15% Class F fly ash replacement was optimal in terms of strength, elasticity modulus and creep. Ghosh and Tikalsky (1981) compared fly ash concrete with reference concrete. The results indicated that concrete containing good quality fly ash had an equal elasticity module and significantly lower creep values than the concrete reference value.

Abbasi and Al-Tayyb (1988) studied the influence of hot weather conditions on concrete tensile strength rupture and splitting modules. They stated that the compressive strength needed was obtained in hot weather conditions, but the respective rupture module and concrete splitting strength was lower by about 20 and 10 percent compared to the concrete reference healed at normal laboratory temperature. Cebeci (1987) investigated the impact of concurrent changes in curing temperatures (17 and 370C) and the relative humidity of the healing medium (100%, 75% and 33%) on concrete strength production up to one year.

Their results showed that the reduction in humidity had a greater effect on the subsequent strength production of concrete than the curing temperature. The compressive strength of concrete kept in low humidity was found to be 30 to 46 percent lower than that of water curing. Ravindrarajah and Tam (1989) studied performance of fly ash concrete under hot climates with a temperature of 28 + 2 ^{0}C and relative humidity of 75 + 15%. The results showed that, under normal temperature conditions, the rapid hydration rate of the reference concrete under hot and humid environments could be altered by adding fly ash to the rates similar to those of the reference concrete.Naik and Singh (2018) analyzed concrete mechanical actions in hot and dry weather conditions as a result of fly ash inclusion and temperature. Their research results are true only for concrete made from low-calcium fly ash, meeting the requirements of ASTM Class F fly ash. The following have been established:

(1) The optimum fly ash level for the concrete with respect to the compressive strength of 28 days was 10 percent at 73 oF (23 oC) and 95 oF (35 oC) temperatures; and 20 percent at 120 oF (49 oC) temperatures.

(2) The maximum fly ash content in concrete was found to be 10 percent in hot and dry weather conditions with respect to the elasticity modulus.

(3) For all test temperatures, the optimal amount of fly ash for the tensile strength was 10 to 20% within the experimental range..

2.6 Fly Ash Based Inorganic Building Material (Geopolymer Concrete)

2.6.1 Environmental Impact

The main reason for global warming is the emission of greenhouse gases such as CO2 and CO (carbon monoxide). As a result, this adverse environmental impact will be resolved by partial or full removal of cement from the concrete mixture. Over the past three decades, GPC (Geo-Polymer Concrete) has been investigated as a popular alternative. The use of fly ash and slag that would otherwise end up in GPC landfills further shows that this material is environmentally friendly. Reducing CO2 emissions for the geopolymer system is due to the use of minimally processed natural minerals and industrial waste as binding agents. The process of using this waste material as a component of binder production helps mitigate environmental issues and provides new green concrete that is environmentally friendly (Joshi & Kadu 2012; Satpute et al. 2012; Subramanian 2007).

2.6.2 Mechanical Properties

Geopolymer binders result from a chemical reaction in which molecules containing silica and alumina in an active pozzolanic material (such as fly ash or slag) react under highly alkaline conditions (Diaz-Loya et al. 2011). The resulting binder reacts as a gel to produce GPC. Several researchers have studied the mechanical properties of this material. These studies have shown that the chemical composition of geopolymer concrete has different mechanical properties compared to OPC. Reviewing the previous geopolymer concrete performance research shows an excellent behavior for this material, making it an alternative building material.

2.6.2.1 Compressive Strength

One of the most important features of concrete is the compressive strength. GPC's compr essive strength depends on various factors such as temperature curing, mixing ratio and alkaline activator molarity. GPC can develop high strength in the earlier age under high curing temperature (Guo et al. 2010; Hardjito et al. 2004, 2005; Kong & Sanjayan 2008; Nasvi et al. 2012; Yost et al. 2013) and it gains target 28 day strength under ambient condition when slag material is added to the mix (Kumar et al. 2010; Li & Liu 2007; Manjunath & Giridhar 2011). The improvement in physical properties is related to the intrinsic structure developed due to enhanced geopolymerisation (Kumar & Kumar 2011; Kumar et al. 2010). Curing at 60 o C for 24 hours produces very rapid strength gain which gives a compressive strength at one day ranging between 47 and 53 MPa (Yost et al. 2013). This feature makes geopolymer concrete suitable for precast applications.

2.6.2.2 Flexural and Tensile Strength

GPC has higher tensile strength than OPC in addition to its higher compressive strength. This improves section capacity, delays the first crack appearance and reduces the percentage of reinforcement to be used. Olivia and Nikraz (2012) indicated that GPC's tensile strength is between 8% and 12% higher than OPC's. As a result, the related sample flexural strength is 1.4 times higher than that of OPC. This activity results from the enhancement of the polymerization-related aluminosilicate network (Nuruddin et al. 2011). Other experiments have shown that the splitting tensile strength and flexural strength are compressive strength functions and compressive strength ratios are equivalent to traditional OPC (Hardjito et al.2005). Bhikshma et al. (2012) explained that its chemical composition is associated with the higher tensile strength of geopolymer concrete. They found that the tensile strength for the alkaline liquid to fly ash ratio varying from 0.3 to 0.5 ranges from 3.72 MPa to 4.95 MPa.

2.6.2.3 Shrinkage and Creep

GPC has low shrinkage and creep properties in addition to the high strength. Pei-Wei et al. (2007) found a 33-40% reduction in the GPC shrinking and expanding strain. Other researchers (Hardjito & Rangan 2005; Hardjito et al. 2004; Olivia & Nikraz 2012) found that drying shrinkage strains were extremely small after one year in the order of 100 micro strains compared to the range of 500 to 800 micro strains reported by OPC. In fact, this behavior is caused by the lower amount of water used in producing GPC. On the other hand, geopolymer concrete has low creep. With the increase in compressive strength, the value of creep deceases is estimated to have no more than 0.4 percent of GPC compared to 0.7 percent of OPC (Hardjito & Rangan 2005; Hardjito et al. 2004; Wallah 2010). Because these factors affect GPC less, it has a lot of advantages over OPC.

2.6.3 Chemical Resistance

Durability of reinforced concrete structures is an important factor affecting the lifetime of structures. The penetration into the concrete of aggressive substances will damage the reinforcement of concrete and corrode. Many research has shown that GPC is more resistant to aggressive environments. As a result, it is possible to use GPC to build structures exposed to aquatic conditions (Reddy et al. 2011). The bulk of previous studies focused on three types of offensive compounds, sulphate, acid and chloride. Wallah and Rangan (2006) researched the impact of immersing low-calcium fly ash GPC concrete in 5 percent sodium sulphate solution for up to one year in different time periods. We concluded that the samples had an outstanding sulfate attack tolerance. Similar to the state before presentation, both samples displayed no change in appearance.

Furthermore, there was no sign of surface erosion, cracking or spalling on the specimensIn terms of acid resistance, GPC has good performance compared to OPC. An experimental study

conducted by Sanni and Khadiranaikar (2012) on the performance of GPC immersed in sulphuric acid and magnesium sulphate showed that the mass loss of GPC specimens for 45 days of exposure was about 3%. On the other hand, the mass loss for the OPC specimens was found to be 20-25% for 45 days of exposure. In addition to this activity, both samples displayed a weight loss decrease of up to 1% for OPC with a marginal improvement for GPC. GPC displayed less compressive strength loss with an average of 15 percent compared to 25 percent for OPC, in addition to its lower mass change (Sanni & Khadiranaikar 2012).

2.6.4 Structure Behavior of Geopolymer Concrete

Yost et al. (2013) conducted an experimental program on geopolymer concrete beam structural performance. They found that the GPC beams have equivalent power and cumulative content similar to OPC beams. GPC beams failed in a more brittle manner than the OPC concrete beams. The researchers suggested that the same method of analysis and layout developed for OPC concrete beams can be used to test the flexural and shear strength for GPC beams. GPC column performance was also studied to ensure that this material is capable of performing in columns as a structural material. Rahman et al. (2011) used twelve reinforced concrete slender columns to investigate the behavior of GPC columns under combined axial load and biaxial bending.

2.6.5 Effect of Temperature and Curing Type on Geopolymer Concrete

Patankar (2014) studied the effect of quantity of water, temperature duration of heating on compressive strength of fly ash based geopolymer concrete. Na2SiO3 solution containing Na2O of 16.45%, SiO2 of 34.35% and H2O of 49.20% and sodium hydroxide solution with concentration of 13 Molar were used in geopolymer concrete as alkaline activators. Fly ash ratio of 0.35 was prepared to processed geo-polymer concrete mixes. Workability was measure by flow table apparatus. Geopolymer concrete cubes of 150 mm X 150 mm X 150 mm were castThe curing temperature ranged from 400C, 600C, 900C and 1200C for each 8, 12 and 24-hour oven heating

period and was tested after 1, 2, 3, 7 and 28 days of concrete cube demolishing. Test results indicate that water quantity plays a major role in balancing workability but does not affect capacity. Thus higher temperature requires less heating time in order to achieve the desired intensity and vice versa. Author says the remaining 3-day cycle is adequate at and above 900C after heating. (SatputeManesh B., WakchaureMadhukar R., PatankarSubhash V. 2012) studied the effect on the compressive strength of geopolymer concrete of duration and temperature curing. Geopolymer concrete is produced by replacing cement with processed fly ash that is activated by alkaline solutions such as Na2Sio3 and NaoH. Cubes of 150 mm X 150 mm X 150 mm X 150 mm was made with 16 Molar concentrated sodium hydroxide solution to fly ash ratio of 0.35. The specimens were cured in the oven for 6, 12, 16, 20 and 24 hours at 600C, 900C and 1200C. Test results show that the compressive strength increases with the duration and temperature of the oven being healed up to 24 hours..

Al-Shathr and Al-Attar (2016) have studied the effect of different curing systems on the strength of Metakaolin (as silica-alumina material) based Geopolymer. Eleven curing systems were used including curing by sun light and laboratory ambient environment at winter (with temperature of 8-19oC) and at summer (with temperature of 32-48oC), curing with halogen lamp, curing by heat at 60oC for 6 hours and at 100oC for 4 hours, water curing, curing by wet burlap, in addition to a mixture of different previous curing systems.

Their results showed that the optimum curing temperature for Geopolymer concrete is (32-48oC) that can be done under sunlight or room temperature, while moist curing was not ideal for this form of concrete. The findings also show that the hardening rate of this form of concrete is high, where it is possible to gain more than 83 percent of the strength of 28 days at 7 days when using

optimum temperature curing. The Geopolymer concrete as a relatively new construction material, still needs to explore.

Since there is no enough information regarding the long term influence of moisture, high temperature, and combined hygrothermal conditions on the mechanical and physical properties of geopolymer concrete, this research will try to conduct it for geopolymer concrete beams and columns.

2.7 Finite element modeling

Finite element method is a powerful alternative approach to solving the governing equations of structural problems. This method consists of envisioning the structure to be composed of discrete parts (i.e. finite elements), which are then assembled in such a way as to represent the distortion of the structure under the specified loads. Each element has an assumed displacement field, and part of the skill of applying the method is in selecting appropriate elements of the correct size and distributions (The FE "mesh"). FEM is useful because only for a simple structure subject to simple loading is an analytical solution available.

2.7.1 Finite element modeling for geopolymer concrete beams

Finite element analysis is used to simulate interactions of all the disciplines of physics, structural, vibration, fluid dynamics, heat transfer and electromagnetic for engineers. By its variety of contact algorithms, time-based loading features and nonlinear material models, FEA can perform advanced engineering analyzes quickly, safely and practically.There were several studies by using FEA software to conduct analytical modeling of geopolymer concrete.

Aleem and Arumairaj (2016) have prepared geopolymer concrete beams of size 100 x 150 x 1000 mm. They used steam curing for 24 hours and then cured under room temperature up to 28 days.

Their beams were tested for three points load methods and deflections were measured. They used ANSYS models to conduct the analytical part of their study.

SOLID187 element, a higher order 3-D, 10-node element was used to model the concrete material. SOLID187 has a quadratic displacement behavior and is well suited to modeling irregular meshes. The element was defined by 10 nodes, with three degrees of freedom at each node: translations in the nodal x, y, and z directions. The SOLID 187 element is shown in the Figure 2.12. Their study showed very similar results between the analytical part and the experimental part.

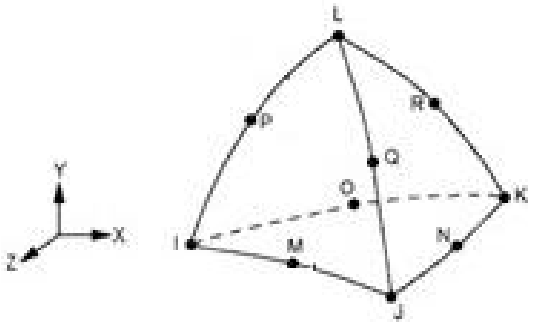

Figure 2.12 SOLID 187 element (Aleem and Arumairaj 2016)

Kumaravel and Thirugnanasambandam, (2013) have studied the flexural behavior of low calcium fly ash based geopolymer concrete beams. They used FEA software ANSYS to predict the load displacement response from the control beams and geopolymer concrete beams numerically. Solid65 was used for beam element (Figure 2.13), and link8 for steel element (Figure 2.14). They conducted that the predicted deflections were in close agreement with the experimental results.

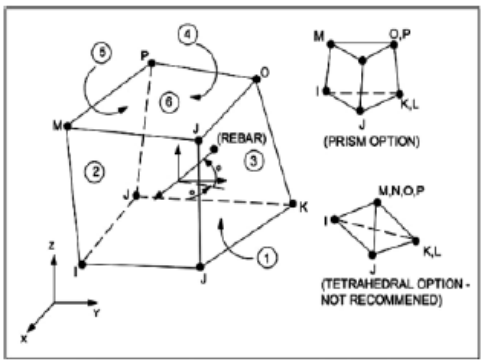

Figure 2.13 Solid65 Geometry

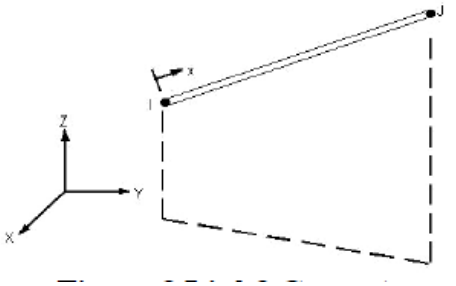

Figure 2.14 Link8 Geometry

2.8 Specification for Hot Weather Concreting (ACI 305.1-06)

2.8.1 Execution

2.8.1.1General

1-Do not place concrete against surfaces of absorbent materials that are dry. Do not place concrete against surfaces that have free water.

2-Prepare all materials required for accepted evaporation control measures and have them available on site so that specified measures can be executed as necessary.

3-Initiate accepted evaporation control measures when concrete and air temperatures, relative humidity of the air, and the wind velocity have the capacity to evaporate water from a free water surface at a rate that is equal to or greater than 1.0 kg/m^2/h (0.2 lb/ft^2/h), unless otherwise specified. Determine the evaporation rate of surface moisture by use of the Menzel Formula:

$$W = 0.315(eo - ea)(0.253 + 0.060V) \text{ [SI units]}$$

$$W = 0.44(eo - ea)(0.253 + 0.096V) \text{ [U.S. Customary units]}$$

Where :

W : mass of water evaporated in kg (lb) per m^2 (ft^2) of water-covered surface per hour;

eo : saturation water vapor pressure in kPa (psi) in the air immediately over the evaporating surface, at the temperature of the evaporating surface. Obtain this value from Table 2.3(a) or (b). The temperature of the evaporating surface shall be taken as the concrete temperature;

ea : water vapor pressure in kPa (psi) in the air surrounding the concrete. Multiply the saturation vapor pressure at the temperature of the air surrounding the concrete by the relative humidity of the air. Air temperature and relative humidity are to be measured at a level approximately 1.2 to 1.8 m (4 to 6 ft) above the evaporating surface on the wind-ward side and shielded from the sun's rays; and:

V: average wind speed in km/h (mph), measured at 0.5 m (20 in.) above the evaporating surface.

- Monitor site conditions (air temperature, humidity, wind speed) to assess the need for evaporation control measures beginning no later than 1 hour before the start of concrete placing operations. Continue to monitor site conditions at intervals of 30 minutes or less until specified curing procedures have been applied.

- For measuring the rate of evaporation of surface moisture, use equipment or instruments that are certified by the manufacturer as accurate to within 1 °C (2 °F), 5% relative humidity, and 1.6 km/h (1 mph) wind speed. Use equipment in accordance with the product manufacturer recommendations.

Air and concrete temperature, °C	Saturation pressure, kPa	Air and concrete temperature, °C	Saturation pressure, kPa
4	0.813	28	3.78
5	0.872	29	4.01
6	0.934	30	4.24
7	1.00	31	4.49
8	1.07	32	4.75
9	1.15	33	5.03
10	1.23	34	5.32
11	1.31	35	5.62
12	1.40	36	5.94
13	1.50	37	6.28
14	1.60	38	6.63
15	1.70	39	6.99
16	1.82	40	7.38
17	1.94	41	7.78
18	2.06	42	8.20
19	2.20	43	8.64
20	2.34	44	9.10
21	2.49	45	9.58
22	2.64	46	10.1
23	2.81	47	10.6
24	2.98	48	11.2
25	3.17	49	11.7
26	3.36	50	12.3
27	3.56		

Data source: *CRC Handbook of Chemistry and Physics*, 68th Edition, 1987, mathematically converted into kPa.

Table 2.3 (a)—Saturation water vapor pressure (kPa) over water (SI units)

Air and concrete temperature, °F	Saturation pressure, psi	Air and concrete temperature, °F	Saturation pressure, psi
40	0.121	81	0.523
41	0.127	82	0.542
42	0.132	83	0.559
43	0.137	84	0.577
44	0.143	85	0.595
45	0.147	86	0.615
46	0.153	87	0.637
47	0.159	88	0.658
48	0.166	89	0.679
49	0.171	90	0.698
50	0.178	91	0.722
51	0.185	92	0.746
52	0.192	93	0.769
53	0.199	94	0.789
54	0.206	95	0.816
55	0.214	96	0.843
56	0.222	97	0.870
57	0.231	98	0.896
58	0.238	99	0.920
59	0.247	100	0.951
60	0.257	101	0.981
61	0.267	102	1.01
62	0.277	103	1.04
63	0.285	104	1.07
64	0.296	105	1.10
65	0.308	106	1.13
66	0.319	107	1.17
67	0.327	108	1.20
68	0.339	109	1.24
69	0.352	110	1.27
70	0.366	111	1.31
71	0.378	112	1.35
72	0.388	113	1.39
73	0.403	114	1.43
74	0.418	115	1.47
75	0.433	116	1.52
76	0.443	117	1.56
77	0.459	118	1.60
78	0.476	119	1.65
79	0.494	120	1.70
80	0.510		

Data source: *CRC Handbook of Chemistry and Physics*, 68th Edition, 1987, mathematically converted into °F and psi.

Table 2.3(b)—Saturation water vapor pressure (psi) over water (U.S. Customary units)

2.8.1.2 Maximum allowable concrete temperature

1- Limit the maximum allowable fresh concrete temperature to 35 °C (95 °F), unless otherwise specified, or unless a higher allowable temperature is accepted by Architect/ Engineer, based upon past field experience or preconstruction testing using a concrete mixture similar to one known to have been successfully used at a higher concrete temperature.

2-Measure the fresh concrete temperature at the point and time of discharge in accordance with ASTM C 1064/C 1064M. Frequency of temperature determination shall be in accordance with ASTM C 94/C 94M and at the option of the inspector.

2.8.1.3 Qualification of concrete mixture proportions

1-Approval of concrete mixture and proposed maximum allowable fresh concrete temperature shall be based, on similar climate and production conditions, materials, mixture proportions and temperatures, placing and finishing methods, and concrete delivery time.

2-Approval of concrete mixture and proposed maximum allowable fresh concrete temperature shall require materials similar to those proposed for use in the project.

3-Laboratory trial batch—Batch the laboratory concrete trial mixture within 2 °C (3 °F) of the proposed maximum allowable concrete temperature and mix in accordance with ASTM C 192/C 192M, except as modified hereinBringing the laboratory mixer into an enclosed, heated and ventilated room, or using heated mixing water or both to achieve and maintain the proposed maximum allowable concrete temperature if necessary. The concrete mixture shall remain in the mixer for 47 minutes after completion of the initial3-minute mixing cycle for drum-type mixers, unless otherwise specified. Cover the mixer opening with a non-absorbent material such as plastic over the 50-minute period to prevent loss of moisture and rotate the mixer continuously at a speed of 6 to 8 rpm. Simulate agitation for laboratory mixers without speed adjustment by rotating the mixer continuously from the horizontal at a drum angle between 45 and 75 degrees. At the end of 50 minutes, mix the concrete mixture for 2 minutes at the manufacturer's designated full mixing speed (8 to 20 rpm). For pan-type mixers, the concrete mixture shall remain in the mixer for 41 minutes after completion of the initial 3-minute mixing period. During the 44-minute period, the mixer shall cycle through periods of rest for 5 minutes, and then mixing for 1 minute. During the rest period, cover the mixer opening with a non-absorbent material, such as plastic, to prevent moisture loss. At the end of 44 minutes, mix the concrete mixture at full mixing speed designated by the manufacturer (8 to 20 rpm) for 2 minutes. During mixing and agitation periods for both

drum-type and pan-type mixers, the addition of water, chemical admixture, or both, to adjust slump is permitted provided that the specified concrete mixture w/cm is not exceeded. As needed, check and adjust the slump of the concrete mixture during the middle 1/3 of the 50- or 44-minute laboratory trial mixing period.

- At the end of the laboratory mixing process, the proposed concrete mixture must meet the specified slump range and meet the required strength at the specified test level.

4- Field test batch — Batch the field concrete test mixture within 2 ° C (3 ° F) of the proposed maximum permissible concrete temperature in a truck mixer with a minimum batch size of 3 m3 (4 yd3). In order to achieve a concrete temperature within the defined tolerance of the proposed maximum allowable concrete temperature, shift the truck mixer into an enclosed, heated and ventilated space if necessary. Unless otherwise specified by the Architect / Engineer, the concrete mixture shall be held in the mixer for 90 minutes. Agitate the mixer at 1 to 6 rpm for the whole 90-minute cycle. Mix the concrete mixture at the manufacturer's full mixing speed (6 to 18 rpm) for 2 minutes at the end of 90 minutes.. It is permissible to add water, chemical admixture, or both during mixing and agitation cycles to modify the slump provided the defined concrete mixture w / cm is not exceeded.- At the conclusion of the 90-minute field mixing cycle, the proposed concrete mixture must meet the required strength at the stated test age within the prescribed slump distance.5-Test values obtained in accordance with the appropriate ASTM Standard shall include compressive strength (C 192/ C 192M or C 31/C 31M, and C 39/C 39M), flexural strength (C 192/C 192M and either C 78 or C 293; C 31/C 31M and either C 78 or C 293), or both; slump (C 143/C 143M); air content (C 231, C 173/C 173M, or C 138/C 138M); concrete density (unit weight) (C 138/ C 138M); and concrete temperature (C 1064/ C 1064M). Slump, air content and measurements of concrete and air temperature shall be performed after initial mixing,

intermediately as required or as needed, and at the end of the mixing duration together with the other specified tests.6- Concrete recognition mixture proportions-Submit a request for acceptance to the Architect / Engineer for a specific higher maximum concrete temperature permitted. Include the constituent materials and proportions of the proposed concrete mixture and all values from past field or pre-construction testing experience. The test results are within the ranges and tolerances of the Project Specification.

2.8.1.4 Concrete production and delivery

1. Concrete is manufactured at a temperature such that its maximum discharge temperature does not exceed the maximum permissible concrete temperature specified. Acceptable production methods for reducing the concrete temperature include: shading aggregate stockpiles, sprinkling water on coarse aggregate stockpiles; using chilled water for concrete production; replacing chipped or shaved iced parts of the mixing water; and cooling concrete materials with liquid nitrogen. The submissions for hot weather concreting shall indicate the methods to be used and the order in which they will be performed when using multiple methods. If requested in the submission and supported by sufficient supporting data, the Architect / Engineer must allow the substitution of other cooling methods.

2. Unless otherwise stated, supply concrete in compliance with ASTM C 94/C 94 M requiring the concrete to be discharged within 1-1/2 hours or 300 revolutions before the truck mixer has revolved..

2.8.1.5 Concrete placement and finishing

1- Concrete placement and finishing operations shall proceed as quickly as conditions will permit.

2.8.1.6 Concrete protection

1- Protection period—Protect the concrete against thermal shrinkage cracking due to rapid drops in concrete temperature greater than 22 °C (40 °F) during the first 24 hours unless otherwise specified.

Protective materials — Acceptable protective materials to prevent excessive drops in temperature include insulating covers, moisture-proof battle insulation, dry porous material layers such as straw, hay or multiple layers of impermeable paper meeting ASTM C 171. These protective materials shall not be applied until the temperature of the concrete surface becomes stable or begins to decline.

CHAPTER 3 EXPERIMENTAL PROGRAM

Introduction

In this chapter, the first step was to choose the best mix design for geo-polymer concrete which will be used in the experimental work. In total, 138 specimens were constructed, cured, and tested under various environmental conditions. 72 specimens were geo-polymer concrete (15 specimens were geo-polymer concrete beams, and 57 specimens were geo-polymer concrete columns). 66 specimens were regular concrete beams and columns (18 specimens were concrete beams, and 48 specimens were concrete columns).

First of all, to get the final composition of geo-polymer concrete that used in this research, 12 geo-polymer concrete cylinder specimens were used to establish four deferent mix design of geo-polymer concrete (3 for each mix sample), and 3 regular concrete specimens were used for comparison in term of compressive strength.

After choosing the final composition of geo-polymer concrete, two different sets of groups were established. The first set was regular concrete specimens, while the second one was geo-polymer concrete specimens. In addition, within each one of these two sets, there were subsets that were subjected to different environmental conditions.

Concrete mix was designed for a nominal compressive strength of 5068 psi (35MPa). The control specimens were tested at the age of 28 days. All specimens were taken out from the molds at the second day of casting and placed into water basin for curing.

All the specimens were subjected to mechanical tests (Flexure test for beams, and compression test for cylinders) using MTS-810 testing machine.

3.1 Geo-polymer Mix Design

To get the final composition of geo-polymer concrete that used in this research, four different compositions were done and tested to choose the most accurate composition. All geo-polymer concrete specimens were made from the following material:

3.1.1 Fly Ash

In the experimental work, dry low-calcium fly ash obtained from thermoelectric power station (Headwaters Resources, lnc.) was used as the base material. American Standard Testing and Material (ASTM C618) classify fly ash into Class F and C depending mainly on CaO content. The fly ash that used in the research was Class F with 5% CaO. The chemical composition of fly ash was described in table 3.1.

Table 3.1. Chemical composition of fly ash

Compounds	SiO2	Al2O3	Fe2O3	SiO2+Al2O3+ Fe2O3	CaO	P2O5	SO3	K2O
Mass (%)	51.3	30.1	4.57	85.9	5.06	1.6	1.4	1.56

3.1.2 Granulated Ground Blast Furnace Slag (GGBFS)

Granulated blast furnace slag (GGBFS) is ground to suitable fineness. It is a recovered industrial by-product of an iron blast furnace . Ground granulated blast furnace slag has been incorporated into concrete projects in the U.S. for over a century to improve durability and reduce life cycle costs .The Granulated blast furnace slag that used in this research was obtained from Standard Lafarge Canfield Laboratory. Standard Specification for Ground Granulated Blast-Furnace Slag for Use in Concrete and Mortars - ASTM C 989.

3.1.3 Aggregates

Coarse and fine aggregates used in this research was mixed between 1/2" Limestone, 3/8″ P-Stone course aggregate, and 2NS-Sand as shown in (Figure 3.1a, b, and c) according to (ASTM

C33-07, 2008) and (ASTM E11-04, 2008) standard limitation for sieve analysis test, to be discussed in the next section.

a) 2NS-sand fine aggregate

b) P-stone coarse aggregate

c)Lime-stone coarse aggregate

Figure 3.1: Geo-polymer aggregate materials

3.1.3.1 Sieve Analysis Test

Sieve analysis, commonly known as the "gradation test" is a basic essential test for both fine and course aggregate. The sieve analysis determines the gradation (the distribution of aggregate particles, by size, within a given sample) in order to determine compliance with design, production control requirements, and verification specifications. The gradation data can be used

to calculate relationships between various aggregate or aggregate blends, to check compliance with such blends, and to predict trends during production by plotting gradation curves graphically and compared with the specifications [17].

In general, the sieve analysis test can be done by following these procedures: weigh a certain weight of a dry sample, a set of sieves should be arranged in order (the top sieve has the largest screen openings and the screen opening sizes decrease with each sieve down to the bottom sieve which has the smallest opening size screen for the type of material specified), the sample is put in the upper sieve, and then shaken by mechanical means for a period of time (about 10 minutes). After shaking the material through the nested sieves, the material retained on each of the sieves is weighed using one of two methods.

The cumulative method requires that each sieve beginning at the top be placed in a previously weighed pan (known as the tare weight) and be weighed. Then the next sieve's contents are added to the pan, and the total is weighed. This is repeated until all sieves and the bottom pan have been added and weighed.

The second method involves weighing separately the contents of each sieve and the bottom pan. Either approach is useful and should lead to the same answer. The sum of the sieve that passes is then measured.

In this research, sieve analysis test has been done for both fine and course aggregates by using the second method according to (ASTM C33-07, 2008) and (ASTM E11-04, 2008) standard limitation. Figure 3.2 shows a mechanical testing sieve shaker.

Figure 3.2: Testing sieve mechanical shaker (CA-1500, Sieve Shaker, 8" Sieves)

a) Sieve analysis for fine aggregate "2NS-sand"

The total weight of the sample was 500g, and the test result is shown in Table 3.2.

Table 3.2: Sieve analysis results for fine aggregate"2NS-sand"

Sieve size (mm)	Weight of remaining (g)	Wt. of remaining Cumulative (g)	Remaining %	Passing %	ASTM Standard limitation C33-08, %
2.36	90	90	18	82	80-100
1.18	129.7	219.7	43.9	56.6	50-85
600 µm	103.5	323.2	64.64	35.36	25-60
300 µm	94	417.2	83.44	16.56	5-30
150 µm	66.9	484.1	96.22	3.18	0-10
Pan	12.1	496.2	100	0	

Based on the above data, the sieve analysis for this sand sample of fine aggregate "2NSsand" is within the ASTM standard limitation. Therefore, this sand had been used in the geo-polymer concrete mix and regular concrete for all this research work. Figure 3.3 shows the curve test result.

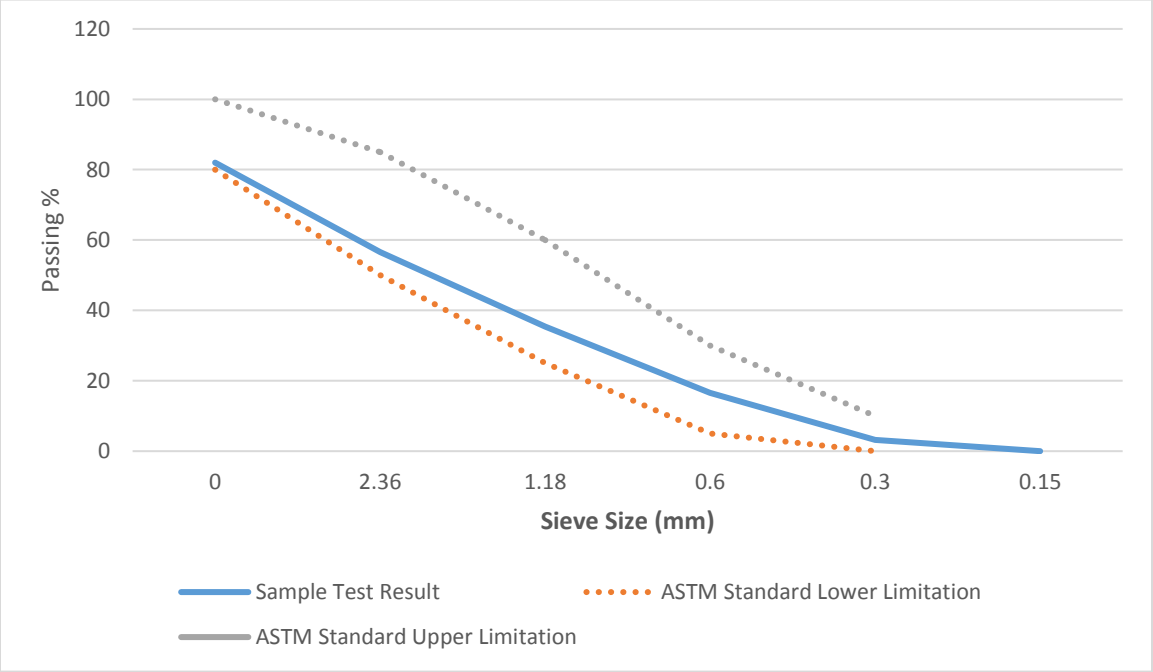

Figure 3.3: Sieve analysis test curve for fine aggregate "2NS-sand"

b) Sieve analysis for Course aggregate

The total weight of the sample "P-stone" was 2800g, and the test result is shown in Table 3.3.

Table 3.3: Sieve analysis results for course aggregate"P-stone"

Sieve size (mm)	Weight of remaining (g)	Wt. of remaining Cumulative (g)	Remaining %	Passing %	ASTM Standard limitation C33-08, %
19	0	0	0	100	100
12.5	2.2	2.2	0.078	99.92	90-100
9.5	334	336.2	12	88	40-70
4.75	2345	2681.2	95.75	4.25	0-15
2.36	102.3	2783.5	99.4	0.59	0-5
Pan	10.4	2793.9	100	0	

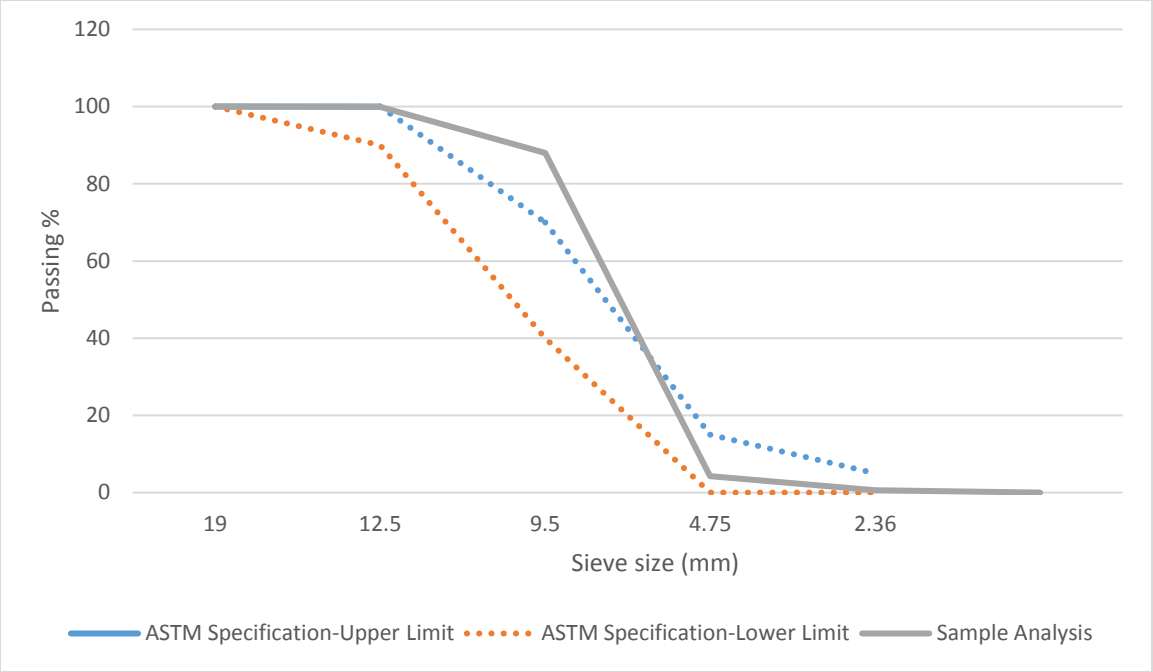

Figure 3.4: Sieve analysis test curve for coarse aggregate "P-Stone"

According to the above test results, this aggregate sample is out of specification due to excessive passing ratio of sieve 9.5mm size.

The total weight of the sample crushed stone "Lime-Stone" was 2800g, and the test result is shown in Table 3.4.

Table 3.4: Sieve analysis results for course aggregate crushed stone "Lime-Stone"

Sieve size (mm)	Weight of remaining (g)	Wt. of remaining Cumulative (g)	Remaining %	Passing %	ASTM Standard limitation C33-08, %
19	1361.9	1361.9	48.6	51.4	100
12.5	1098.3	2460.2	87.86	12.13	90-100
9.5	283.1	2743.3	97.97	2.025	40-70
4.75	46.8	2790.1	99.64	0.35	0-15
2.36	0.2	2790.3	99.65	0.346	0-5
Pan	8.8	2800	100	0	

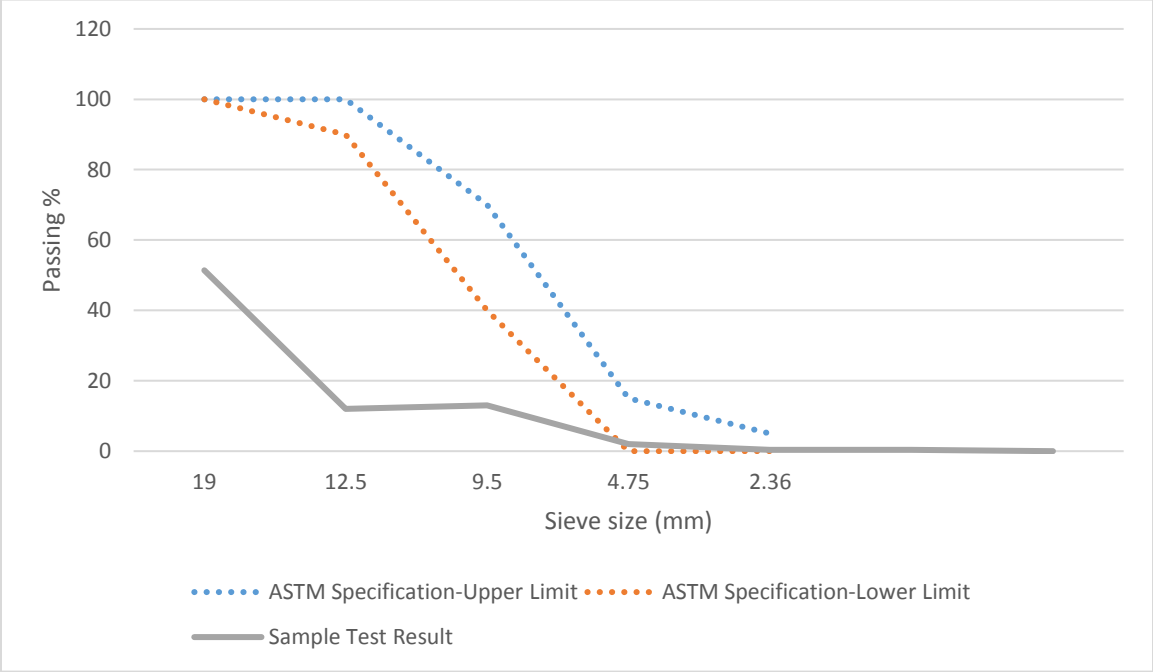

Figure 3.5: Sieve analysis test curve for coarse aggregate "Lime-Stone

Table 3.4 and figure 3.5 show that the sieve analysis test results of that sample is out of specification as well due to a low passing ratio of sieves 19mm, 12.5mm, and 9.5mm size. Therefore, those two course aggregate samples had been mixed together by using trial and error method. Several trials had been done until an optimum ratio was found. The resulting curve fit within the ASTM standard limits. The optimum ratio of the P-stone sample to the lime stone sample was 1:1. Table 3.5 and figure 3.6 show the sieve analysis results of the hybrid sample.

Table 3.5: Sieve analysis test results for the mixing sample, sample weight =2800g.

Sieve size (mm)	Weight of remaining (g)	Wt. of remaining Cumulative (g)	Remaining %	Passing %	ASTM Standard limitation C33-08, %
19	0.00	0.00	0.00	100	100
12.5	127.95	127.95	4.57	95.43	90-100
9.5	955.65	1083.6	38.70	61.30	40-70

4.75	1588.20	2671.8	95.42	4.57	0-15
2.36	102.5	2774.3	99.08	0.91	0-5
Pan	24.8	2799.1	100	0	

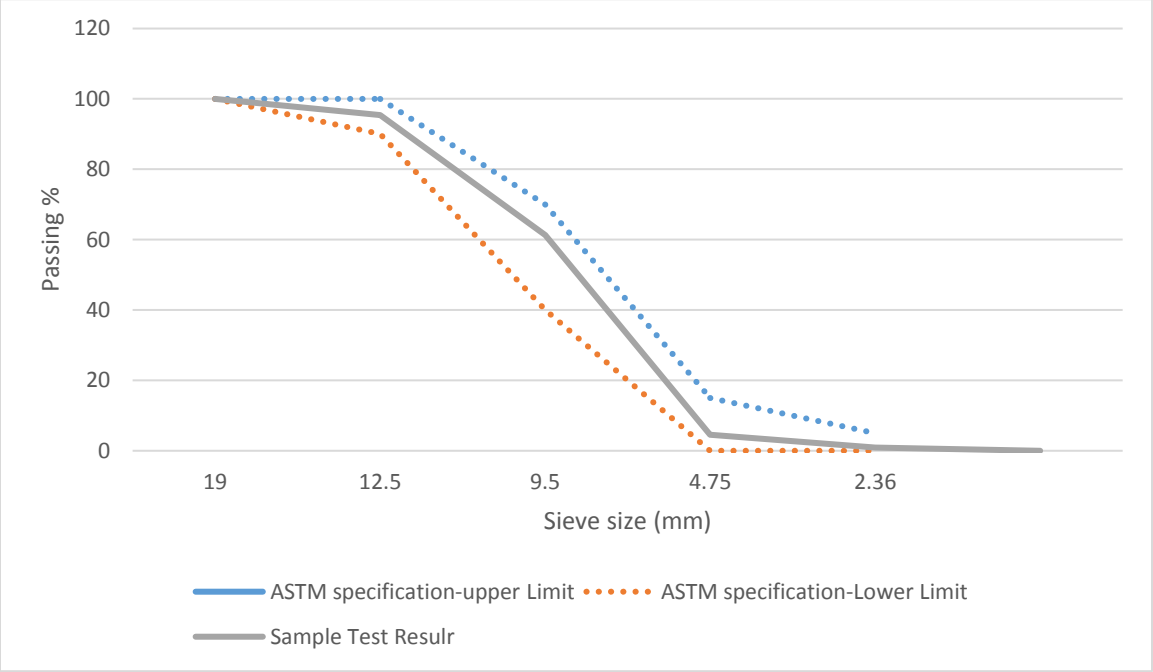

Figure 3.6: Sieve analysis for course aggregate "hybrid sample"

From Table 3.5 and Figure 3.6, the above mixed sample is appropriate per the ASTM standard. Therefore, the 1:1 ratio is used throughout this study.

3.1.4 Alkaline Solution

Alkaline solution plays an important role in geo-polymer synthesis for the dissolution of silica and alumina as well as for the catalysis of polymerization reaction [57]. In this experiment, a combination of sodium silicate and sodium hydroxide was chosen as the alkaline liquid. Sodium silicate was obtained from HTI (High Temperature Ins. Portland, Oregon, United States), and the sodium hydroxide was obtained from (Duda Energy LLC). Sodium silicate (Na2SiO3) used with a composition of 40% water and SiO2 /Na2O =2.

To make the alkaline activator, sodium hydroxide (NaOH) was first dissolved in distilled water to avoid the effect of unknown contaminants in the mixing water. The different concentration of NaOH solution was 8M, 12M & 14M. NaOH solution with a concentration of 8M consisted of 8x40 = 320 grams of NaOH solids (in flake or pellet form) per liter of the solution, where 40 is the molecular weight of NaOH. In order to make 1 Kg of 8M, 12M &14M solutions, 68%, 52%, and 44% of water were added to the pellets to make the solutions 8M, 12M &14M respectively, then the sodium silicate (Na2SiO3) was added to sodium hydroxide solution and stayed for one day.

3.1.5 Super plasticizer (SP)

The Super plasticizer (Sodium naphthalene sulfonate formaldehyde condensate) was used to increase the workability of geo-polymer Concrete. The super plasticizer that used in this research was obtained from (Art-stone-USA). The amount of SP used in this research can be found in table 3.6 as well as the amount of water used in the mix design if any.

3.2 Geopolymer Mixing Procedures

Fly ash, granulated Ground Blast Furnace slag (GGBS) and the aggregates were first mixed together for about 3 minutes (hand mixing). Mix compositions are given in table 3.6. The sodium silicate solution and the sodium hydroxide solution were mixed together one day prior as described before to prepare the alkaline liquid. On the casting day of the specimens, the alkaline liquid was mixed together with the super plasticizer and the extra water (if any) to prepare the liquid component of the mixture. The liquid component of the mixture was then added to the dry materials and the mixing continued for further about 4 minutes using a small mixer (figure 3.7) to manufacture the fresh geo-polymer concrete.

Figure 3.7 Blakeslee Model F-30 Floor Mixer

3.3 Casting and Curing

Cylindrical molds of 150 mm high and 75mm in diameter (According to ASTM C39-08) were used to cast the samples in three layers. Each layer was compacted by tamping rod of diameter 16 mm.

Thermal curing was chosen because compressive strength increases with increase in duration and temperature of oven curing up to 24 hrs [70, 71]. After 24 h of thermal curing (heating) in 60oC, all specimens were demolded and then placed in water for 28 days.

Table 3.6 Mix design proportion

Mix Sample	Fly Ash	GGBS	coarse agg.	fine agg.	Na-Silicate	NaOH	S.P	Water	Curing	
									Time	Tem.
	Kg/m3	Kg/m3	Kg/m3	Kg/m3	Kg/m3	Kg/m3	Kg/m3	Kg/m3	Days	Co
S1	340	60	1280	560	104	40(14M)	0	22.5	28	60
S2	340	60	1280	560	104	40(8M)	6	22.5	28	60
S3	340	60	1280	780	104	40(14M)	6	22.5	28	60
S4	340	60	1240	600	72	72(12M)	6	25.0	28	60

3.4 Test Procedure

To choose the final composition of geo-polymer concrete that will be used in this research, 3 tests have been done to establish that.

3.4.1 Setting time

The initial setting time is the time period between the alkali activator solution added to binder (fly ash_and GGBS) and the time at which Vicat's needle stops around 4mm to 5mm before striking the glass plate, and the finale setting time is the time period between alkali activator solution is added to binder and the time at which Vicat's needle doesn't make any impression on the surface of the paste. The setting time test was done for all the four compositions according to ASTM C191 by using Vicat's needle. The test was done at room temperature (23oC) (see figure 3.8).

Figure 3.8: Vicat's needle for setting time test

3.4.2 Slump test

The slump test is an empirical test that is used for the measurement of the fresh property of geopolymer concrete such as consistency and workability. The test has been done per ASTM C143-08 “Standard Test Method for Slump of Hydraulic-Cement Concrete”. The procedures which had been followed to find the slump value were as follows: a standard concrete slump test cone with 305 mm (12″) high, the base 203mm (8″) diameter, and 102mm (4″) diameter at the top. The cone was placed on a smooth surface plate, the small diameter at the top, and the cone was filled with fresh geoploymer concrete in three layers. Each layer was tamped 25 times with a standard 16 mm (5/8″) diameter steel rod before add the next layer. The final top surface of geopolymer concrete was struck off by means of a screeding and rolling motion of the tamping rod. The cone was firmly held by foot-rests against its base during the operation. After the filling, the cone was slowly lifted and put it upside down and then measure the slump value (see figures 3.9a, b, c, and d).

Figure 3.9a: measure the slump value (S1)

Figure 3.9b: measure the slump value (S3)

Figure 3.9c: measure the slump value (S2)

Figure 3.9d: measure the slump value (S4)

3.4.3 Compressive Strength Test

To measure the compressive strength of the samples, 3 cylinder samples for each composition were tested (Figure 3.10a).

A high capacity MTS-810 testing machine was used (Figure 3.10b). The test had been done at laboratory temperature (23oC).

Figure 3.10a: cylinder mold sample

Figure 3.10b: A high capacity MTS-810 testing machine

3.5 Regular concrete composition for comparison

To get the final composition for geo-polymer concrete, 3 cylinder samples of regular concrete were established and tested for compressive strength to use them for comparison. The mix design of the regular concrete specimens that used for comparison was the same that established for all the experimental study (see table 3.10). The average compressive strength at 28 days was 35MPa.

3.6 Results and discussion

1. Effect of Super Plasticiser (SP) on the workability and the strength of the geopolymer concrete The relative slump and compressive strength of the geopolymer concrete with using sodium hydroxide solution (14 M concentration) with and without using SP are presented in Fig 3.11. As can be seen in this figure, relative slump of the geopolymer concrete mix composition S3 with using SP was significantly increased with respect to that of the mix composition S1 without using any SP, and it can be seen also that S2 and S4 have better degree of workability but they have different M concentration, while the compressive strength of the mix composition S3 with using SP has a reduction of 5.26% with respect to that of the mix composition S1without using any SP. The increase in relative slump was 42.85% for the mix composition S3 with using SP with reference to the mix composition S1 without using any SP.

It can be concluded that in the case of fly ash based geopolymer activated by NaOH solution (14.0 M concentration), SP are an effective additive resulted in 42.85% increase in relative slump without having any large negative effect on compressive strength with reference to the mix composition without using any SP.

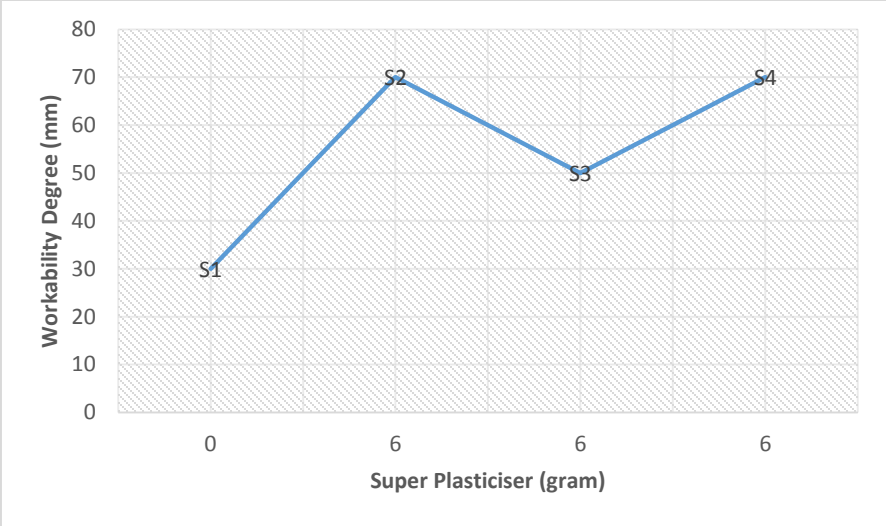

(Figure 3.11 . Effect of Super Plasticiser on the workability of the geopolymer concrete)

2. Effect of Sodium hydroxide solution concentration on the workability, setting time, and the strength of the geopolymer concrete.

The relative slump, compressive strength, and the setting time of the geopolymer concrete with using sodium hydroxide solution concentration 8M, 12M, and 14M with using SP are presented in Fig3.12a, b and c respectively. As can be seen in these figures, relative slump of the geopolymer concrete with NaOH concentration 8M, and 12M has no change, however, the relative slump of the geopolymer concrete with NaOH concentration 14M was decreased by 28.57% (from 70mm to 50mm). The initial setting time as well was decreased from 130min to 115min by increasing the concentration of sodium hydroxide solution from 8M to 14M, while the compressive strength was increased from 35MPa to 45MPa by increasing the concentration of sodium hydroxide solution from 8M to 14M.

It can be concluded that, workability, and the setting time will decrease by increasing the concentration of NaOH, while the compressive strength will increase by increasing the concentration of NaOH.

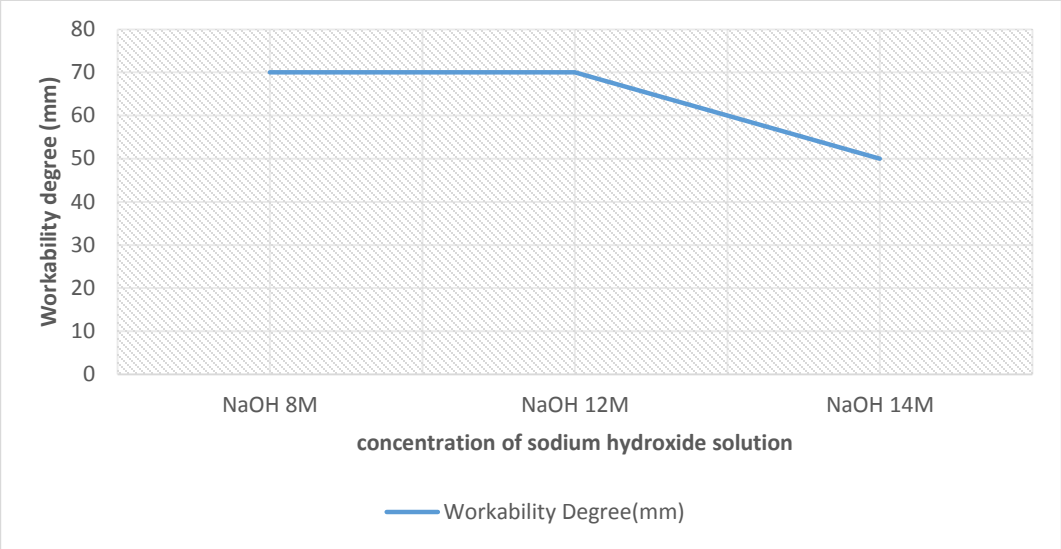

(Figure3.12a. Effect of Sodium hydroxide solution concentration on the workability of the geopolymer concrete)

mm

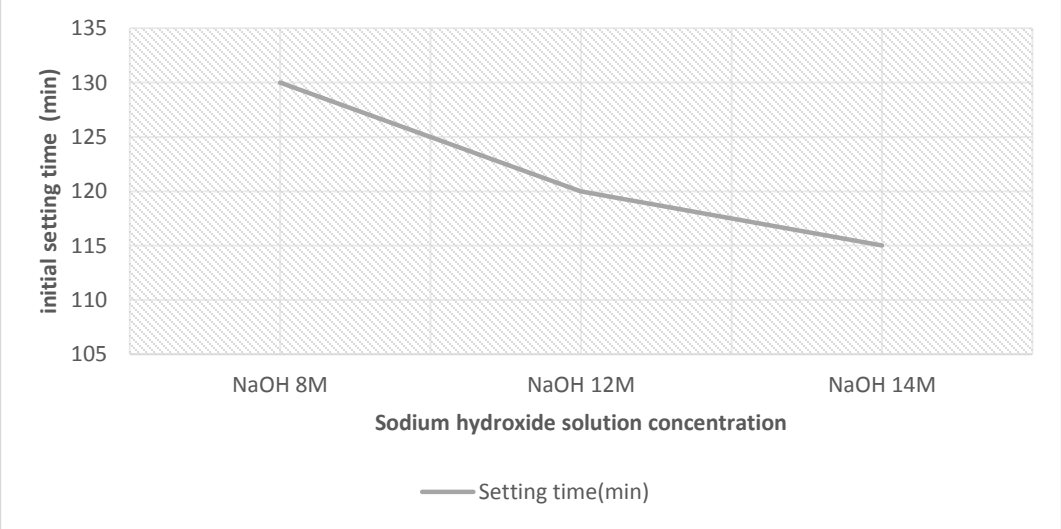

(Figure3.12b. Effect of Sodium hydroxide solution concentration on the initial setting time of the geo-polymer concrete)

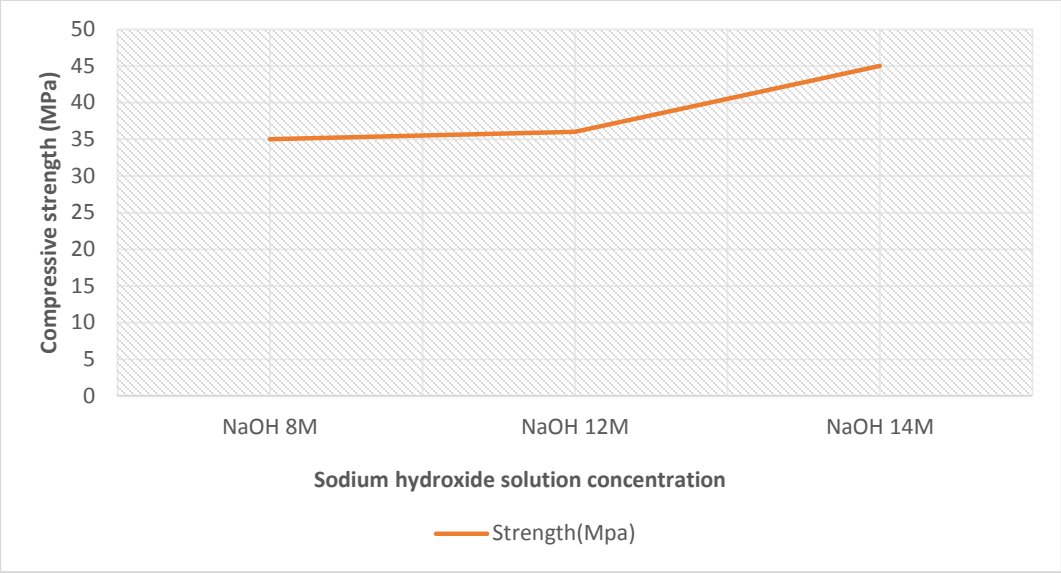

(Figure3.12c. Effect of Sodium hydroxide solution concentration on the strength of the geopolymer concrete)

3. Effect of the ratio of sodium silicate solution to sodium hydroxide solution on the workability and the strength of the geopolymer concrete.

The relative slump and compressive strength of the geopolymer concrete with using different ratio of sodium silicate solution to sodium hydroxide solution are presented in Fig 3.13a, and b respectively. As can be seen in these figures, relative slump of the geopolymer concrete and the compressive strength have no large change in term of changing sodium silicate solution to sodium hydroxide solution ratio. The benefit of using less sodium silicate is the cost. The cost of Na2SiO3 is more expensive than NaOH, so it should be noted that when the ratio of the sodium silicate solution to sodium hydroxide solution is decreased from 2.6 to 1, it is cost effective, and it has no large effect on the workability, and the strength of geopolymer concrete.

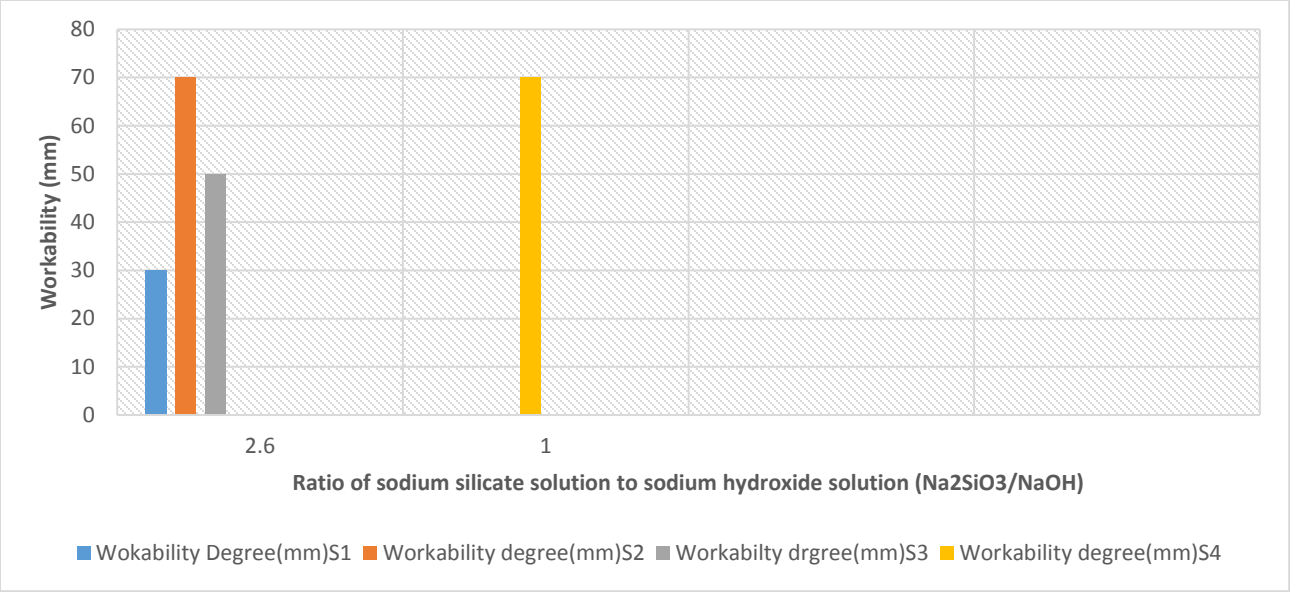

(Figure 3.13a Effect of the ratio of Sodium silicate solution to Sodium hydroxide solution on the workability of the geo-polymer concrete.)

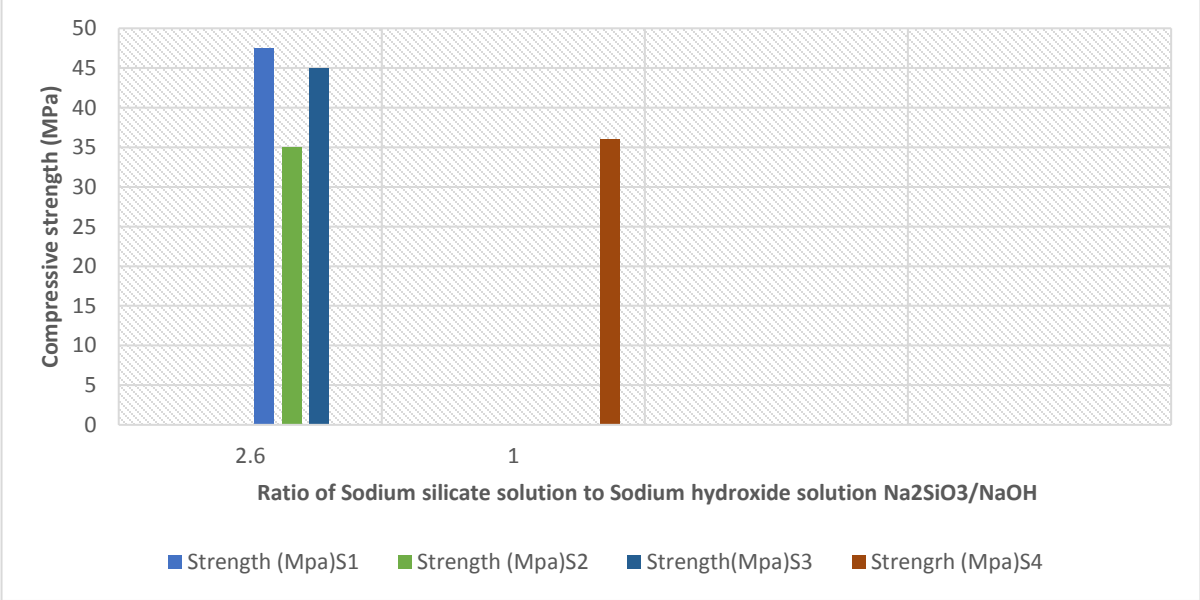

(Figure 3.13b Effect of the ratio of Sodium silicate solution to Sodium hydroxide solution on the strength of the geo-polymer concrete.)

As a result of the above discussion, S4 mix proportion was chosen to be the geo-polymer concrete composition that used in this research work as listed in Table 3.7. Many considerations have been taken for this choice. The workability, the strength, and the cost. The composition (S4) has medium workability (70mm). The strength of the composition (S4) was equal to (36Mpa), and the ratio of Sodium silicate solution to Sodium hydroxide solution equal 1, so it is more effective in term of cost since the cost of Na2SiO3 is more expensive than NaOH.

Table 3.7: Mix compositions of geo-polymer concrete

Mix sample Kg/m3	Fly ash Kg/m3	GGBS Kg/m3	Coarse agg. Kg/m3	Fine agg. Kg/m3	Na. Silicate Kg/m3	NaOH Kg/m3	S.P Kg/m3	Water Kg/m3
S4	340	60	1240	600	72	72(12M)	6	25

3.7 Concrete Mix Design

The ACI Standard Practice ACI 211.1-91 was used to determine the mix portion of this study. We require a mix with a mean 28-day compressive strength (measured on standard cylinders) of 35 MPa and a slump of 50 mm, ordinary Portland cement being used. The maximum size of well-shaped, angular aggregate is 20 mm, its bulk density is 1680 kg/m3, and its specific gravity is 2.7. The available fine aggregate has a fineness modulus of 2.40 and a specific gravity of 2.54. No air entrainment is required. For the sake of completeness, all steps, even when obvious, will be given.

Step 1: A slump of 50 mm is specified.

Step 2: The maximum size of aggregate of 20 mm is specified.

Step 3: From Table 3.8 for a slump of 50 mm and a maximum size of aggregate of 20 mm (or 19 mm), the water requirement is approximately 190 kg per cubic meter of concrete.

Step 4: From experience, the water/cement ratio was assumed as equal to 0.54 to result in concrete with a compressive strength, measured on cylinders, of 35 MPa. There are no special durability requirements.

Step 5: The cement content is 190/0.54 = 351 kg/m3.

Step 6: From Table 3.9, when used with a fine aggregate having a fineness modulus of 2.40, the bulk volume of oven-dry rodded coarse aggregate with a maximum size of 20 mm is 0.66. Given that the bulk density of the coarse aggregate is 1680 kg/m3, the mass of coarse aggregate is 0.66 × 1680 = 1109kg/m3.

Step 7: To calculate the mass of fine aggregate, we need first to calculate the volume of all the other ingredients. The required values are as follows:

Volume of water is 190/1000=0.190m3

Solid volume of cement, assuming usual specific gravity of 3.15, is 351/ (3.15×1000) =0.111m3

Solid volume of coarse aggregate is 1109/ (2.7× 1000) =0.41m3

Volume of entrapped air, given in table 3.5, is 0.02× 1000=0.020m3

Hence, total volume of all ingredients except fine aggregate =0.731m3

Therefore, the required volume of fine aggregate is 1- 0.731= 0.269m3

Hence, the mass of fine aggregate is 0.269× 2.54× 1000= 685kg/m3

From the various steps, we can list the estimated mass of each of the ingredients in kg/m3 of concrete as listed in table 3.10.

Table 3.8. Approximate Mixing Water and Air Content Requirements for Different Slumps and Nominal Maximum Sizes of Aggregates given in ACI 211.1-91

Slump, mm	*Water, kg/m³ of concrete for indicated nominal maximum sizes of aggregate*							
	9.5	*12.5*	*19*	*25*	*37.5*	*50*	*75*	*150*
Non-air-entrained concrete								
25 to 50	207	199	190	179	166	154	130	113
75 to 100	228	216	205	193	181	169	145	124
150 to 175	243	228	216	202	190	178	160	—
Amount of entrapped air, per cent	3	2.5	2	1.5	1	0.5	0.3	0.2
Air-entrained concrete								
25 to 50	181	175	168	160	150	142	122	107
75 to 100	202	193	184	175	165	157	133	119
150 to 175	216	205	197	184	174	166	154	—
Total air content, (per cent) for:								
Improvement of workability	4.5	4.0	3.5	3.0	2.5	2.0	1.5	1.0
Moderate exposure	6.0	5.5	5.0	4.5	4.5	4.0	3.5	3.0
Extreme exposure	7.5	7.0	6.0	6.0	5.5	5.0	4.5	4.0

Table 3.9. Bulk Volume of Coarse Aggregate per Unit Volume of Concrete

Maximum size of aggregate		*Bulk volume of oven-dry rodded coarse aggregate per unit volume of concrete for fineness modulus of fine aggregate of:*			
mm	*in.*	*2.40*	*2.60*	*2.80*	*3.00*
9.5	$\frac{3}{8}$	0.50	0.48	0.46	0.44
12.5	$\frac{1}{2}$	0.59	0.57	0.55	0.53
20	$\frac{3}{4}$	0.66	0.64	0.62	0.60
25	1	0.71	0.69	0.67	0.65
37.5	$1\frac{1}{2}$	0.75	0.73	0.71	0.69
50	2	0.78	0.76	0.74	0.72
75	3	0.82	0.80	0.78	0.76
150	6	0.87	0.85	0.83	0.81

Table 3.10: Mix compositions of regular concrete

Concrete Material	Quantity (Kg/m3)
Cement	351
Coarse Aggregate	1109
Fine Aggregate	685
Water	190

3.8 Concrete Mixing Procedures

A 6 cubic foot heavy duty concrete mixer was used to produce concrete, as shown in Figure 3.14. All concrete compositions were measured by weight by using a digital balance (Figure3.15).

All dry constituents were mixed for one minute before water was added and mixed for three more minutes to provide a homogeneous concrete mix. The composition ratio of the overall concrete mix was 1: 3.2: 1.95: 0.54 (cement: coarse aggregate: fine aggregate: water) respectively.

Figure 3.14: Heavy duty concrete mixer.

Figure 3.15: All concrete compositions

All the specimens were casted from the same batch, and cured for 28-days in a water tank (Figure 3.16).

Figure 3.16: the specimens in the water tank

3.9 Concrete Slump Test

The slump test was as described before for geo-polymer concrete (see 3.4.2) .The slump value for regular concrete as seen in figures 3.17 a, b.

Figure 3.17a: Slump test cone filled out by concrete

Figure 3.17b: measure the slump value

3.9 Geo-polymer Concrete Mixing Procedures

The same 6 cubic foot heavy duty concrete mixer that was used to produce concrete was used for geo-polymer concrete. All geo-polymer compositions were measured by weight by using a digital balance.

Fly ash, Granulated Ground Blast Furnace slag (GGBS) and the aggregates were first mixed together for about 3 minutes. The sodium silicate solution and the sodium hydroxide solution were mixed together one day prior to use to prepare the alkaline liquid. On the casting day of the specimens, the alkaline liquid was mixed together with the super plasticizer and the extra water to prepare the liquid component of the mixture. The liquid component of the mixture was then added to the dry materials and the mixing continued for further about 4 minutes to manufacture the fresh geopolymer concrete.

3.10 Description of Test Specimens

16″, 4.3″, 4.1″ (length, width, and height) respectively, rectangular beam molds, (see Figure 3.18a) has been used for beam specimens, and 3″ diameter with 6″ height cylindrical molds were used to produce column specimens (figure 3.18b). The dimensions of the beam molds were selected according to the ASTM standard C293-8 for flexural strength concrete using simple beam with center-point loading, whereas the effective span length was three times of the beam depth and the distance from the center of the support to the beam edge was 2″ each side. The cylindrical column molds has been used according to ASTM C39-08 for compressive strength of cylindrical specimen. Plastic molds were used with height equals two times of the diameter.

Figure 3.18a: rectangular beam molds

Figure 3.18b: cylindrical Molds

3.11 Environmental Conditioning

In the mechanical properties of regular concrete and geopolymer concrete, temperature and humidity play an important role. The following procedures were carried out to investigate the effects of hot weather and hygrothermal aging on the mechanical properties of the geo-polymer based on fly ash. After curing, the aim specimens of samples was submitted to accelerated aging conditions throughout expose them to the temperature and humidity sources for certain period of time before tested.

3.11.1 Temperature

The influence of temperature on regular concrete and geo-polymer concrete was a most important part of this research. In addition to room temperature, specimens have been exposed to four different temperatures (25$_o$C, 100$_o$C) with 100% humidity, and (45$_o$C, 70$_o$C) with 0% humidity. Two furnaces with a maximum heat power range of 400$_o$C, (figure 3.19), and one environmental chamber with a maximum temperature of 200$_o$C, (see figure 3.20), have been used for this purpose.

Figure 3.19: Laboratory furnaces (, model #21-350)

3.11.2 Relative Humidity

Another factor that has been investigated in this research is relative humidity. For this experimental work, two levels of relative humidity were performed. Such relative humidities are 0.0% and 100%. The two furnaces were used at 0 percent humidity for all conditioned specimens, while the environmental chamber was used for the humidity tests of 100 percent.

Figure 3.20: Temperature/Humidity environmental chamber

3.12 Age Accelerating

To evaluate the durability performance of the geo-polymer concrete, the environment factors that have been considered in this test program are number of thermal cycles, cycle length, exposure time, and media type including various degrees of humidity and dry air.

In this study, flexural strength and compression strength tests were carried out to evaluate the deterioration after 0, 40, 100, 250, 625, and 1250 cycles. The cycle period was 2hrs.

The temperature and humidity regime cycles for 2 hrs for 100oC of temperatures are shown in figures (3.21). This was for 100% humidity condition. The 0% humidity condition was done by using two different temperatures ((45oC, and 70oC) with the same duration of the cycles (40, 100, 250, 625, and 1250 cycles).

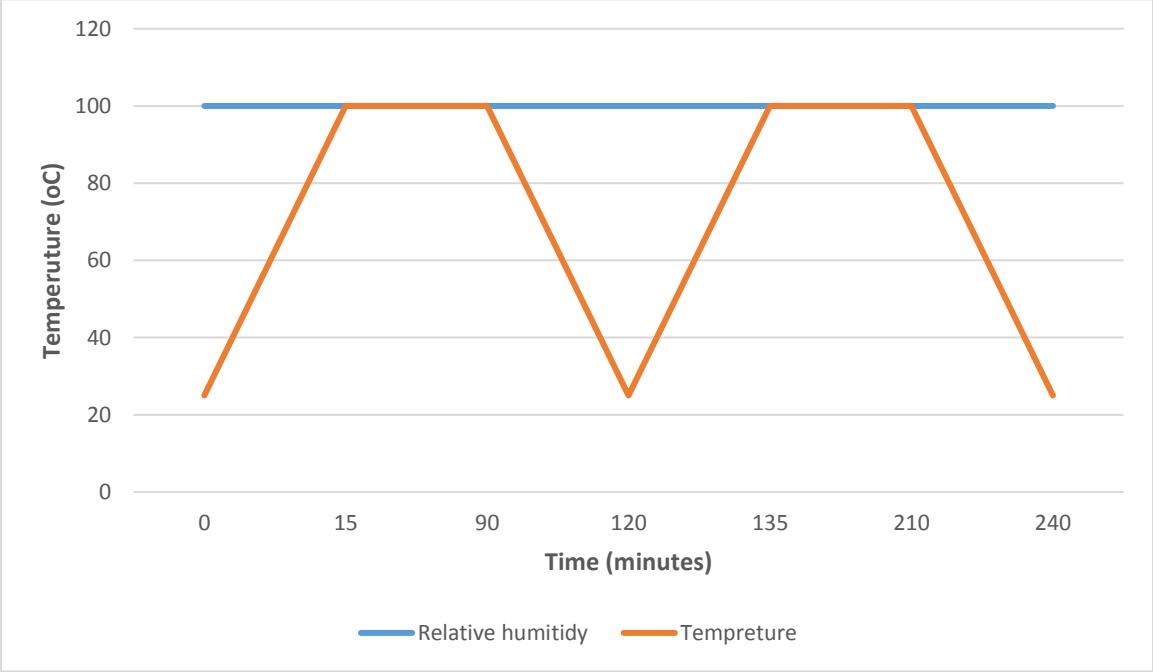

Figure 3.21: Temperature and humidity regime cycles (2 hrs-cycles)

3.13 Mechanical Test Procedures

Two different mechanical tests have been carried out in this experimental program, flexural strength test and compressive strength test. All plain concrete beams, and geo-polymer concrete beams have been subjected to flexural strength testing. While all concrete columns and geo-polymer concrete columns were subjected to compressive strength testing.

3.13.1 Flexural Strength Test Procedures

The 16″x4.3″x4.1″ concrete beams were simply supported over a 12 ″ span and loaded at the middle of the span according to ASTM C293. The load was applied monotonically under displacement control at a constant rate of 0.003 mm/sec. The load and displacement data were recorded every 0.8 sec up to the test specimen failure.

Figure 3.22 shows the MTS-810 testing machine which was used for all flexural strength tests. All tests were done at laboratory temperature and humidity (74oF and 25%) respectively.

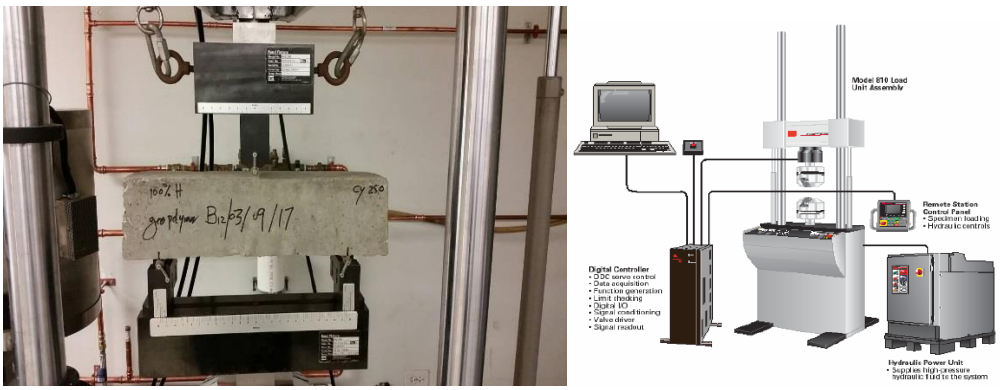

Figure 3.22: MTS-810 material test system

3.13.2 Compressive Strength Test Procedure

Cylindrical samples of 3″ diameter and 6″ height were loaded axially according to ASTM (C39-2008) until failure (see figure. 3.23). MTS-810 testing machine was used. The test had been done at laboratory temperature and humidity (74oF and 25%) respectively.

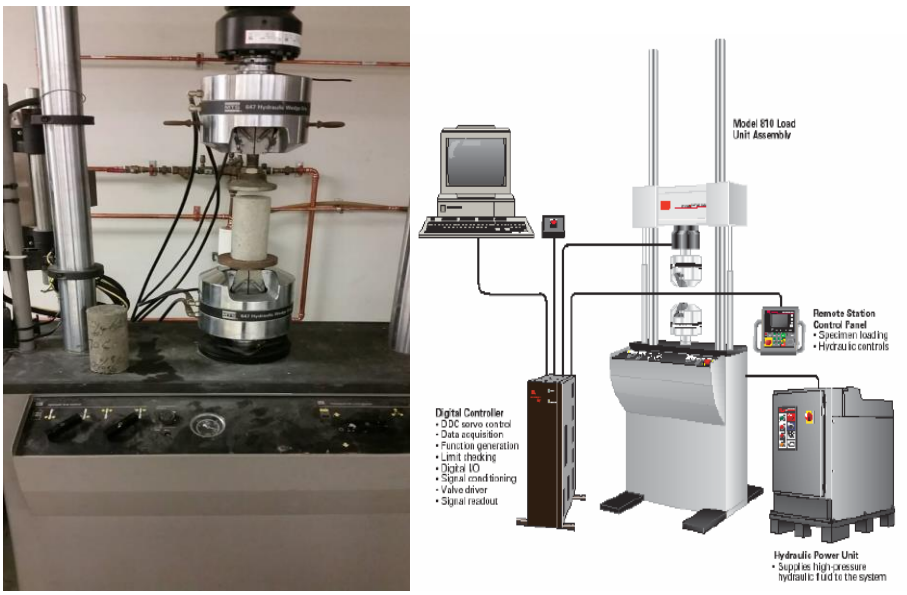

Figure 3.23: MTS -290 material test system

CHAPTER 4 EXPERIMENTAL RESULTS AND DISCUSSIONS

4.1 Introduction

In this chapter, all the results of the experimental work have been discussed (Total of 126 specimens). 60 specimens were geo-polymer concrete (15 specimens were geo-polymer concrete beams, and 45 specimens were geo-polymer concrete columns). 66 specimens were regular concrete beams, and columns (18 specimens were concrete beams, and 48 specimens were concrete columns).

4.2 Experimental Results and Discussions for Regular Concrete Specimens

To make this study comprehensive, the influence of temperature (T), relative humidity (RH), number of cycles (Cy), and the cycle period (Cp) on the compressive and flexural strength of concrete were of significant interest in this research. 48 plain concrete beams, (Figure 4.1) and 48 cylindrical plain concrete column specimens, (Figure 4.2) were implemented and tested after subjected to diverse environmental conditions.

Figure 4.1: Concrete beam specimens

Figure 4.2: Cylindrical concrete column specimens

4.2.1 Experimental Results for regular Concrete Beams (100% relative humidity)

Three plain concrete beams B1, B10, B15 have been utilized as the control beam. These beams were tested for flexural strength using three-point loading according to ASTM C293-08 after 28 days in water. As shown in table 4.1, the average maximum flexural load of these three specimens was 3051.1lbs. The type of failure of these three beams was flexural failure.

The relationship curves between flexural load and deflection of these specimens are shown in figure 4.3.

Table 4.1: Flexural strength test results of control beam specimens

Beam #.	Max deflection (in)	Max. load (lbs)	Mean (lbs)	Max. flexural strength (psi)	Stiffness (lbs/in)	Failure mode
B1	0.0261	2996.5	3051.1	844.08	100382	FLEXTURE
B10	0.0272	3050.4		859.26	102188	FLEXTURE
B15	0.0276	3106.4		875.04	101064	FLEXTURE

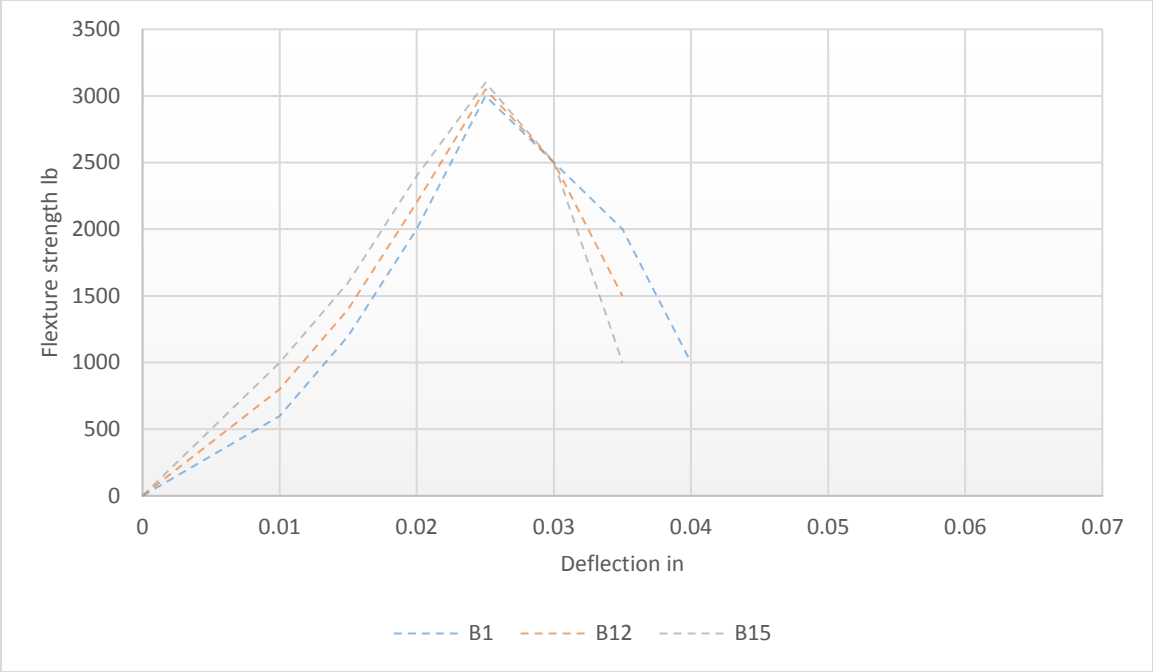

Figure 4.3: Control-concrete beams, flexural load- deflection results

To study the effect of hygrothermal condition on concrete flexural strength, 15 plain concrete beams have been subjected to 100% relative humidity, number of cycles, and cycle periods. Table 4.2 shows the average results of the specimens. Figure 4.4 shows Concrete beam specimen.

Table 4.2: Flexural strength test results of concrete beam specimens at 100% relative humidity

Temp. *oC*	Cy	CP (*Hr*)	Max deflection (in)	Mean (lbs)	Max. flexural strength (psi)	Failure mode	Strength Comparing with control beam	Deflection comparing with control beam	Stiffness (lbs/in)
25-100	40	2	0.0273	3061	862.25	FLEXTURE	0.32% increase	1.1% increase	112124.54
	100		0.0347	4020	1132.39	FLEXTURE	31.75% increase	28.5% increase	115850.14
	250		0.0341	4350	1225.35	FLEXTURE	42.57% increase	26.3% increase	127565
	625		0.040	3810	1073.23	FLEXTURE	24.87% increase	48.1% increase	95250
	1250		0.0271	1940	546.47	FLEXTURE	36.4% decrease	0.37% increase	71587

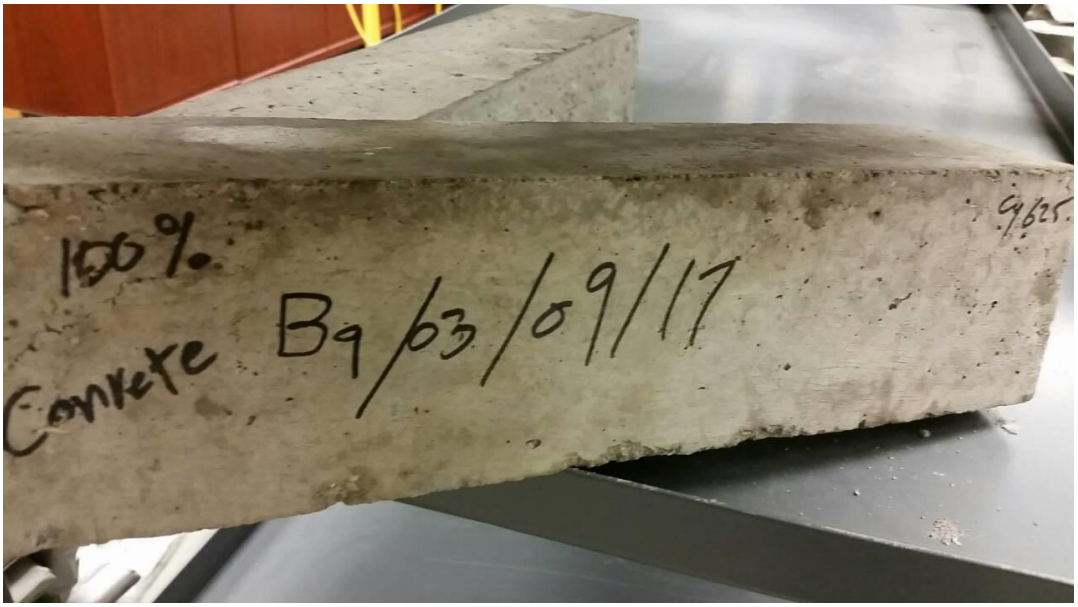

Figure 4.4: Concrete beam specimen

All the above 15 specimens failed due to flexural crack at the center of the beam, Figure 4.5 shows the mode of failure for one of these beams.

Figure 4.5: Flexural failure of concrete beam-100% relative humidity

The relationship curve between flexural load and deflection of the average of regular concrete beam specimens are shown in figure 4.6.

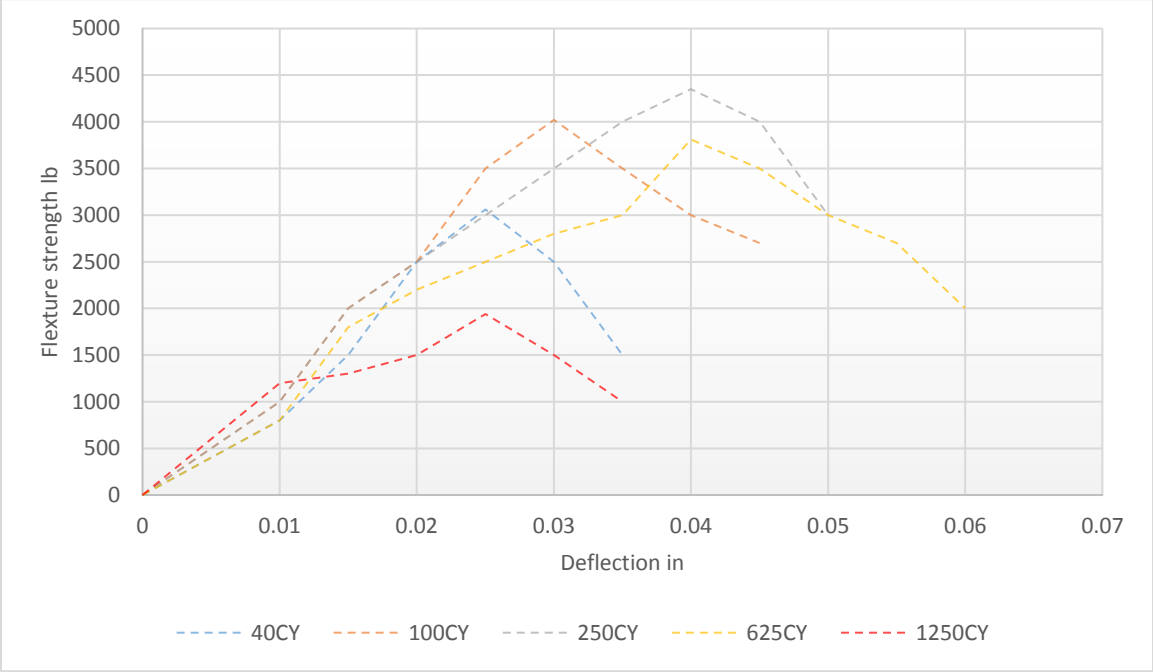

Figure 4.6: Concrete beams, flexural load - deflection results

The above results showed that the flexural strength of concrete beams increased due to subjecting to 100% relative humidity with temperature changing from 25^{o}C *to 100* ^{o}C, the magnitudes of flexural strength increases varied with the number of cycles. The strength was the highest after 250 cycles, comparing to 100 cycles, and 40 cycles, then the strength was reduced after 625 cycles. This can be due to the change of the chemical and the physical properties of the plain concrete (Naus 2005). The increase of temperature will increase the hydration process of the Portland cement and the chemical reaction will fast in certain point. The modules of elasticity (stiffness) will increase by increasing the temperature cycle, and because of the humidity, concrete members will still keep some moisture and the strength will keep increasing in certain point (from 40cy into 250cy). Then because of the duration of exposing time of the temperature, the

properties of plain concrete will start lose some of its advantages. The modules of elasticity will start decreasing and the strength as well (625cy into 1250cy).

Figures 4.7 and 4.8 shows the relationship between the temperature with the ultimate strength, and the temperature with modules of elasticity respectively (Naus 2005). Figures 4.9a and 4.9b shows the relationship between the flexure load with number of cycle temperature, and the relationship between the deflection with number of cycle temperature respectively. Figure 4.10 shows the relationship between the stiffness and number of cycle temperature comparing with control specimens.

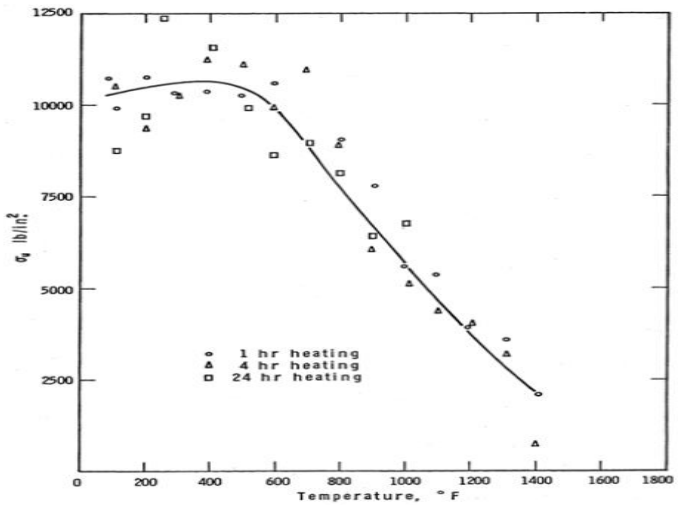

Figure 4.7: Ultimate strength of hydrated Portland cement at elevated temperature (Naus 2005).

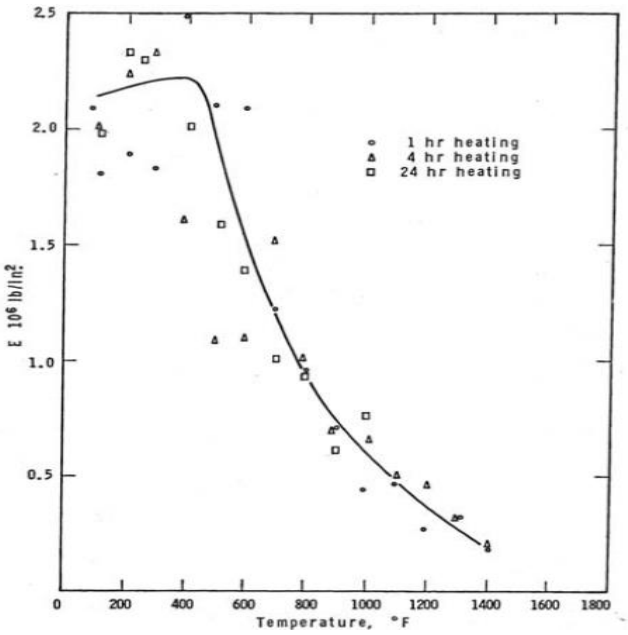

Figure 4.8 Modulus of elasticity of hydrated Portland cement at elevated temperature (Naus 2005).

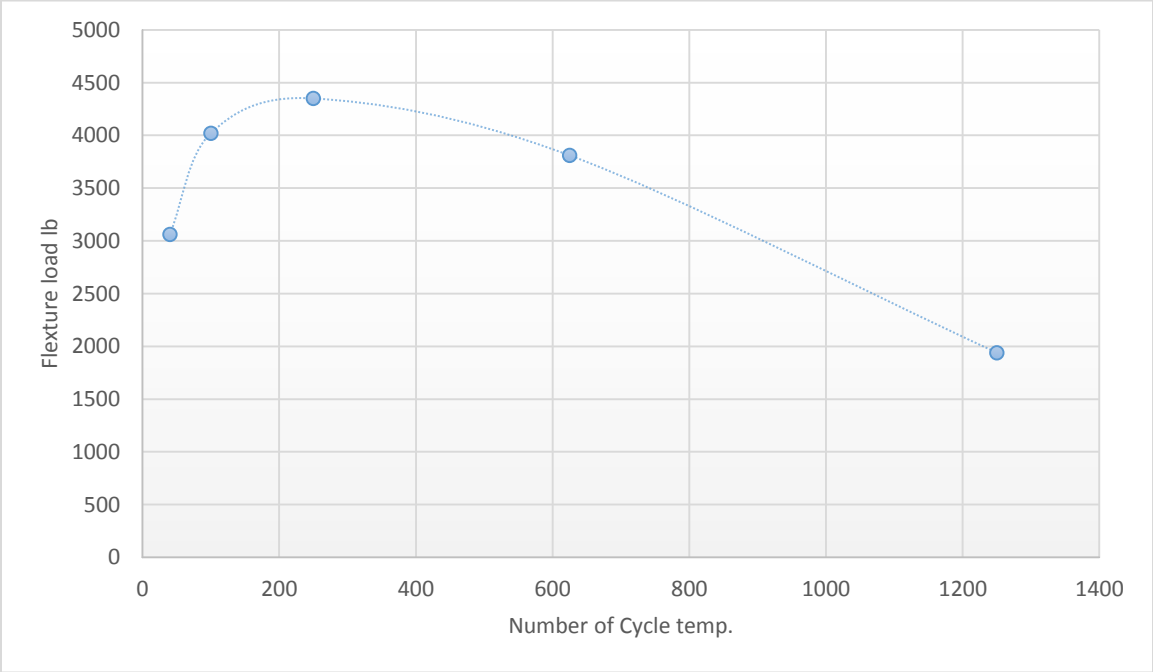

Figure 4.9a: Concrete beams, max flexural load results vs number of cycles

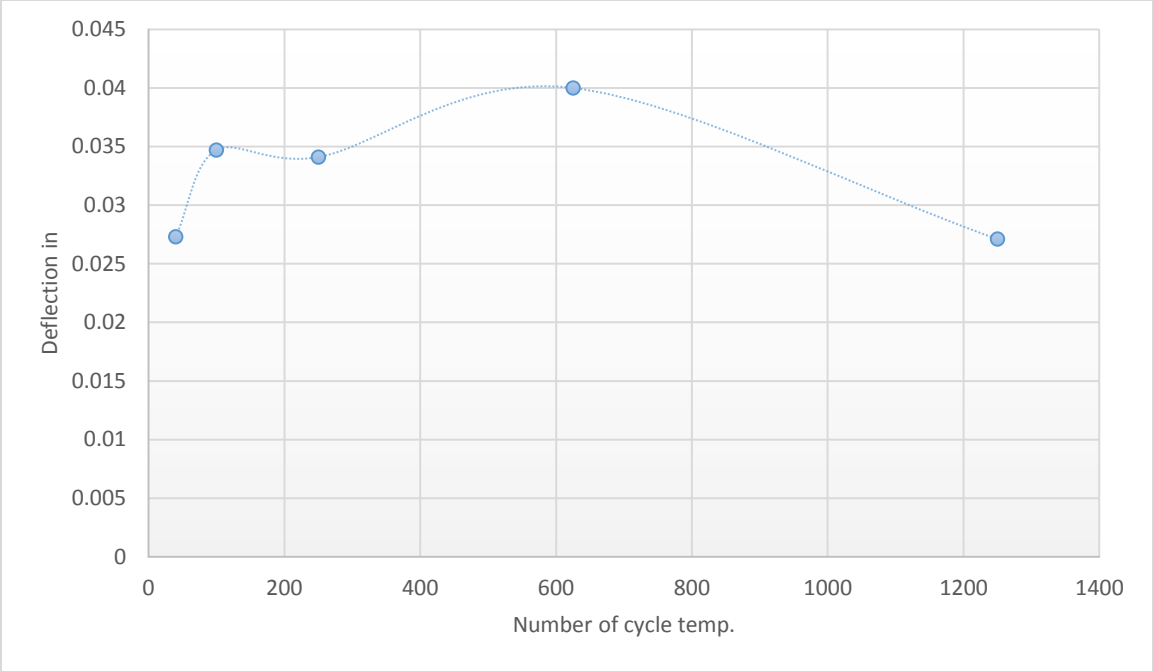

Figure 4.9b: Concrete beams, max deflection results vs number of cycles

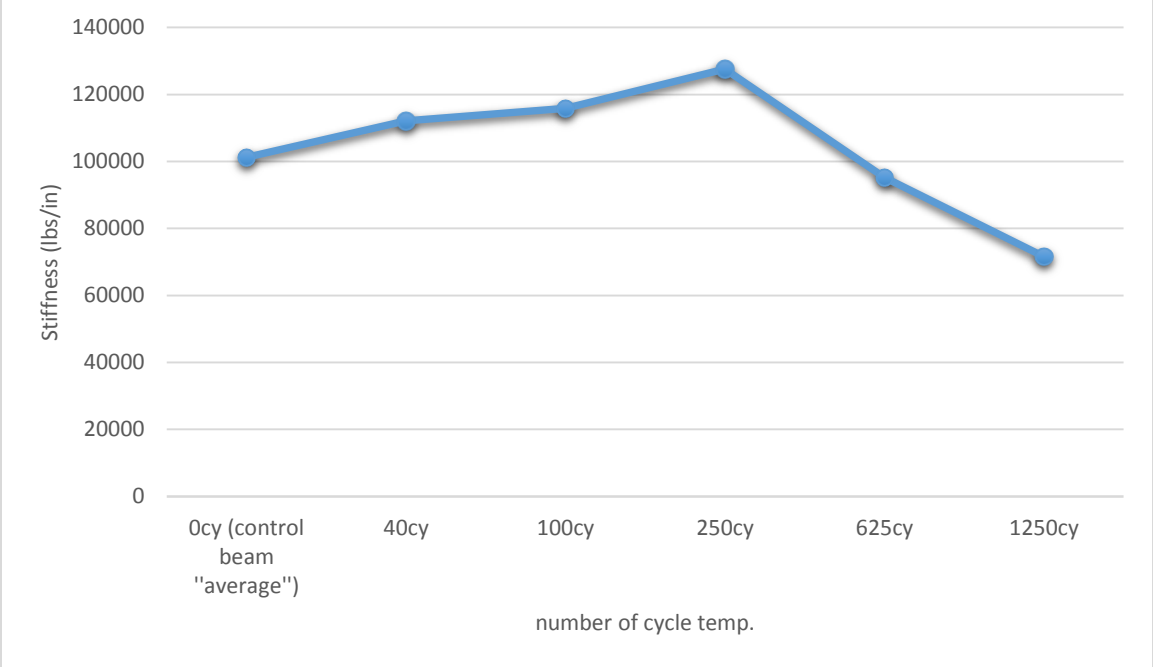

4.10: Relationship between the stiffness and number of cycle temperature comparing with control specimens.

4.2.2 Experimental Results for regular Concrete Columns (100% relative humidity)

Three plain concrete columns C1, C12 and C15 have been randomly selected and utilized as control. They were tested after 28 days of curing in water. All columns were tested for compressive strength according to ASTM C78-08, Figure (4.11). The mode of failure was concrete compression failure, (see figure 4.12). Table 4.3 shows the deflection at maximum load, maximum compressive load, maximum compressive strength, stiffness, and the mode of failure of these three control specimens, where, the average maximum compressive strength of three specimens was 5067.63 psi, (35.0Mpa).

Figure 4.11: Compressive strength test "control specimen"

Table 4.3: Compressive strength test results for control specimens (28 days)

Column #.	Max deflection (in)	Max. load (lbs)	Mean (lbs)	Max. compr. strength (psi)	Stiffness (lbs/in)	Failure Mode
C1	0.0481	37418	35800.66	5296.25	777920	compression failure
C12	0.0502	34602.2		4897.70	689287	compression failure
C15	0.0494	35381.8		5008.04	716231	compression failure

Figure 4.12: Concrete compression failure of Control specimen

Figure 4.13 represents the relationship between compressive load and deflection of three control column specimens. The figure shows that the deflection at maximum load for all specimens is closed to each other.

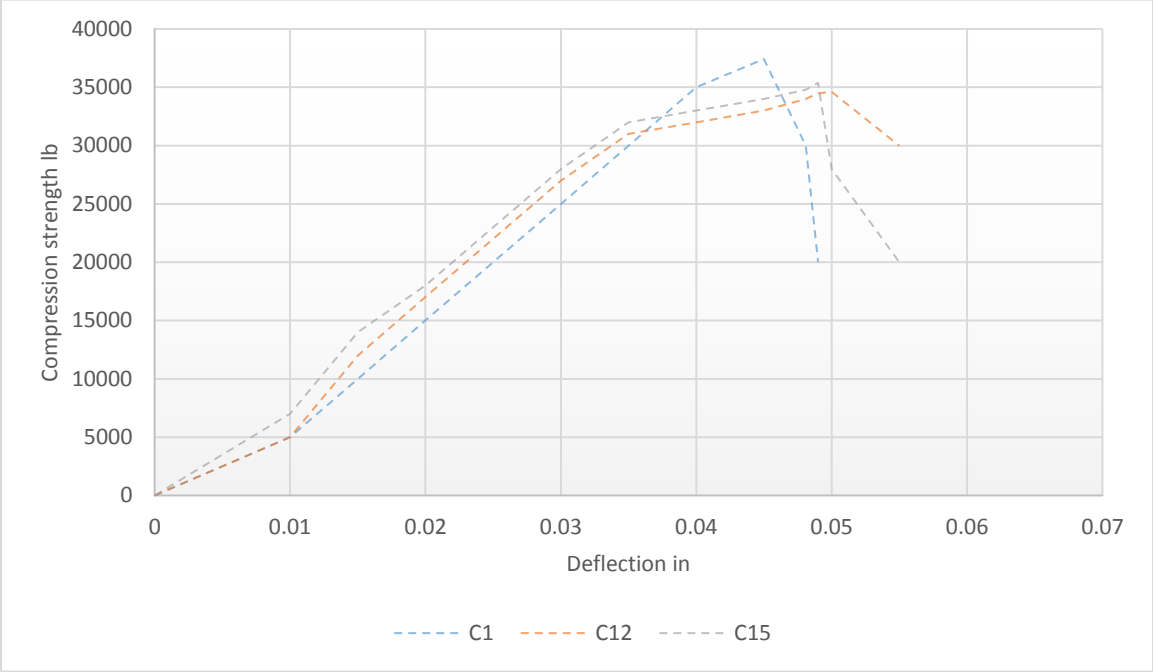

Figure 4.13: Compressive load- deflection results – "control specimens"

15 plain concrete columns have been subjected to 100% relative humidity, number of cycles, and cycle periods. Table 4.4 shows the average results of the specimens. Figure 4.14 shows Concrete column compressive strength test.

Table 4.4: Compressive strength test results of concrete column specimens

Temp. *oC*	Cy	CP (*Hr*)	Max deflection (in)	Mean (lbs)	Max. Compr. strength (psi)	Failure mode	Strength Comparing with control column	Deflection comparing with control column	Stiffness (lbs/in)
25-100	40	2	0.050	35925.5	5085	Compression	0.34% increase	2% increase	718510
	100		0.0521	47180	6678	Compression	32% increase	6.3% increase	905566
	250		0.051	51044.6	7225	Compression	43% increase	4.1% increase	1000875
	625		0.0481	44708	6328.1	Compression	25% increase	18% decrease	931416
	1250		0.037	22763.4	3222	Compression	36% decrease	24.5% decrease	615227

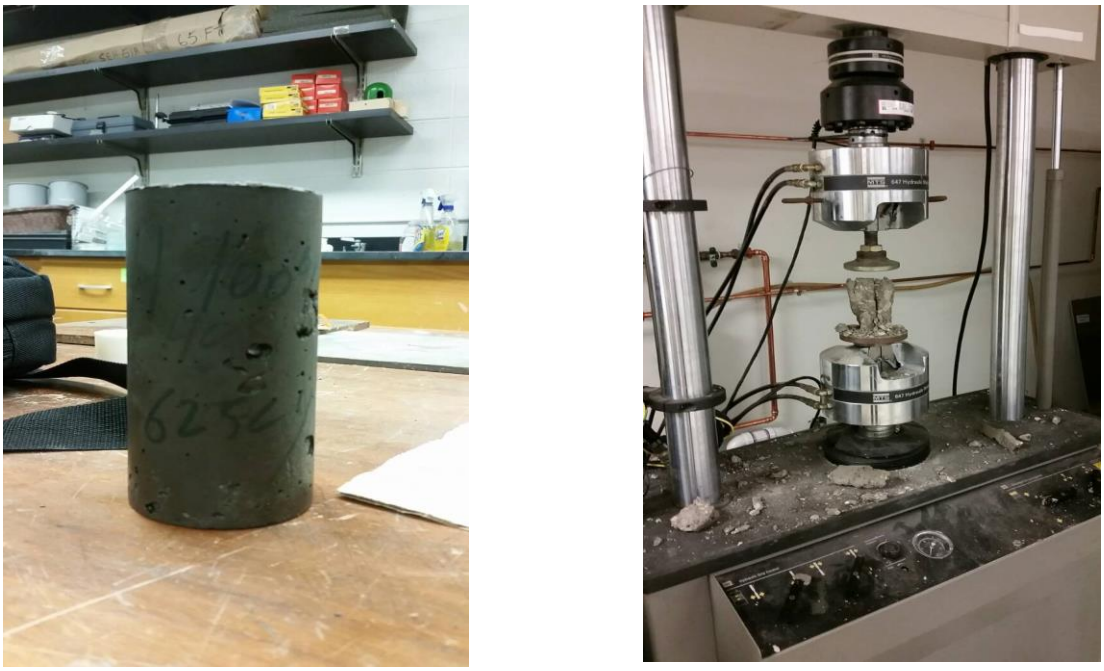

Figure 4.14: Compressive strength test

The relationship curves between compression load and deflection of the average specimens are shown in figure 4.15.

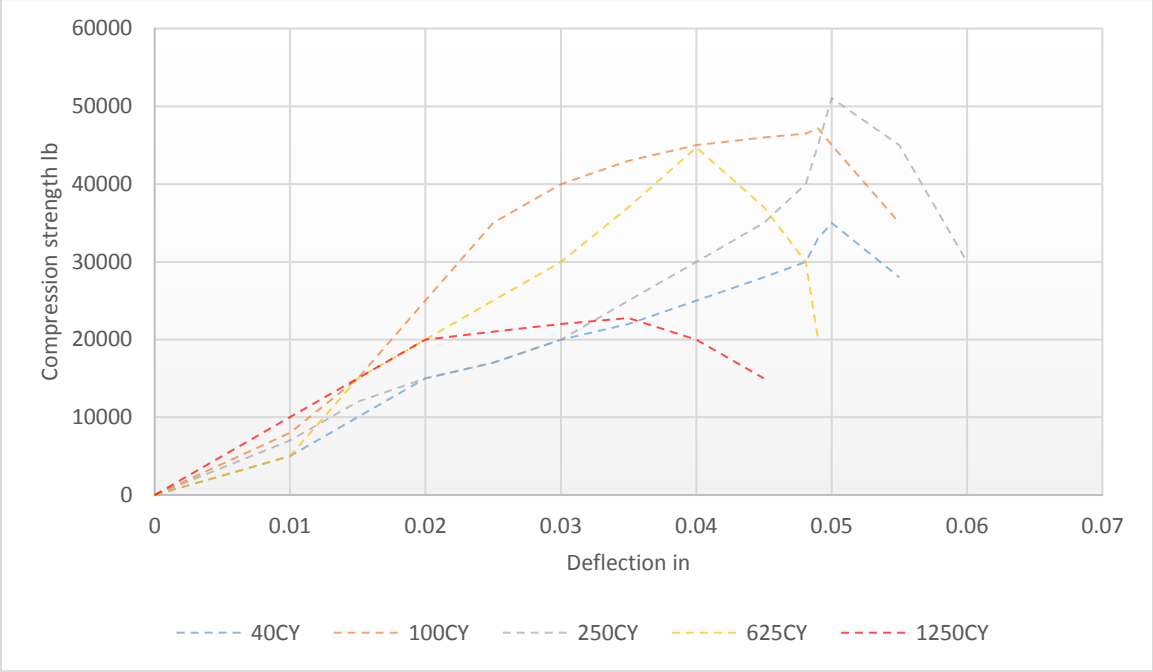

Figure 4.15: Concrete columns, compression load –deflection results

Figures 4.16a and 4.16b illustrate the relationship between the maximum compressive load and maximum deflection results vs. number of cycles respectively. Figure 4.17 shows the relationship between the stiffness and number of cycle temperature comparing with control specimens. The figures showed similar results to the beam specimens.

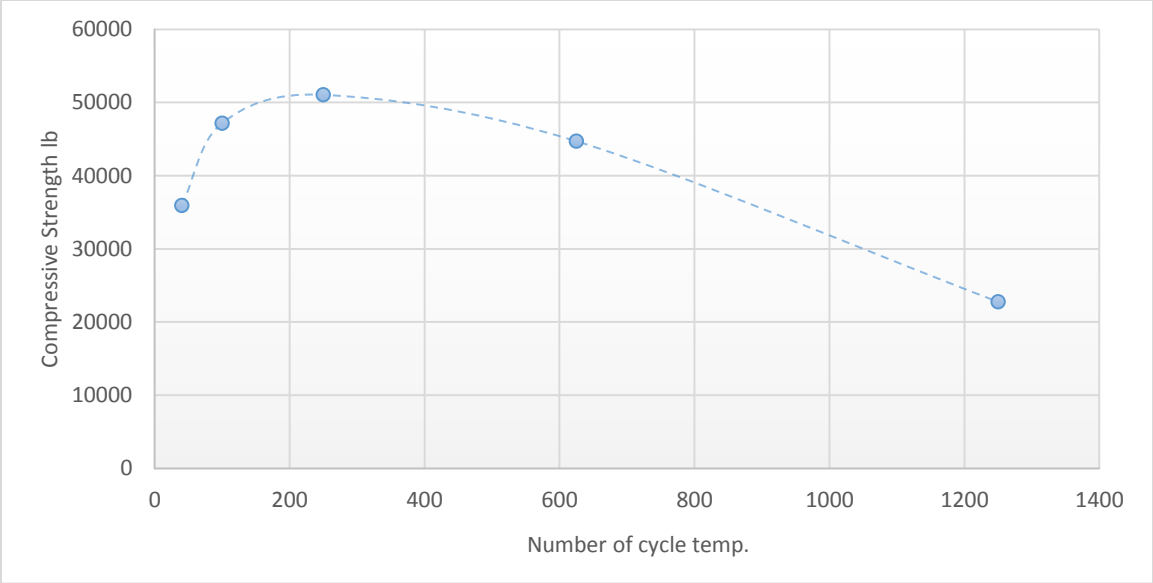

Figure 4.16a: Concrete columns, max compressive load vs number of cycle

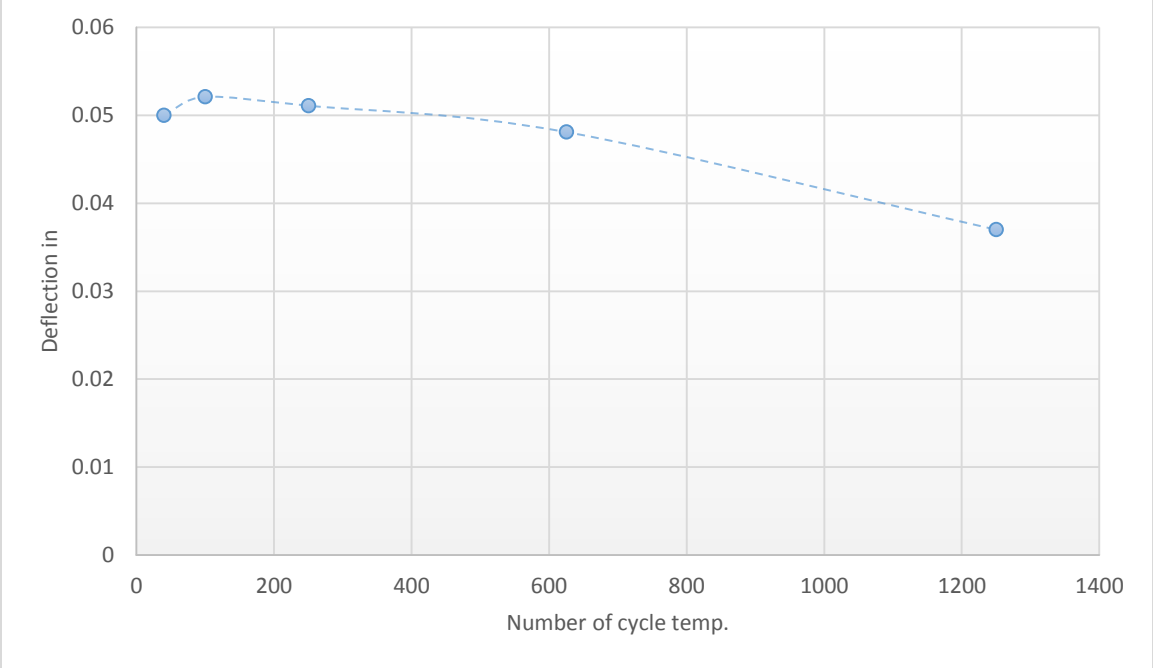

Figure 4.16b: Concrete columns, max deflection vs number of cycle

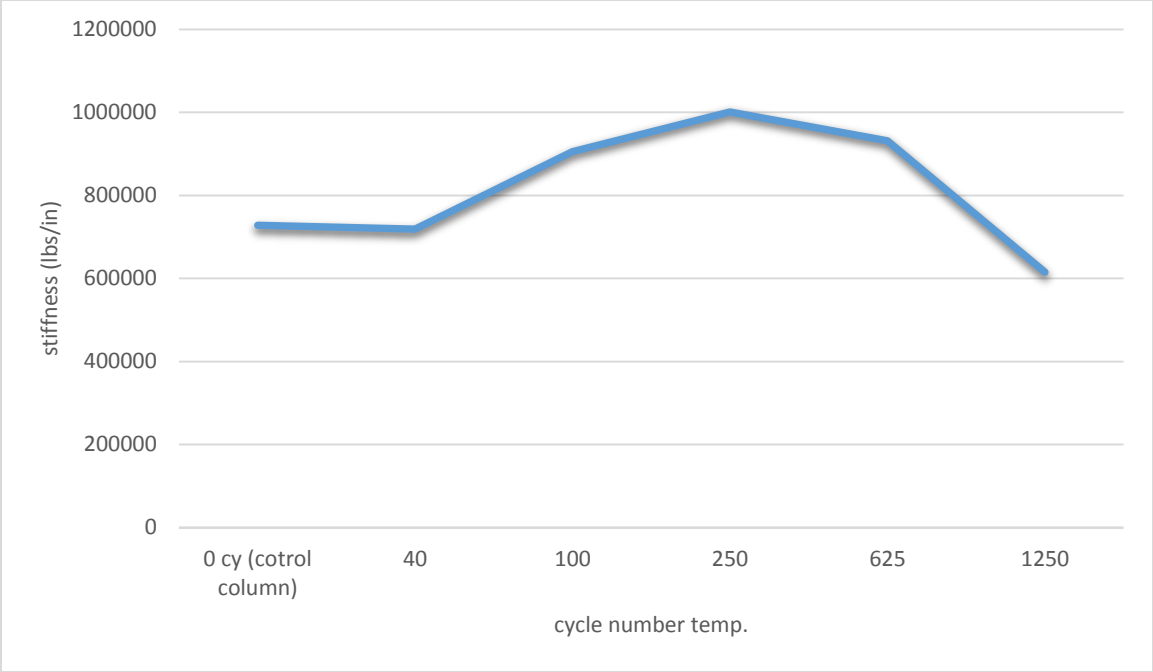

Figure 4.17: relationship between the stiffness and number of cycle temperature

The above results showed almost the same results of concrete beams. The strength increased due to subjecting to 100% relative humidity with temperature changing from 25^{o}C *to 100* ^{o}C, the magnitudes of compressive strength increases varied with the number of cycles. The strength was the highest after 250 cycles, comparing to 100 cycles, and 40 cycles, then the strength was reduced after 625 cycles.

This is also due to the change of the chemical and the physical properties of regular concrete as has been explained before in the concrete beams.

4.3 Experimental Results and Discussions for Geo-polymer Concrete Specimens

15 geo-polymer concrete beams, and 45 cylindrical geo-polymer concrete column specimens, were implemented and tested after subjected to diverse environmental conditions as well as the regular concrete specimens.

4.3.1 Experimental Results for geo-polymer Concrete Beams (100% relative humidity)

To study the effect of hygro-thermal condition on geo-polymer concrete flexural strength, 15 geo-polymer concrete beams have been subjected to 100% relative humidity, number of cycles, and cycle period. Table 4.5 shows the average results of the geo-polymer concrete beams. Figure 4.18a shows flexural load test.

Table 4.5: Flexural strength test results of geo-polymer concrete beam specimens at 100% relative humidity

Temp. *oC*	Cy	CP (*Hr*)	Max deflection (in)	Mean (lbs)	Max. flexural strength (psi)	Failure mode	Strength Comparing with control beam	Deflection comparing with control beam	Stiffness (lbs/in)
25-100	40	2	0.0263	3100	873.23	FLEXTURE	1.6% increase	2.5% decrease	117870.7
	100		0.0319	4150	1169.01	FLEXTURE	36% increase	18% increase	130094
	250		0.0356	4520	1273.23	FLEXTURE	48.14% increase	31.8% increase	126966
	625		0.0440	3708	1044.50	FLEXTURE	21.52% increase	63% increase	84273
	1250		0.0268	2021	569.29	FLEXTURE	33.76% decrease	0.74 decrease	75410

Figure 4.18a: geo-polymer Concrete beam subjected to flexural load test

All the above 15 specimens failed due to flexural crack at the center of the beam, Figure 4.18b shows the mode of failure for one of these beams.

Figure 4.18b: Flexural failure of geopolymer concrete beam-100% relative humidity

Figure 4.19 shows the relationship between flexural load and deflection of the average specimens.

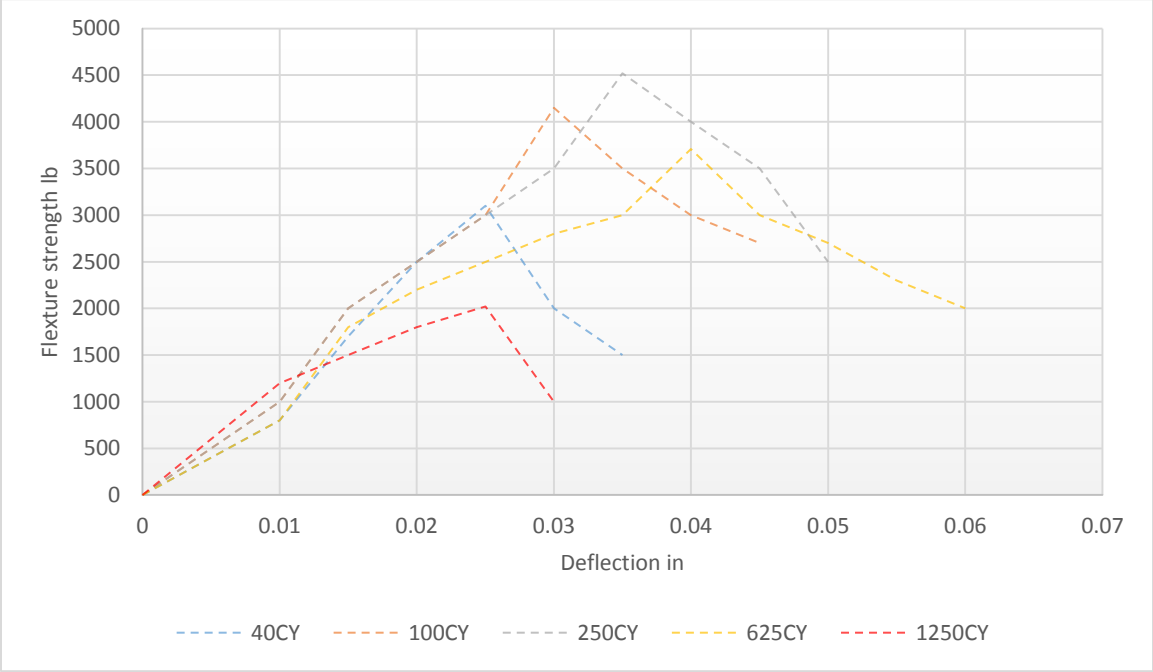

Figure 4.19: geo-polymer Concrete beams, flexural load – deflection results

The above results showed that the flexural strength of geo-polymer concrete beams increased due to subjecting to 100% relative humidity with temperature changing from 25^{o}C *to 100* ^{o}C, the magnitudes of flexural strength increases varied with the number of cycles. The strength was the highest after 250 cycles, comparing to 100 cycles, and 40 cycles, then the strength was reduced after 625 cycles. The increase in the geo-polymer concrete is slightly larger than the increase in the regular concrete case.

The explanation of this behavior is that the polymerisation process is generally accelerated in the higher temperature than in the normal temperature (Krishnaraja, Sathishkumar, Kumar, P. Kumar 2014). Geo-polymer concrete produced in hygro-thermal condition achieves lower strength in the early days as compared to the late days. The flexural strength increases as the age of geo-polymer

concrete increases from 40cycles to 250 because of the appropriate temperature at first days accelerate the Geopolymerisation process then the other days with moderate temperature lead to continuous Geopolymerisation with homogenous structure and less porosity that effect positively on strength (Davidovits, 2011), and also because of the humidity, most of the water did not released during the chemical reaction which induced drying shrinkage is low, and the stiffness is high. Figures 4.20 and 4.21 represents the maximum flexure, maximum deflections vs. number of cycles respectively.

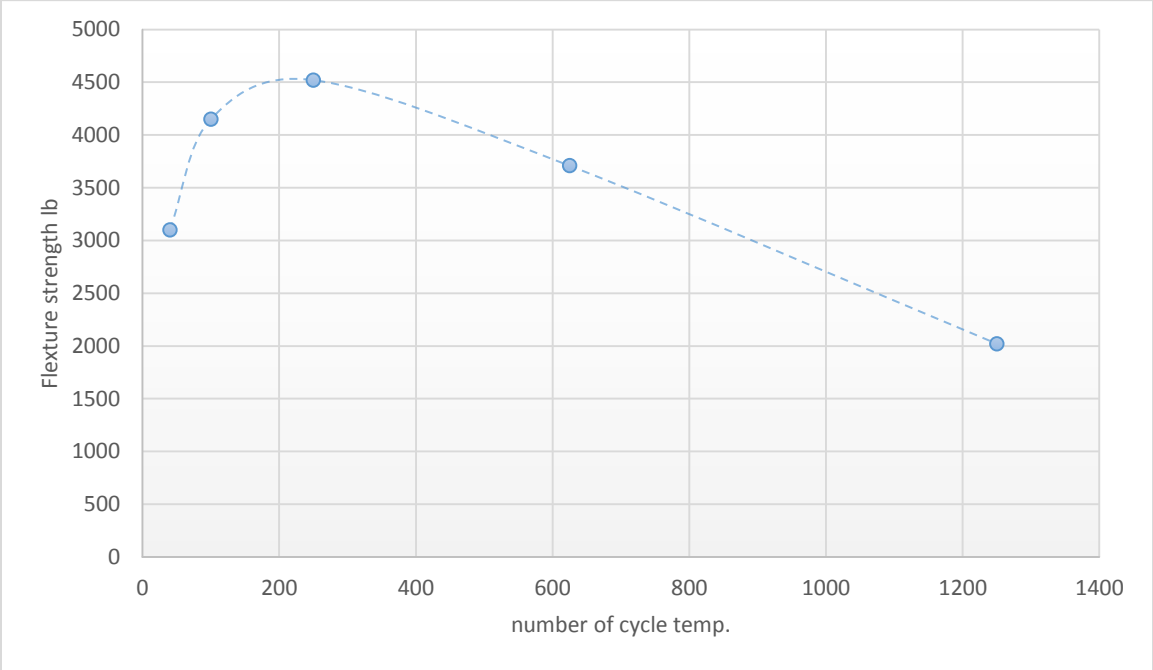

Figure 4.20: the maximum flexure vs. number of cycles.

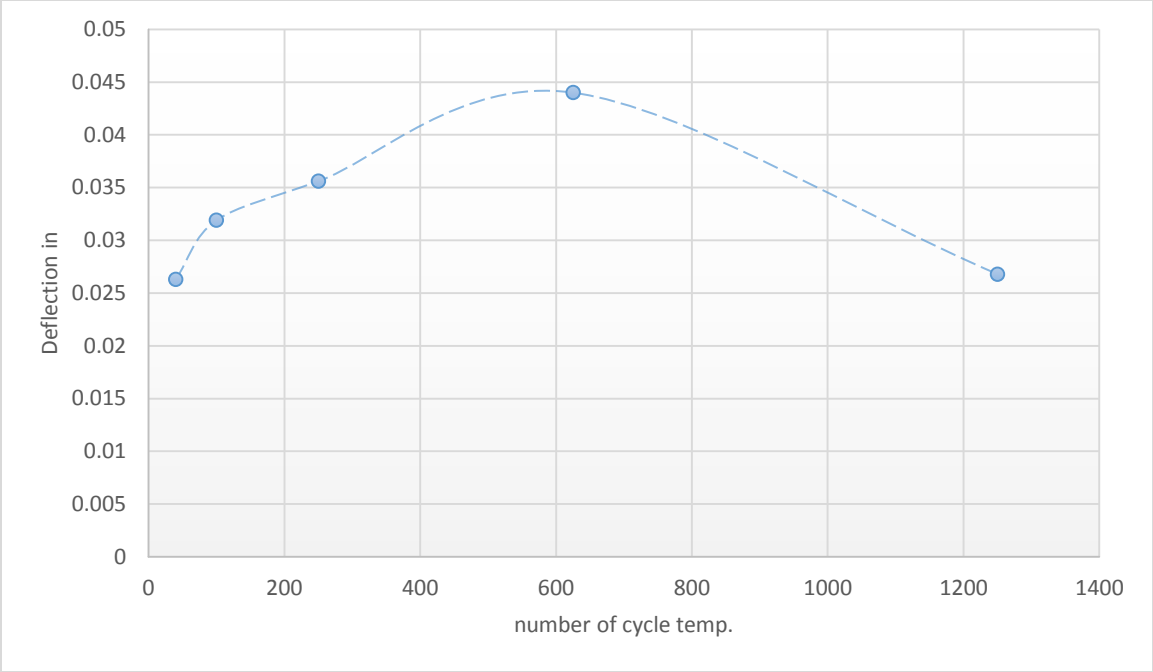

Figure 4.21: the maximum deflection vs. number of cycles.

Figures 4.22a, 4.22b, and 4.22c represents comparison between the regular concrete strength, deflection, and stiffness with geo-polymer concrete strength, deflection, and stiffness respectively. It shows that geo-polymer concrete has more strength than regular concrete when both specimens subjected to the same environmental condition. Table 4.6 shows the different between the strength for both cases (geo-polymer concrete beams, and regular concrete beams).

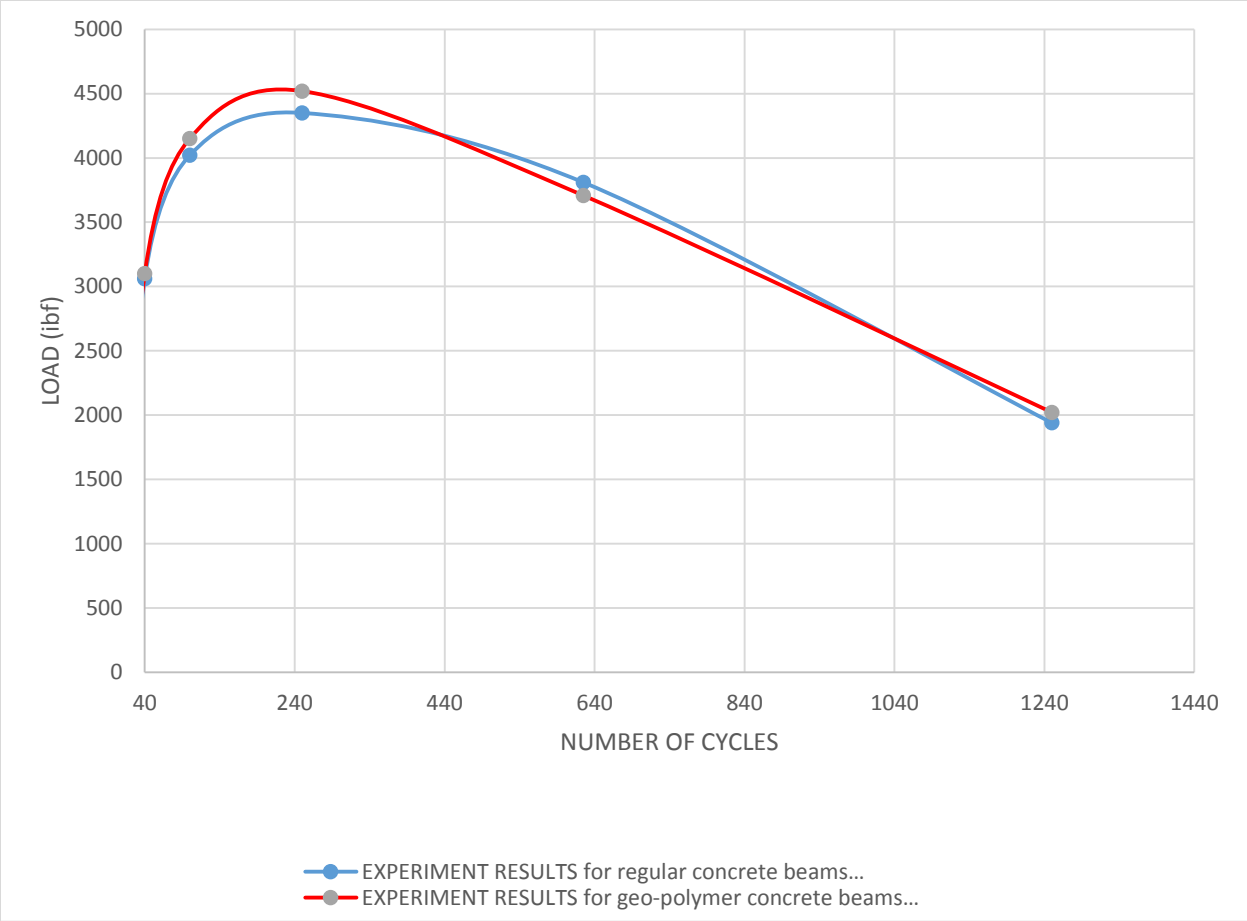

Figure 4.22a: comparison between the regular concrete beams strength and geo-polymer concrete beams strength

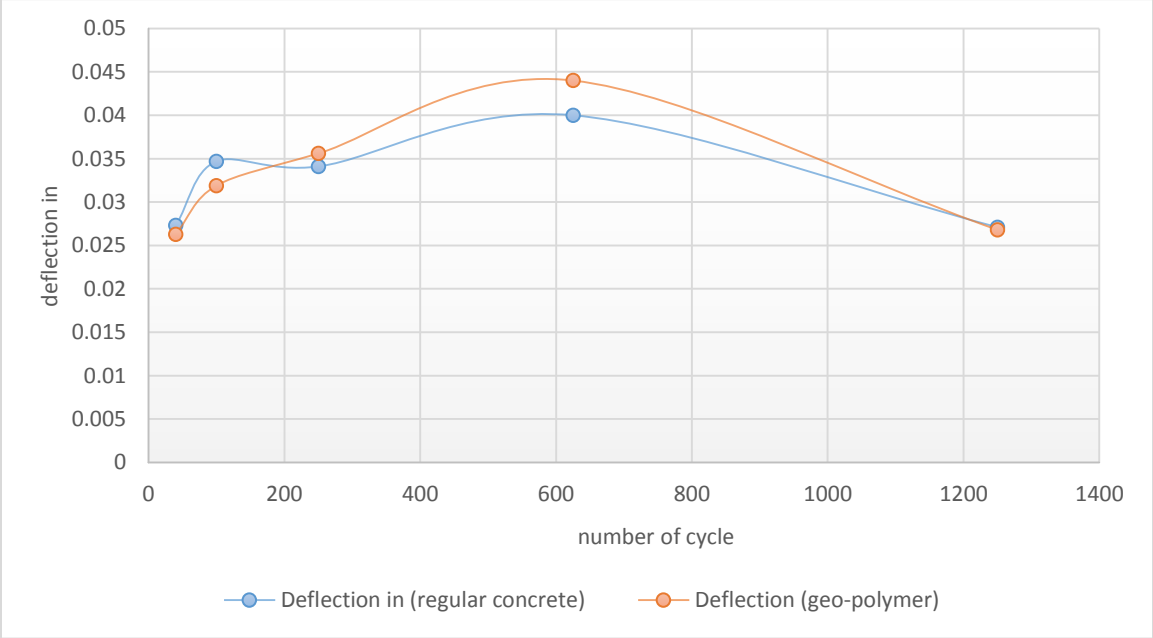

Figure 4.22b: comparison between regular concrete beams deflection and geo-polymer concrete beams deflection

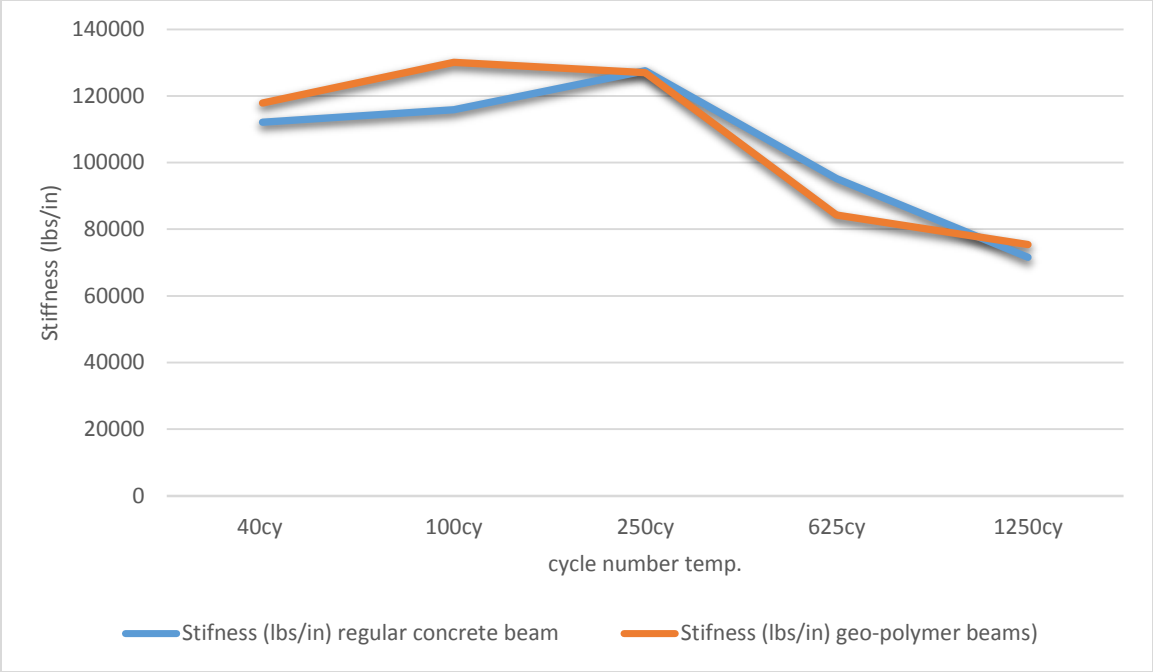

Figure 4.22c: comparison between regular concrete beams stiffness and geo-polymer concrete beams stiffness

Table 4.6: the different between the strength for both cases (geo-polymer concrete beams, and regular concrete beams).

CY	Regular concrete strength (lbs)	Geo-polymer concrete strength (lbs)	The differences
40	3061	3100	1.258% increase
100	4020	4150	3.132% increase
250	4350	4520	3.761% increase
625	3810	3708	2.750% decrease
1250	1940	2021	4.007%increase

It's very clear that the geo-polymer concrete showed more improvement in term of strength than regular concrete. This is due to the behavior of both, regular concrete, and geo-polymer concrete. Both material has different reaction when they expose to hygro-thermal condition, however, geo-polymer material is gain more strength by exposing it to hygro-thermal condition because of the

polymerisation process is generally accelerated in the higher temperature. And also because of the Geopolymerisation process will accelerate by accelerating the duration of exposing to the temperature which will lead to continuous Geopolymerisation with homogenous structure and less porosity that effect positively on strength. The regular concrete has similar reaction. The temperature will increase the hydration presses of the Portland cement, but the regular concrete will start losing the water faster than the geo-polymer concrete which will lead to decrease of the hydration reaction and then loss some advantage of its properties like stiffness, and strength.

4.3.2 Experimental Results for geo-polymer Concrete Columns (100% relative humidity)

15 geo-polymer concrete columns have been subjected to 100% relative humidity, number of cycles, and cycle periods. Table 4.7 shows the average result of the specimen's tests. Figure4.23 shows the compressive strength test of one of these specimens.

Table 4.7: Compressive strength test results of geo-polymer concrete column specimens

Temp. *oC*	Cy	CP (*Hr*)	Max deflection (in)	Mean (lbs)	Max. Compr. strength (psi)	Failure mode	Strength Comparing with control column	Deflection comparing with control column	Stiffness (lbs/in)
25-100	40	2	0.0511	36243.4	5130	Compression	1.23% increase	4.3% increase	709264
	100		0.0517	49511.5	7008	Compression	38.3% increase	5.5% increase	957670
	250		0.0501	53870.6	7625	Compression	50.5% increase	2.2% increase	1075262
	625		0.0441	47534	6728.1	Compression	32.8% increase	6% decrease	1077868
	1250		0.041	26013.3	3682	Compression	27.3% decrease	16.3% decrease	634471

Figure 4.23: Compressive strength test for geo-polymer concrete columns

Figure 4.24 shows the relationship between, compressive load and deflection for geo-polymer Concrete columns.

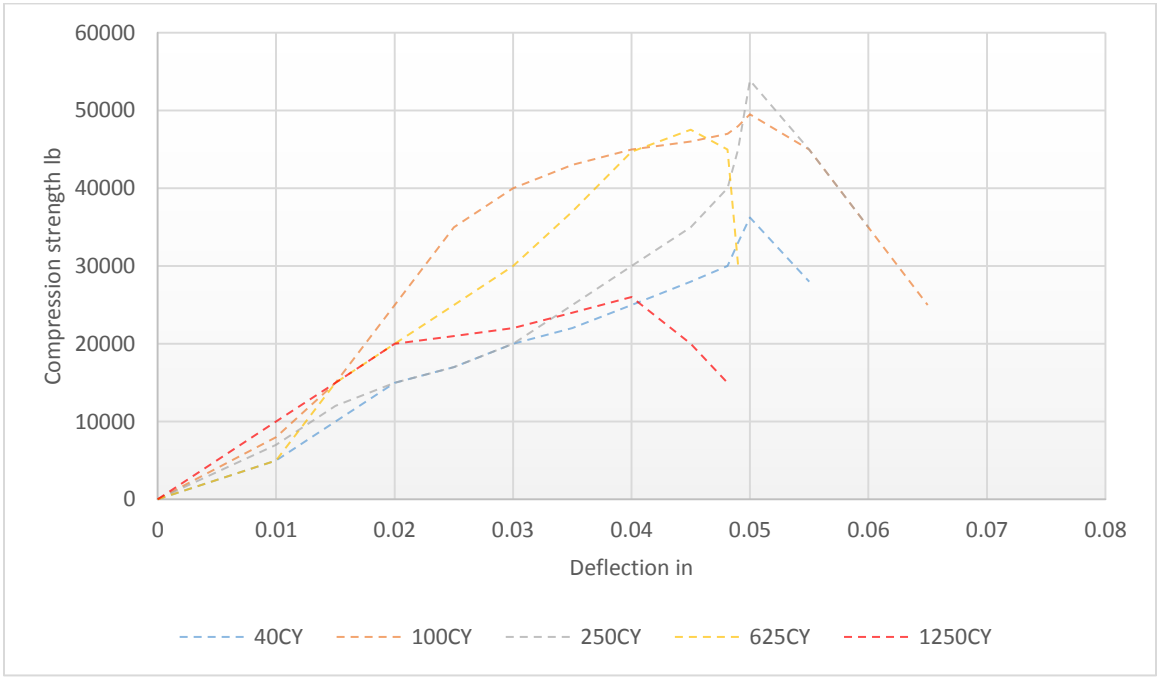

Figure 4.24: geo-polymer Concrete columns, compressive load – deflection results

Figures 4.25, and 4.26 illustrate the relationship between the maximum compressive load and maximum deflection results vs. number of cycles respectively. The figures show similar results to regular concrete columns specimens, however, the increase in the geo-polymer concrete is larger than the increase in the regular concrete case. The explanation of this was discussed on the geo-polymer concrete beam section (4.3.1).

That can be due that the geo-polymer column showed more stiffness, and less permeability.

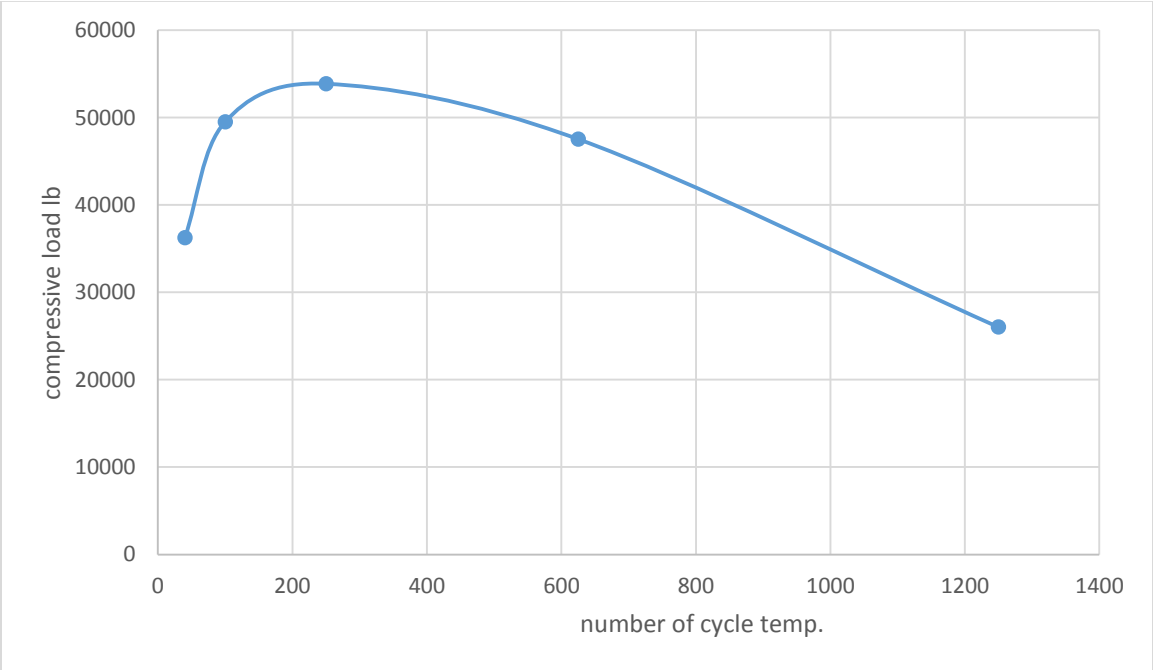

Figure 4.25: maximum compressive load vs. number of cycles

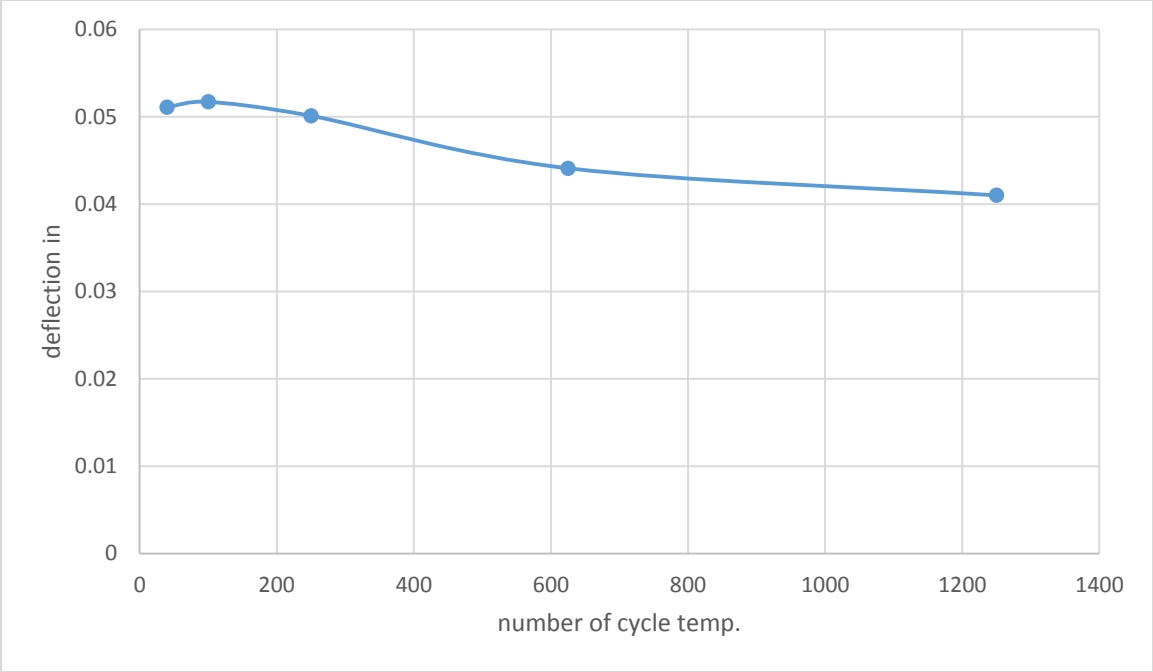

Figure 4.26: maximum deflection vs. number of cycles

Table 4.8 show comparison between regular concrete columns and geo-polymer concrete columns in term of strength.

It shows clear improvement at all cycle temperature similarly to geo-polymer concrete beams.

Figures 4.27a, 4.27b, and 4.27c show the different between geo-polymer concrete columns and regular concrete columns in term of strength, deflection, and stiffness respectively, and they support what have been discussed in geo-polymer concrete beam section.

Table 4.8: the different between the strength for both cases (geo-polymer concrete columns, and regular concrete columns).

CY	Regular concrete strength (lbs)	Geo-polymer concrete strength (lbs)	The differences
40	35925.5	36243.4	0.877% increase
100	47180	49511.5	4.7.9% increase
250	51044.6	53870.6	5.245%increase

625	44708	47534	5.945%increase
1250	22763.4	26013.3	12.493%increase

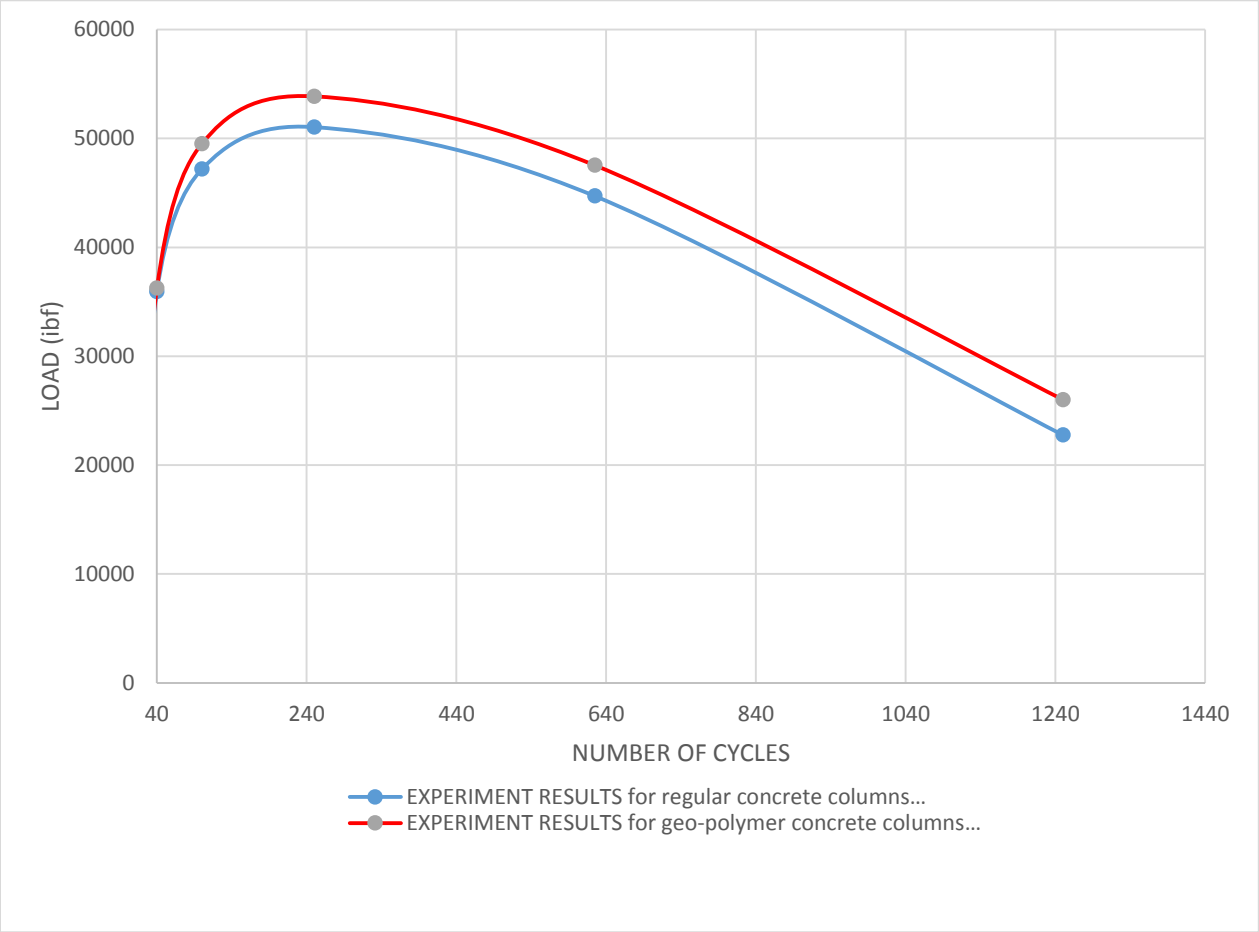

Figure 4.27a: comparison between the regular concrete columns and geo-polymer concrete columns

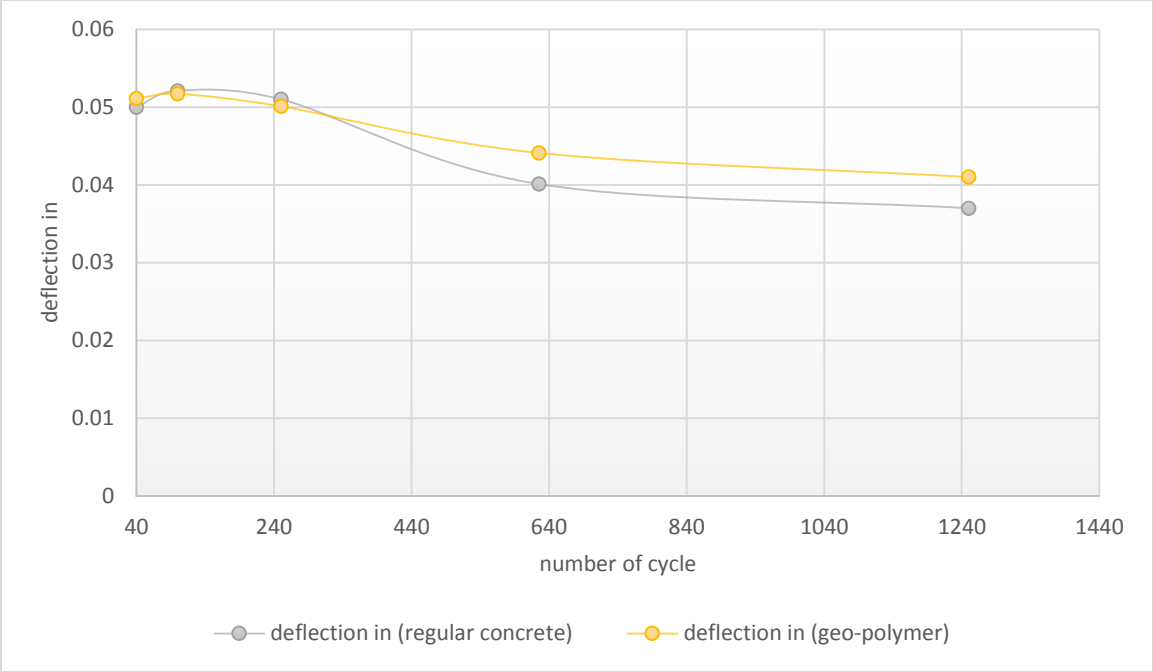

Figure 4.27b: comparison between the regular concrete columns and geo-polymer concrete columns

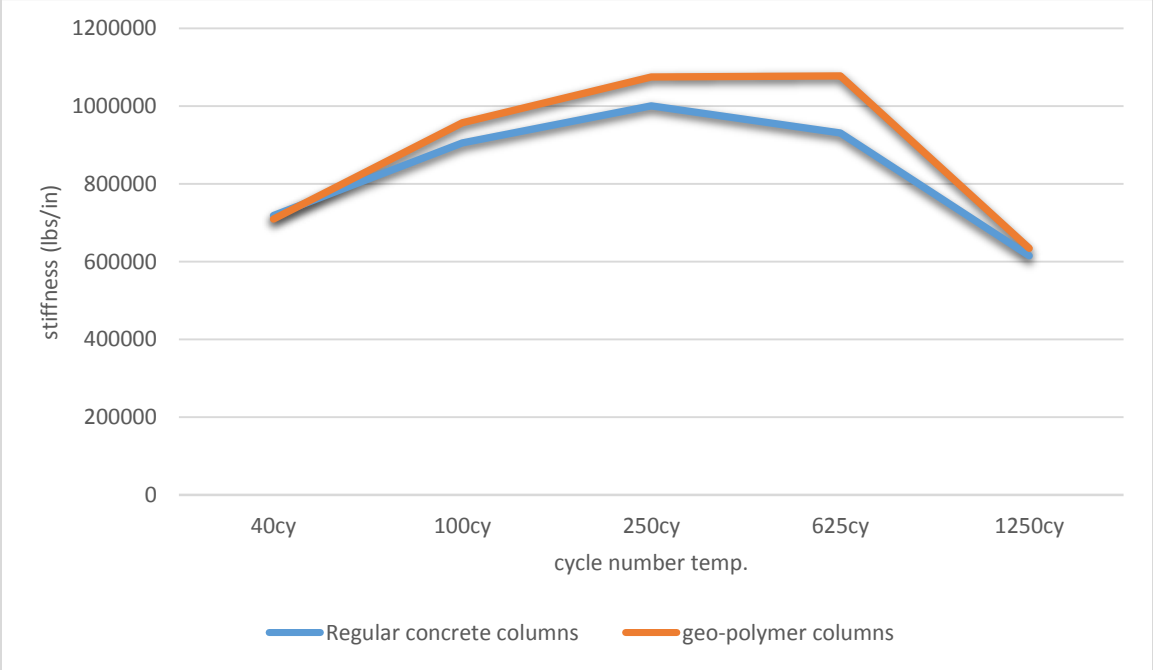

Figure 4.27c: comparison between the regular concrete columns and geo-polymer concrete columns

4.4 Experimental Results for regular Concrete columns (0% relative humidity)

30 plain concrete columns have been subjected to 0% relative humidity with two fixed temperature (T= 45$_o$C & T=70 $_o$C), and various period of times as shown in table 4.9. Figure 4.28 shows Concrete column specimens.

Table 4.9: Compressive strength test results of regular concrete column specimens (0% relative humidity)

Temp. $_oC$	Time (*Hr*)	Mean (lbs)	Max. Compr. strength (psi)	Failure mode	Comparing with control Column
45	80	35854.87	5075	Compression	0.14% increase
	200	43923.10	6217	Compression	22.7% increase
	500	47392.72	6708.1	Compression	32.4% increase
	1250	44156.25	6250	Compression	23.3% increase
	2500	20147.96	2851.8	Compression	43.7% decrease
70	80	35741.83	5059	Compression	0.17% decrease
	200	45533.92	6445	Compression	27.1% increase
	500	49440.87	6998	Compression	38% increase
	1250	44177.44	6253	Compression	23.4% increase
	2500	18095.51	2561.29	Compression	50% decrease

Figure 4.28: Concrete column specimens (0% relative humidity)

Figure 4.29 represents comparison between the regular concrete columns subjected to 100% relative humidity and regular concrete columns subjected to 0% relative humidity. It shows that regular concrete columns with 100% relative humidity has more strength than regular concrete columns with 0% relative humidity.

This can be due to that: when the specimens subjected to 0% relative humidity, they will lose water because of the temperature faster than the specimens that subjected to 100% relative humidity, and as a result of that they will be more shrinkage at 0% relative humidity than 100% relative humidity, and they will be more cracks for the specimens that subjected to 0% relative humidity (Figure 4.30a &b).

Furthermore, the hydration reaction of Portland cement will start slowdown because of losing water by increasing the temperature duration exposure.

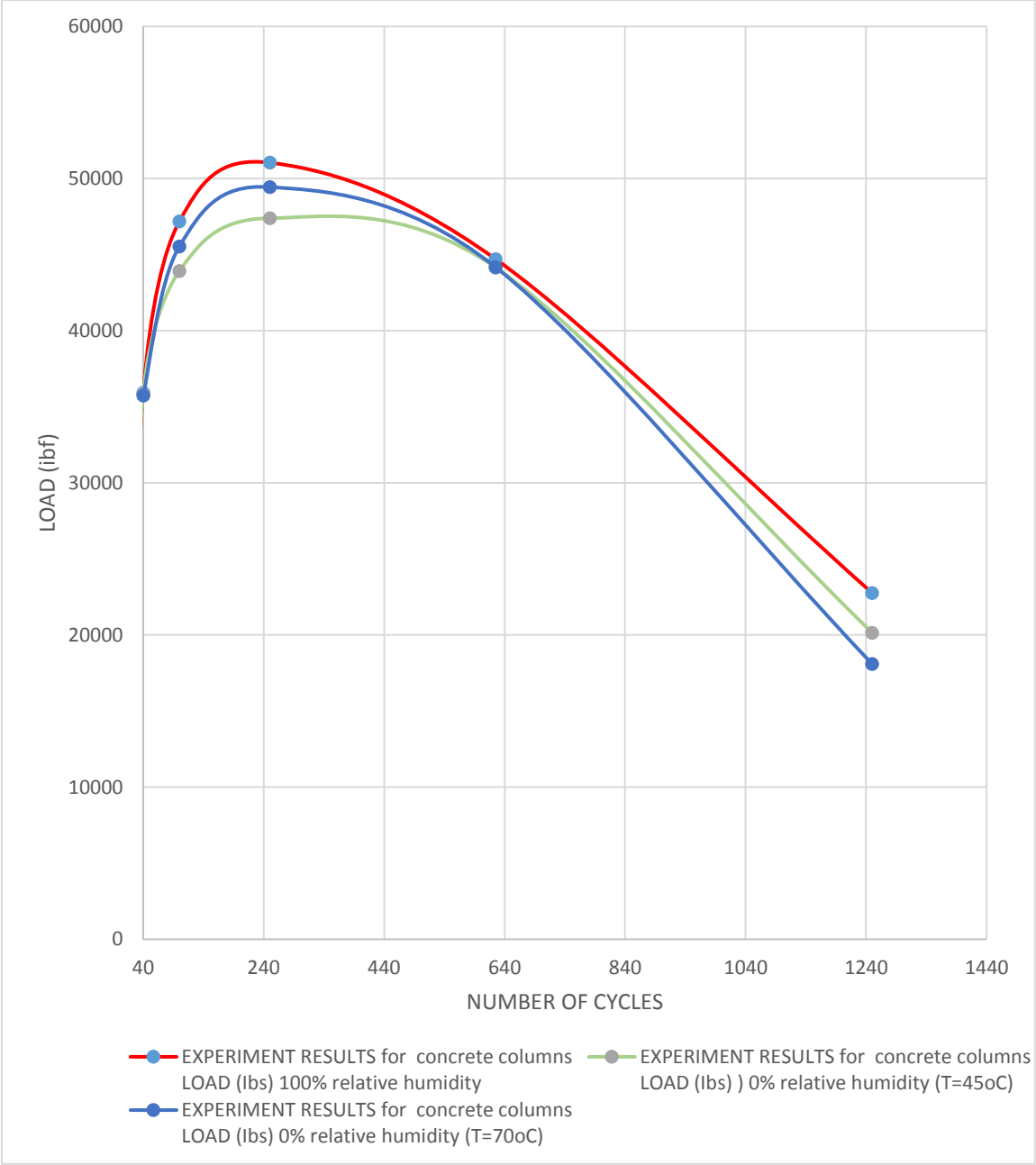

Figure 4.29: compression between the regular concrete columns with 100% relative humidity and regular concrete columns with 0% relative humidity

Figure 4.30a: Concrete column subject to 100% relative humidity

Figure 4.30b: Concrete column subject to 0% relative humidity

4.5 Experimental Results for geo-polymer Concrete columns (0% relative humidity)

30 geo-polymer concrete columns have been subjected to 0% relative humidity with two fixed temperature (T= 45$_o$C & T=70 $_o$C), and various period of times as shown in table 4.10.

Table 4.10: Compressive strength test results of geo-polymer concrete column specimens (0% relative humidity)

Temp. $_oC$	Time (*Hr*)	Mean (lbs)	Max. Compr. strength (psi)	Failure mode	Comparing with control column
45	80	36208.12	5125	Compression	1.13% increase
	200	49560.97	7015	Compression	38.4% increase
	500	53778.78	7612	Compression	50.2% increase
	1250	47356.69	6703	Compression	32.2% increase
	2500	25539.97	3615	Compression	28.6% decrease
70	80	36702.67	5195	Compression	2.5% increase
	200	49878.9	7060	Compression	39.3% increase
	500	54047.25	7650	Compression	51.0% increase

	1250	46946.92	6645	Compression	31.1% increase
	2500	26981.23	3819	Compression	24.6% decrease

Figure 4.31 represents comparison between regular concrete columns and geo-polymer concrete columns subjected to 0% relative humidity with regular concrete columns and geo-polymer concrete columns subjected to 100% relative humidity. It shows that geo-polymer concrete columns has more strength than regular concrete columns in both cases, and it shows as well that geo-polymer concrete columns has no big change in term of strength between 0% relative humidity and 100% humidity. That means, the humidity does not affect the strength of geo-polymer concrete.

This is because the geo-polymers possess excellent physic-chemical and mechanical properties, including low density, micro- or Nano- porosity, negligible shrinkage, high strength, great surface hardness and significant thermal stability, fire and chemical resistance (Panias D., Giannopoulou I. P. 2006).

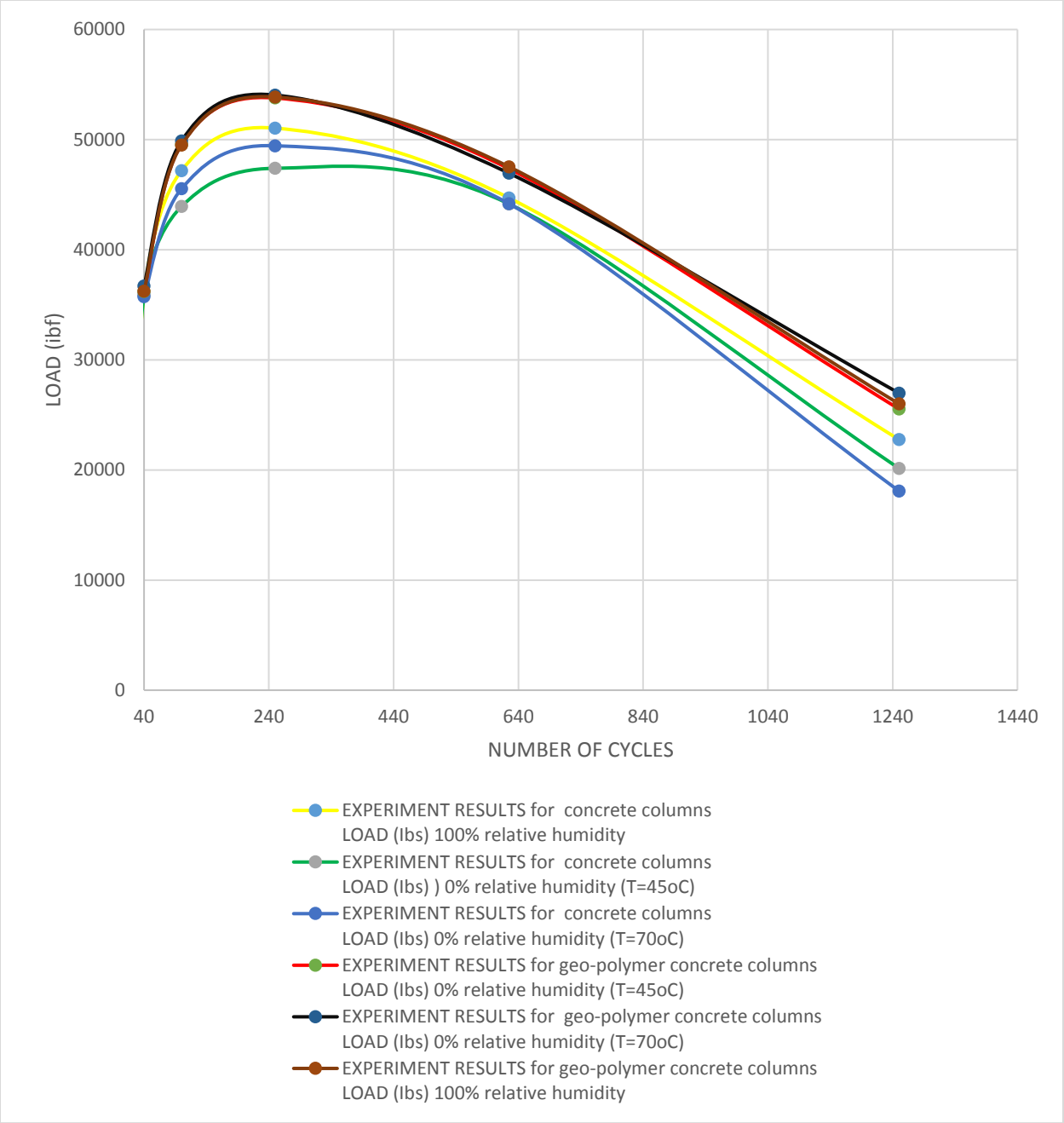

Figure 4.31: compression between all cases

4.6 Summary

Total of 126 specimens were constructed, cured, and tested under various environmental conditions. 60 specimens were geo-polymer concrete (15 specimens were geo-polymer concrete beams, and 45 specimens were geo-polymer concrete columns). 66 specimens were regular concrete beams, and columns (18 specimens were concrete beams, and 48 specimens were concrete columns).

As a result of all the above tests, the mode of failure of all the beam specimens were flexure failure, while the failure mode of all the columns specimens were compression failure.

The environment has clearly effect on regular concrete specimens and geo-polymer concrete specimens.

According to the above results and observations, the following conclusions have been drawn:

1. The flexural and the compression strength of concrete and geo-polymer concrete increased due to subjecting to 100% relative humidity and 0% relative humidity with temperature changing from 25^{o}C *to 100* ^{o}C, the magnitudes of flexural and compression strength increases varied with the number of cycles. The strength was the highest after 250 cycles, comparing to 100 cycles, and 40 cycles, then the strength was reduced after 625 cycles.

2. The humidity has very clear effect on the strength of regular concrete. The flexural and the compression strength of regular concrete that subjected to 100% relative humidity are higher than the flexural and the compression strength of regular concrete that subjected to 0% relative humidity.

3. The humidity has no large effect on the strength of geo-polymer concrete.

4. The geo-polymer concrete has more strength in term of flexure and compression than the regular concrete when both subjected to the same environmental condition.

CHAPTER 5 DURABILITY PERFORMANCE PREDICTION USING ANALYTICAL MODELING

5.1 Introduction

Temperature and humidity (hygro-thermal) cycles cause degradation in composite strengthening materials by changing the properties of based material due to plasticization and hydrolysis.

Although there is no comprehensive mechanistic modeling of the hygro-thermal effect on durability/life-prediction including temperature, relative humidity, aging of exposure, and cycle periods, fairly precise predictions can be made through the sensible use of an equation based on micro mechanics and semi-empirical approaches that are based on extensive prior experimental testing results.

This chapter includes equations related to the prediction of hygro-thermal effects, and then describes the predicting results on long-term strength of concrete and geo-polymer concrete that exposed to various environmental conditions.

William-Landel-Ferry (WLF) equation was employed here to develop the shift factor for regular concrete and geo-polymer concrete exposed to different environmental conditions. The shift factors were determined empirically based on experimental test results.

An extensive experimental research has been carried out throughout this study. The test results showed that the most influence on the strength of either concrete or geo-polymer concrete was temperature.

5.2 Temperature and Aging effects

In chapter four of this dissertation, the accelerating aging effects on the strength behavior

of plain concrete, and geo-polymer concrete beams and columns have been experimentally investigated. In this section, the temperature and aging effects are considered empirically for both regular concrete and geo-polymer by utilizing the WLF equation.

The combined effect of temperature and time on the strength of various materials could be represented by the time-temperature superposition (TTS) principle. One of the common applications of TTS is to expand the time range of short-term strength test results by taking such data at various temperatures and shifting them along the time axis, and then fitting the curve to find a master curve at the reference temperature which usually was the standard lab temperature (25_oC). The TTS principle was employed to construct the master curves for regular concrete and geo-polymer that were utilized in the experimental work of this research. The master curves were determined separately by using linear strength and time data, and also by logarithmic scale of these strength and time data.

5.2.1 Temperature and Aging Effects on regular Concrete Material

The experimental data of regular concrete beams was applied to obtain the master curve of concrete material.

The William-Landel-Ferry (WLF) equation is:

$$\log aT = -\frac{C1\ (\mathrm{T}-\mathrm{Tr})}{C2+(T-Tr)} \qquad (5.1)$$

Where:

aT = temperature-dependent shift factor

T= temperature

T_r= reference temperature,

C_1 and C_2 are material constants.

By using the flexural strength data under various aging conditions for regular concrete beam specimens that were determined from the experimental tests, the original data on flexural strength-time are plotted in figure 5.1 using linear scales. Figure 5.2 shows the logarithmic curves of these original data.

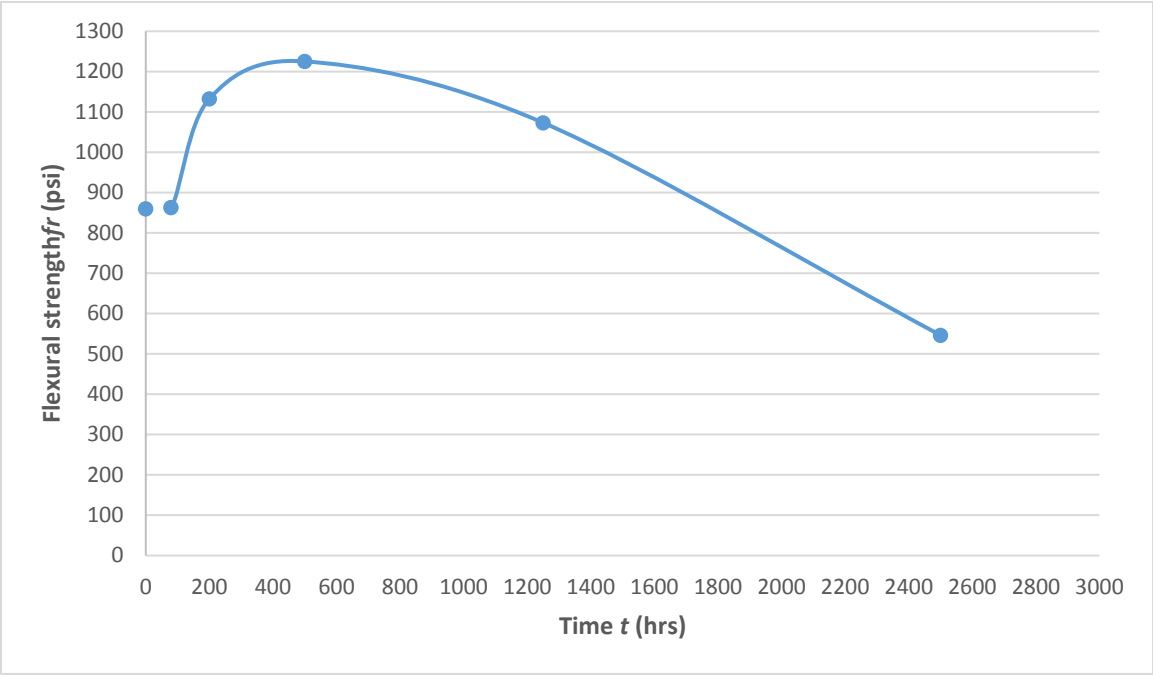

Figure 5.1 Flexural strength vs. time curves for concrete beams

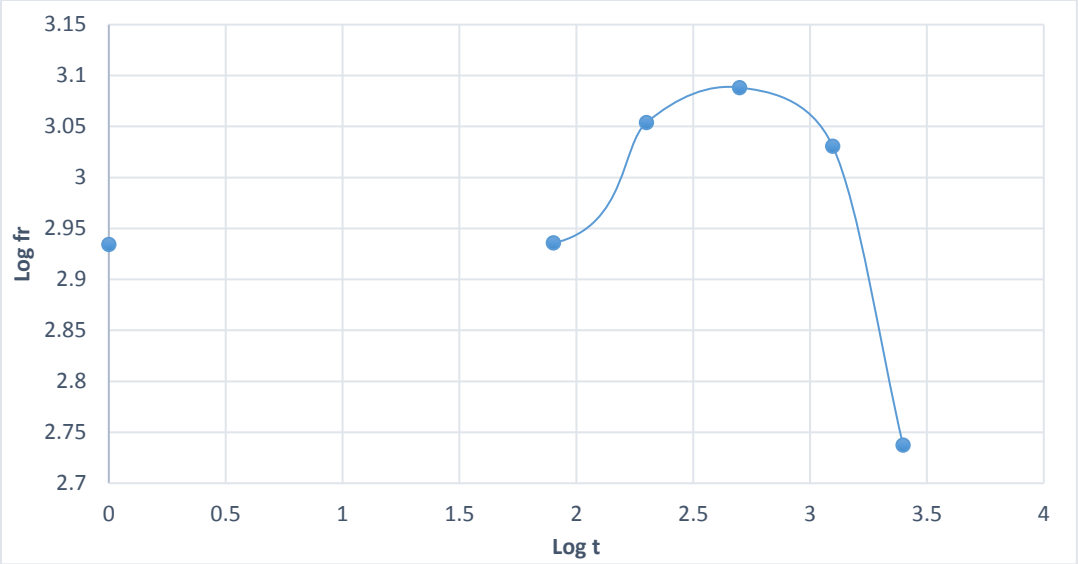

Figure 5.2: Flexural strength vs. time curves for concrete beams (logarithmic scale)

By using the WLF equation and substituting T by 100$_o$C and T_r was 25$_o$C, and assuming c_1= -8260.30 and c_2 = 146.26 (note: these values of c_1 and c_2 were obtained by using linear data from other experimental study (Elarbi 2011). When the logarithmic data were used, the constants of c_1 and c_2 were equaled - 38.40 and 2325.0 respectively.

As a result of applying time-temperature superposition (TTS) using the available experimental data and shifting 100$_o$C curve, the new curve was combined to generate the master curve (see figures 5.3 and 5.4).

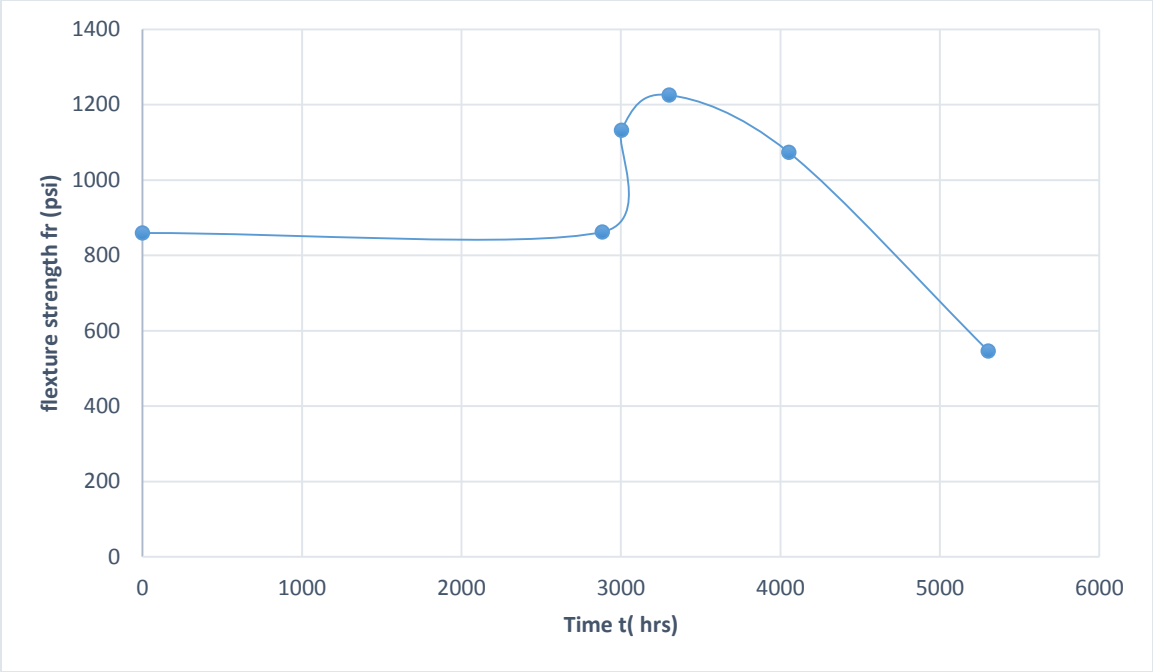

Figure 5.3: Shifting of flexural strength vs. time curves for concrete beams

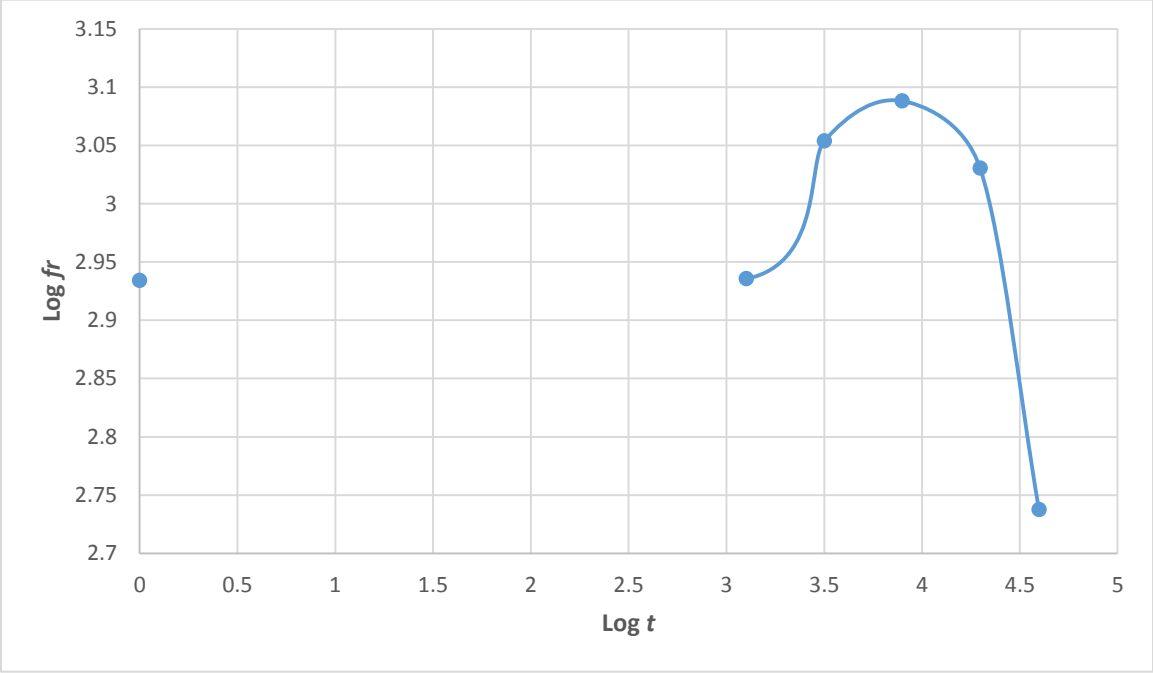

Figure 5.4: Shifting of Flexural strength vs. time curves for concrete beams (logarithmic scale)

The master curves at the reference temperature (25oC) were obtained by fitting all the data points in figures 5.3 and 5.4, and were shown in figures 5.5 and 5.6. The normalized strength equations as a function of time are equal:

$$f_{r(t)} = -6\times10^{-5}\,(t^2) + 0.2622(t) + 839.41 \quad \text{(linear scale)} \quad (5.2)$$

$$f_{r\,(\log(t))} = -0.0356\log(t^2) + 0.1522\log(t) + 2.9263 \quad \text{(logarithmic scale)} \quad (5.3)$$

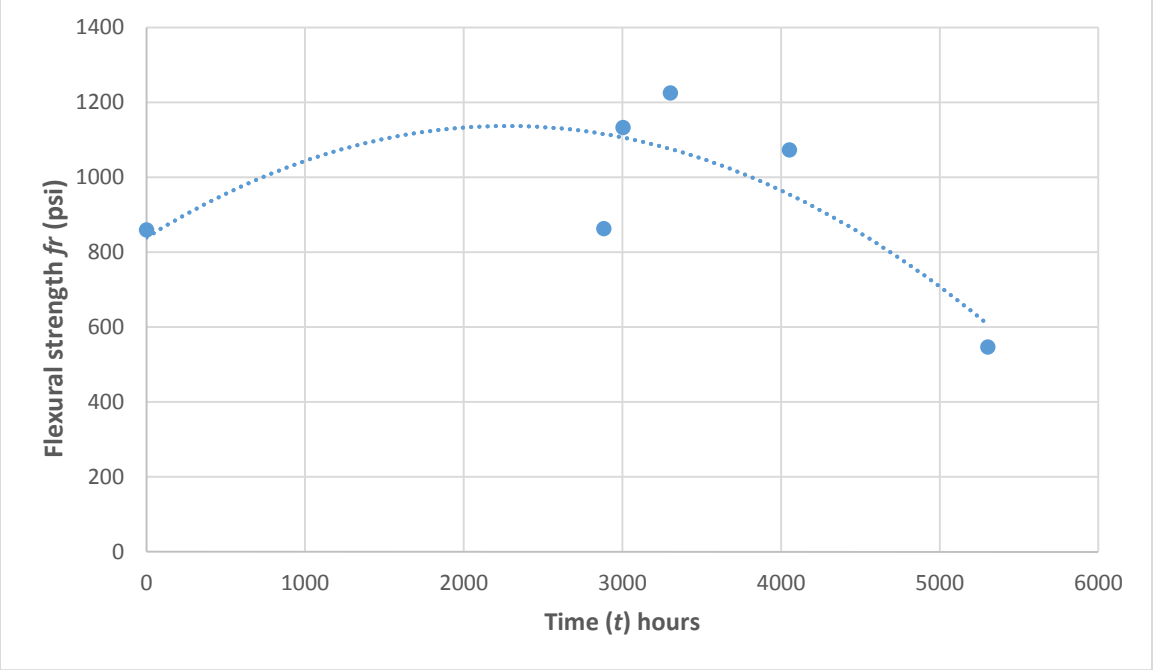

Figure 5.5: Master curve for concrete at reference temperature (linear scale)

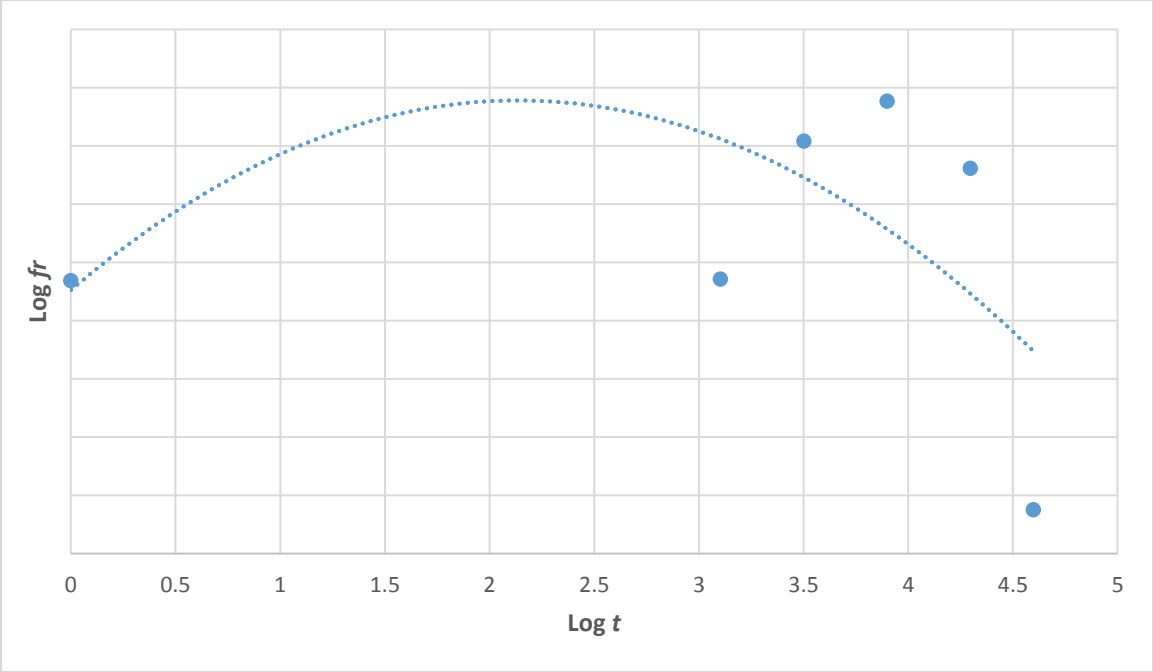

Figure 5.6: Master curve for concrete at reference temperature (logarithmic scale)

The above master curves that are shown in figures 5.5 and 5.6 can be used to predict the compressive strength for regular concrete columns.

5.2.2 Temperature and Aging Effects on geo-polymer Concrete Material

Similarly to regular concrete, the experimental data of geo-polymer concrete beams was applied to obtain the master curve of geo-polymer material.

The same equation was used (The William-Landel-Ferry (WLF) equation):

$$\log a_T = \frac{-c_1(T - T_r)}{c_2 + (T - T_r)}$$

Where:

a_T = temperature-dependent shift factor

T= temperature

T_r = reference temperature,

c_1 and c_2 are material constants.

By using the flexural strength data under various aging conditions for geo-polymer concrete beam specimens that were determined from the experimental tests, the original data on flexural strength-time are plotted in figure 5.7 using linear scales. Figure 5.8 shows the logarithmic curves of these original data.

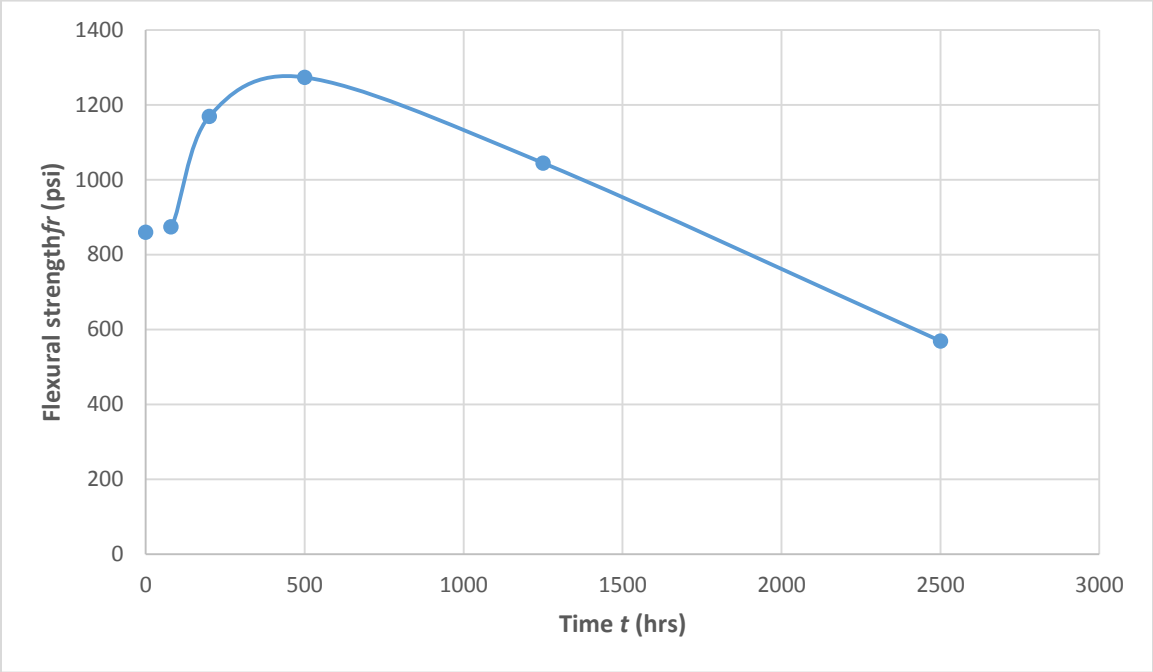

Figure 5.7: Flexural strength vs. time curves for geo-polymer concrete beams

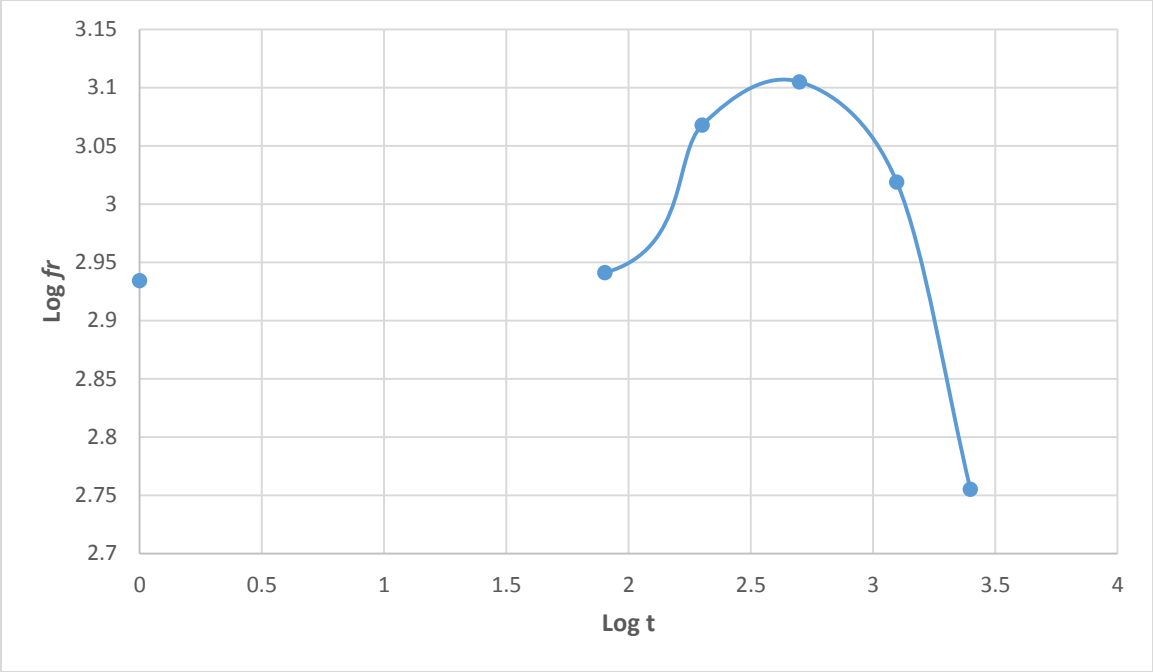

Figure 5.8: Flexural strength vs. time curves for geo-polymer concrete beams (logarithmic scale)

By following the same concept that used in regular concrete. Using the WLF equation and substituting T by 100$_o$C and T_r was 25$_o$C, and assuming c_1= -8260.30 and c_2 = 146, and when the logarithmic data were used, the constants of c_1 and c_2 were equaled - 38.40 and 2325.0 respectively. As a result of applying time-temperature superposition (TTS) using the available experimental data and shifting 100$_o$C curve, the new curve was combined to generate the master curve (see figures 5.9 and 5.10).

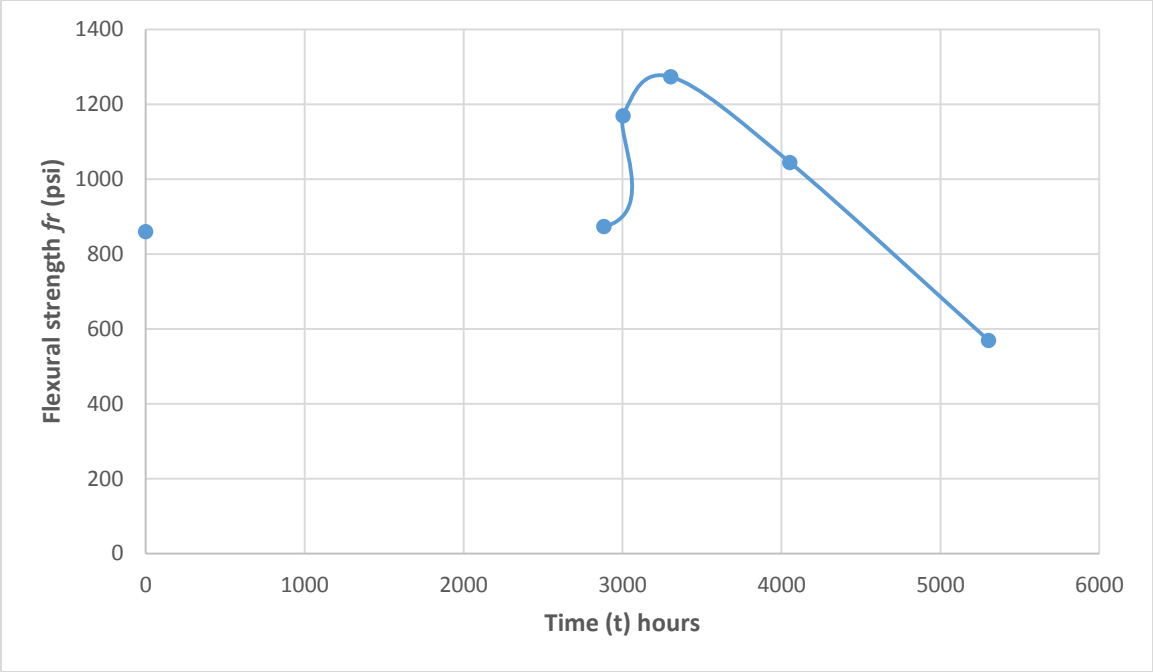

Figure 5.9: Shifting of flexural strength vs. time curves for geo-polymer concrete beams

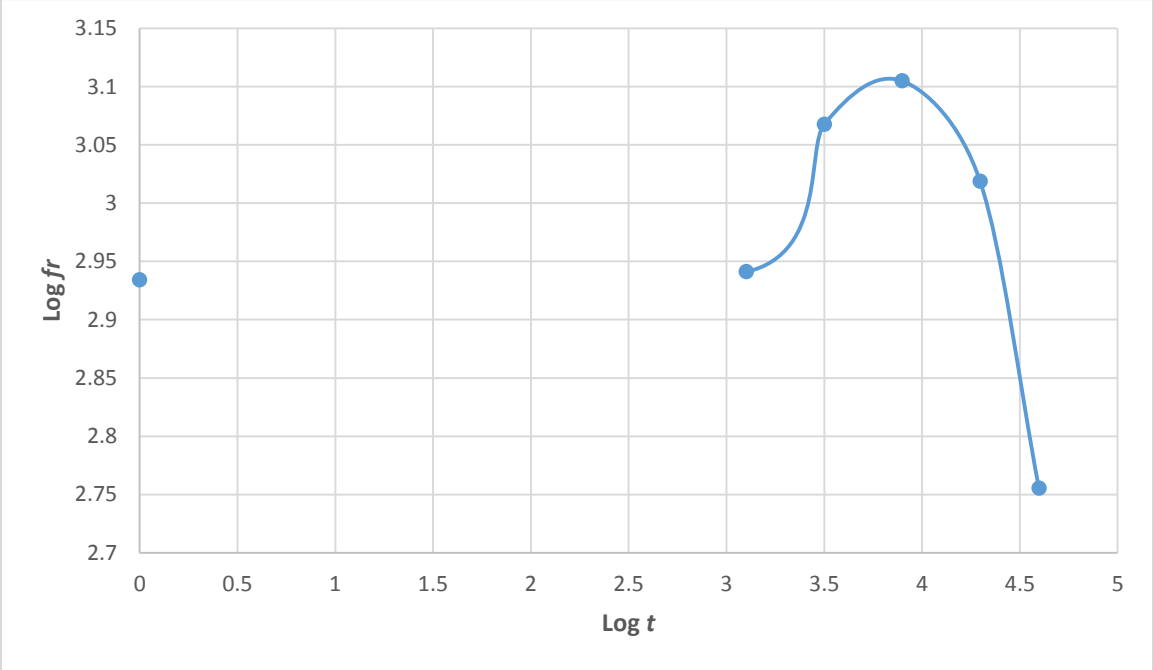

Figure 5.10: Shifting of Flexural strength vs. time curves for geo-polymer concrete beams (logarithmic scale)

The master curves at the reference temperature (25oC) were obtained by fitting all the data points in figures 5.9 and 5.10, and were shown in figures 5.11 and 5.12. The normalized strength equations as a function of time are equal:

$$f_{r(t)} = -6\times10^{-5}(t^2)+0.274(t)+842.02. \quad \text{(linear scale)} \quad (5.4)$$

$$f_{r\,(log(t))} = -0.0364\ log\,(t^2)+0.1575\ log(t)+2.9263 \quad \text{(logarithmic scale)} \quad (5.5)$$

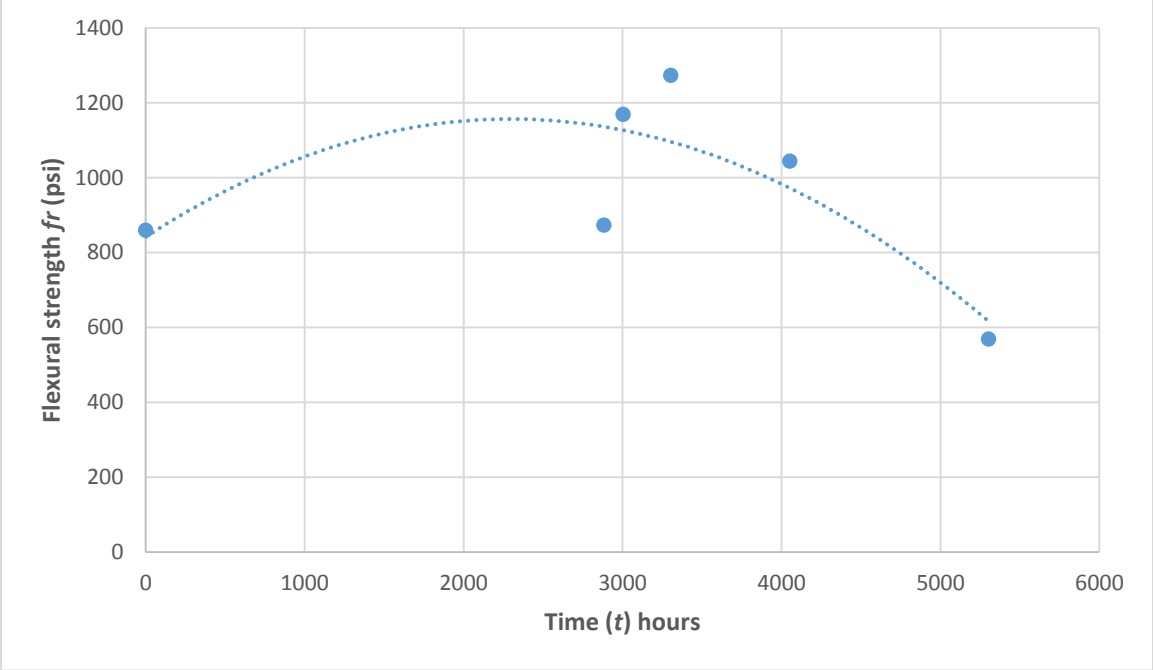

Figure 5.11: Master curve for geo-polymer concrete at reference temperature (linear scale)

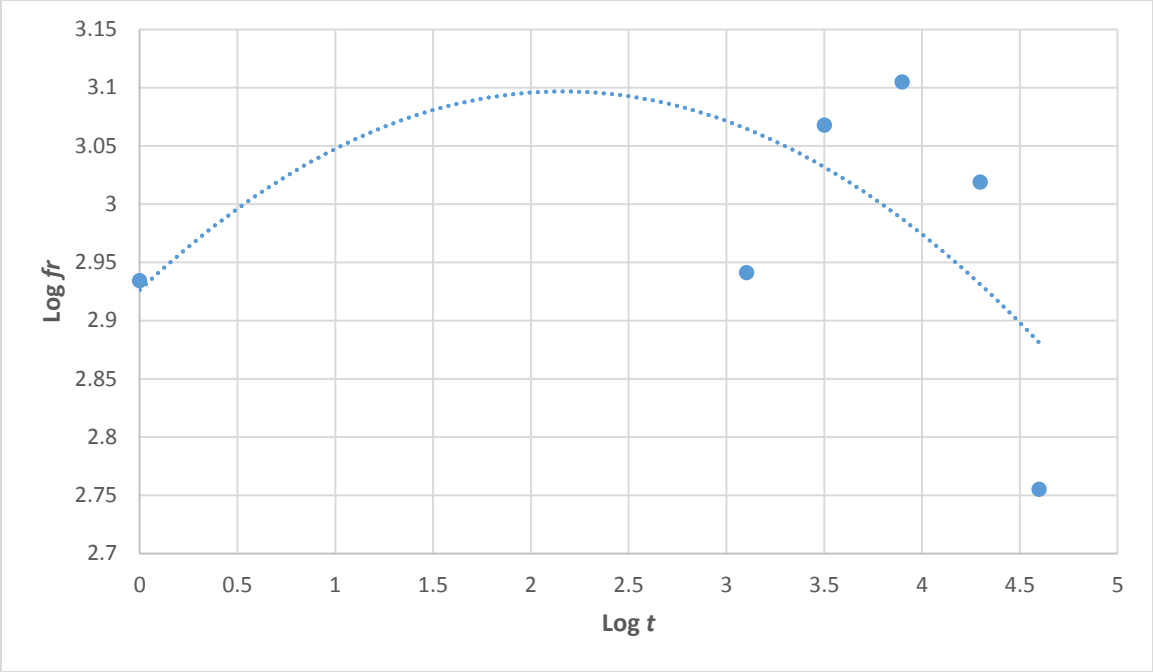

Figure 5.12: Master curve for geo-polymer concrete at reference temperature (logarithmic scale)

The above master curves that are shown in figures 5.11 and 5.12 can be used to predict the compressive strength for geo-polymer concrete columns.

CHAPTER 6 NUMERICAL MODELING

6.1 Introduction

Since the early years of the mathematical modeling of problems in continuum mechanics, the numerical analysis have concluded that the exact solution to some of the controlling differential equations hardly ever exists, and even if it did, it is frequently hard to accustom for common use. Analytical approaches like series expansions asymptotic integration have been used in solving some problems, but they still fall short of general applicability (Matthew J. P.,Ho Kim; and Davis 2010).

Recently, numerical analysis has become the essential tool for design and research problems. Analytical solution can be found for certain simplified situations. For problems concerning complex materials properties and boundary conditions, numerical methods are typically used, that give approximate and suitable solutions. In the numerical methods, the solution more commonly capitulates approximate values of unidentified quantities only at a separate number of points in the structure. The way of choosing only a certain number of discrete points in the body structure can be described as "discretization". One of the ways of discretizing a body or a structure is to split it into an equivalent system of small bodies or structures. These bodies are then assembled to represent the solution for the original body, and inside this combination, the bodies are assumed to be connected to each other at separate points called nodes.

Many numerical methods had been developed before the electronic computers being. The best well know methods are the finite difference method, residual methods for instance, the method of least squares and variational methods such as the Rayleigh-Ritz method, in which approximate functions are assumed for the unknown functions to be determined. Both these methods take linear combination of approximating functions which makes a given function stationary. But the major

difference between these two methods is that assumed approximating functions, in the finite element methods are not defined over the entire solution domain, but only in the small domain (element) and mainly at the nodes, and they are not necessary to satisfy boundary conditions, but it has to satisfy the continuity condition at the nodes. In the Ritz method, functions are defined over the whole domain, therefore, it can be used only for domains of relatively simple geometric shapes, while in finite element method the same constraint exists but for the elements only, since element of simple shape can be collected to present complex geometries (Jensen, E., Grace, N., Eamon, C.D., Shi, X., and Matsagar, V. 2009).

6.2 Finite Element Method

Finite element method came into the sight of numerical analysis about seven decades ago; it has been developed in 1943 by R. Courant. Finite element method started as an extension to the matrix methods and their applications to trusses and frames of directly connected members by matching the nodal displacements and with no consideration for the inter-element continuity. Since that time, finite element method has expended beyond proportions to the extent of covering more fields than structural mechanics such as heat flow, fluid flow, seepage of water, and others (Elarbi 2011).

The formulation of finite element method was mainly based on two principles. The first is the principle of minimum potential energy, which is concerned with satisfying the continuity conditions within the structure and the kinematic boundary conditions, but no requirements that the equilibrium of stress and boundary conditions be satisfied (displacement or stiffness model); the second is a principle of minimum complementary energy which is concerned with the stress fields that satisfy the conditions of equilibrium, but not necessarily the requirements of compatibility (stress or flexibility model).

In general, two types of analysis are used in finite element to model any type of structure, 2-D modeling, and 3-D modeling.

Although 2-D modeling has advantage of simplicity and allows the analysis to be run on a normal-speed computer, it tends to yield less accurate results.

However, 3D modeling results more accurately while sacrificing the ability to operate eff ectively on all but the fastest computers. Within each of these modeling systems, the users can insert many functions which may make the system conduct linear or non-linear analysis.

Linear systems are less complex and generally do not need to take plastic deformation in the consideration. While non-linear systems do account for plastic deformation.

FEA uses a complex point system called nodes that make a mesh grid. This mesh is designed to c ontain the material and structural properties that define how the structure will react to certain loa ding conditions. Nodes are assigned throughout the material at a certain density depending on a given area's predictable stress levels. Sections that receive large amounts of stress typically have a higher density of nodes than those with little or no stress.. Points of interest may be the breaking point of previously tested material, filets, edges, complex measurements, and areas of high pressure. The mesh functions as a spider web in that a mesh component spreads to each of the adjacent nodes from each node. This vector web is what brings to the object the material properties, creating many elements. One of the important applications of FEM is the analysis of crack propagation problems.

Basics of the current form of linear elastic fracture mechanics (LEFM) emerged literally in marine laboratories during the First World War. Since then, LEFM has been productively applied to a variety of classical crack and defect problems, but remained relatively limited to simple geometries and loading conditions.

The development of the finite element method has quickly changed the scope of LEFM's application. FEM was virtually unlimited in solving complex geometries and loading conditions and was soon extended to nonlinear materials and major deformation problems.

FEM's use in linear elastic fracture mechanics and its extension to mechanics of elastic plastic fracture (EPFM) has now extended to almost all crack problems. The introduction of new design codes for stable cracks has even resulted in parametric tests and experimental findings. The core of analyzes, however, remained almost unchanged: LEFM basic principles coupled with FEM techniques focused on classical continuum by smeared or discrete crack models. A major breakthrough in the basic idea of part of unity and the eXtended Finite Element Method (X-FEM or XFEM) seemed to evolve after that. (N. Moës, N. Sukumar, B. Moran and T. Belytschko (2000)).

6.3 Extended Finite Element Method

The Extended Finite Element Method (XFEM) is a model used to model strong and weak discontinuities independent of the finite element mesh using the finite element partition method (Matthew J. P., Kim; and Davis 2010).

The first attempt to develop the extended method of finite elements could be dated back to 1999 when Belytschko and Black (1999) presented a method for crack growth with minimal re-meshingof finite elements. The concept was constructed by adding discontinuous enrichment functions to the approximation of the finite element to account for the crack.. The method allowed the crack to be arbitrarily combined within the mesh, despite the need to remediate for harshly curved cracks (Elarbi 2011).

Moës et al. developed the method in 1999, naming it the expanded method of finite elements (XFEM). This improvement allowed the entire crack to be represented independently from the

mesh, based on the construction of the enriched approximation of the crack geometry interaction with the mesh.

In 2000, Dolbow et al. 2000 also presented a system for modeling arbitrary discontinuities within the framework of finite elements by locally enriching a displacement-based approximation by means of a unity method partition (Elarbi 2011).

In addition, in 2000, Sukumar et al. expanded the XFEM to three-dimensional crack modeling and discussed geometric issues related to crack representation and finite-element approximation enrichment..

Daux et al. (2000) studied another topic as extensions to the original XFEM. They focused on modeling randomly branched cracks with multiple branches, multiple holes and cracks from holes.

Gradually, level set methods expanded to reflect the location of crack, including the position of crack tips. In 2001, Stolarska et al. presented a way to coupl the level-set method (LSM) to model crack growth with XFEM. By the year 2001, Belytschko et al. introduced a technique in finite elements to model arbitrary discontinuities in the function and its derivatives. The discontinuous approximation was developed as a signed distance variable, so that level sets could be used to modify discontinuity position. Sukumar et al. (2001) also made a further effort to describe modeling holes and level sets inclusions in the extended finite element method.

Meanwhile, in 2002, Moës et al and Gravouil et al discussed the mechanical model and level update for non-planar three-dimensional crack growth based on a Hamilton – Jacobi formula to update level sets with a velocity extension approach to maintain the old crack surface (N. Moës, N. Sukumar, B. Moran and T. Belytschko 2000).

The extended method of finite elements (X-FEM) has recently emerged as a powerful numerical procedure to analyze crack problems. It has been widely acknowledged that, under the assumptions of linear elastic fracture mechanics (LEFM), the method facilitates crack growth modeling. Several new extensions and applications have appeared in the scientific literature since the introduction of the method about a decade ago, with significant contributions to X-FEM in recent years.

The X-FEM offers significant advantages in the numerical modeling of crack propagation compared to the standard finite element method.. In the traditional concept of the FEM, the presence of a crack is based on the requirement that the crack follow the edges of the object. On the contrary, it is not necessary to align the crack geometry in the X-FEM with the edges of the elements that provide flexibility and versatility in modeling. The method is based on enriching the finite element model with additional degrees of freedom (DOFs) linked to the nodes of the elements discussed by the crackThe discontinuity is thus included in the numerical model without altering the discretization, as the mesh is generated without taking into account the crack's being. Therefore, for any crack length and orientation, only one mesh is needed. Furthermore, nodes around the crack tip are filled with DOFs associated with functions copying LEFM asymptotic fields. This allows the simulation of the crack discontinuity within the crack-tip component and significantly increases the accuracy of the measurement of stress intensity factors (SIFs) (Elarbi 2011).

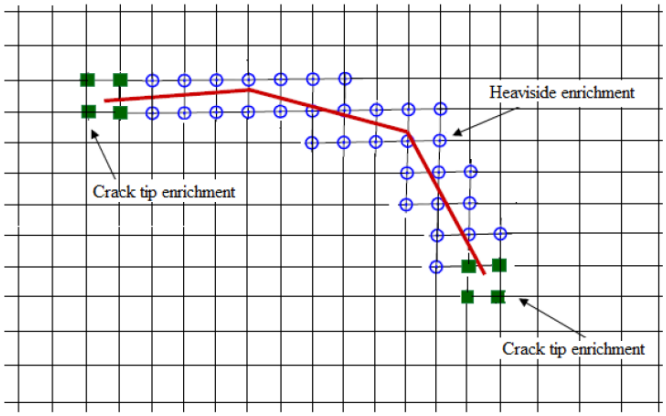

Figure 6.1: The nodes enriched with the Heaviside and crack tip enrichment functions (IFOSC 2001).

As shown in figure 6.1, the circled nodes are the nodes enriched by two additional DOFs (total of four DOFs per node), while the nodes marked with a square are enriched by eight additional DOFs (total of ten DOFs per node). It is known as enriched elements that contain at least one enriched node. Nodes with two additional DOFs (one for each coordinate direction) have shape functions multiplying the Heaviside function H(x) (unit magnitude function whose sign changes through the crack, H(x)=±1), whereas H(x) is positive above the crack and negative below the crack. This role essentially creates discontinuity across the faces of the crack. In the two Cartesian directions, nodes with eight additional DOFs are enriched with four Fα(x) crack tip functions (IFOSC 2001).

$$[F_\alpha(r,\theta), \alpha = 1-4] = \left[\sqrt{r}\sin\frac{\theta}{2}, \sqrt{r}\cos\frac{\theta}{2}, \sqrt{r}\sin\frac{\theta}{2}\sin\theta, \sqrt{r}\cos\frac{\theta}{2}\sin\theta\right] \quad (6.1)$$

Where: r,θ represent local polar co-ordinates defined at the crack tip. The displacement approximation for crack modeling in the extended finite element method can be written in the form

$$u_{xfem}(x) = \sum_{i\epsilon I} N_i(x)u_i + \sum_{i\epsilon j} N_i(x)H(x)a_i + \sum_{i\epsilon k}\left[N_i(x)\sum_{\alpha=1}^{4} F_\alpha(x)b_{i\alpha}\right] \tag{6.2}$$

Where: I represents the set of all nodes in the mesh, $N_i(x)$ is the nodal shape function and u_i is the standard DOF of node i (u_i represents the nodal displacement for non-enriched nodes only). j and k contain the nodes enriched with Heaviside function $H(x)$ or crack-tip functions $F_\alpha(x)$, respectively, and a_i, $b_{i\alpha}$ are the corresponding DOFs. In case there is no enrichment, then the above equation reduces to the classical finite element approximation

$$u_{fe}(x) = P_i N_i(x)u_i \tag{6.3}$$

The additional functions are used in the displacement approximation are typically called enrichment functions and the approximation is written as

$$u^h(x) = \sum_I N_I(x)\left[u_I + \sum_j v^j(x)a_I{}^j\right] \tag{6.4}$$

Where: u_I represents the classical finite element degrees of freedom, $v(x)$ is the j_{th} enrichment function, and aI^j is the enriched degrees of freedom corresponding to the j_{th} enrichment function at the I_{th} node. The enriched degrees of freedom defined by Eq. (6.1) generally do not have a physical meaning and instead can be considered as a calibration of the enrichment functions which result in the correct displacement approximation. Equation (6.4) does not satisfy the interpolation property, $u_I = u_h(x_I)$ because of the enriched degrees of freedom, instead additional calculations are required in order to calculate the physical displacement by utilizing equation (6.4). The interpolation property is important in practice in applying boundary or contact conditions. Therefore, it is a common practice to shift the enrichment function to the shape:

$$\gamma_I^J(x) = v^J(x) - v_I^J(x) \tag{6.5}$$

Where:

$v_I^J(x)$ is the value of the J_{th} enrichment function at the I_{th} node. As the shifted enrichment function now takes a value of zero at all nodes, the solution of the resulting system of equations satisfies $u_I = u_h(x_I)$ and the enriched degrees of freedom can be used for additional actions such as interpolation and post-processing. Here, the shifted enrichment functions are referred to with upper case characters, and the unshifted enrichment functions are referred to with lower case font. The shifted displacement approximation is in the form

$$u^h(x) = \sum_I N_I(x)\left[u_I + \sum_j \gamma_I^J(x) a_I{}^j\right] \tag{6.6}$$

Where:

$\gamma_I^J(x)$ represents the J_{th} shifted enrichment function at the I_{th} node.

6.4 Finite Element Simulation by Using ABAQUS- CAE Software

ABAQUS / CAE is a complete ABAQUS environment that provides a simple, consistent interface for ABAQUS / Standard and ABAQUS / Explicit simulation results creation, submission, monitoring and evaluation. ABAQUS / CAE is divided into modules in which each module defines a logical aspect of the modeling process, such as geometry definition, material properties definition and mesh generation. You can build the model from which ABAQUS / CAE generates an input file submitted to the ABAQUS / Standard or ABAQUS / Explicit analysis product as one moves from module to module. The result of analysis conducts the analysis, sends information to

ABAQUS / CAE to allow you to track the work progress and produce a list of outputs. The analytical model consists at least of the following information:• Discretized geometry.

• Element section properties.

• Material data.

• Loads and boundary conditions.

• Analysis type.

• Output requests.

In this research, ABAQUS/CAE 6.9 release has been utilized to implement the scope of work. Compared with other computer softwares, one of the major advantages of this software is the flexibility of implementing, revising, analyzing the model, and getting results. But the more important function of this release of ABAQUS/CAE 6.9 is that it allows a crack to grow up with or without specifying the locations of the crack initiation.

6.4.1 Concrete Beam Simulation

For non-linear finite element analysis, ABAQUS-CAE software was used to model the behavior of plain concrete. The modeling space was chosen 2D planar and the type was deformable, (figure 6.2).

Figure 6.2: 2D planar concrete beam model

The element has been considered as an elastic-isotropic material. The material behaviors have been selected to be “Maxps Damage”, and the properties are shown in table 6.1.

Table 6.1: Concrete material properties

Young's Modulus	4.058x10$_6$ psi
Compressive Strength	5068 psi
Poisson's ratio	0.18
Density	0.0867 lb/in$_3$

The element has been meshed by size of 0.8 and for the mesh control the element shape was considered a quad-dominated structured, Figure (6.3).

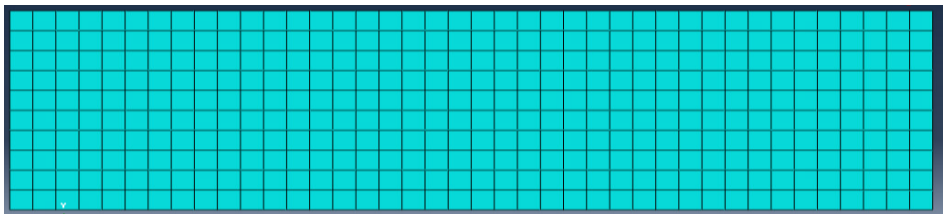

Figure 6.3: Mesh of the 2D planar concrete beam model

The load has been used as a static concentrated dead load and the type of boundary conditions was selected displacement/rotation, one support was considered as a pin and the other roller, figure (6.4).

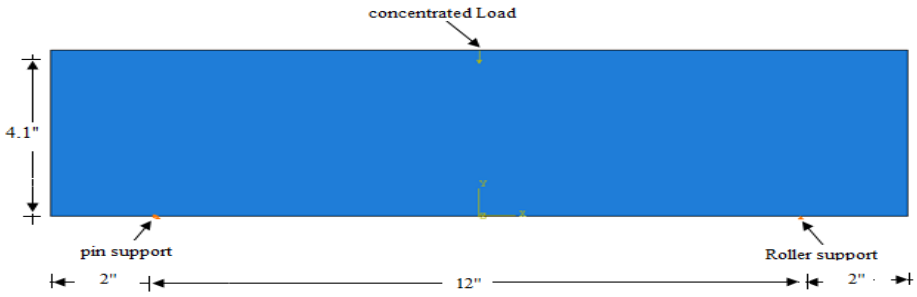

Figure 6.4: Load and boundary conditions of concrete beam model

6.4.2 Concrete Column Simulation

ABAQUS-CAE software was used to model the behavior of concrete column. The modeling space was chosen 3D and the type was deformable (see figure 6.5).

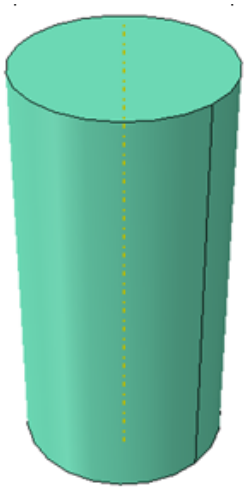

Figure 6.5: 3D Concrete column model

Similar to the concrete beam model, the element has been considered as an elasticisotropic material. The material behaviors have been selected “Maxps Damage”, and the properties are listed in Table 6.1.

The element has been meshed by size of 0.2 and for the mesh control the element shape was considered “Hex” while the element shape technique has been chosen “sweep” and the element type was “3D stress”. The fine mesh of the concrete column is shown in figure 6.6.

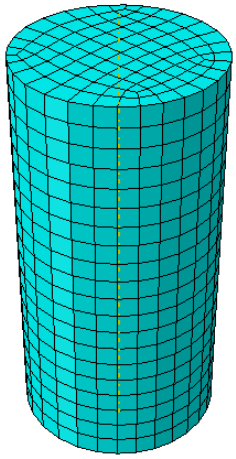

Figure 6.6: Mesh of 3D concrete column model

The type of load has been used as a static pressure on the upper surface and the type of boundary conditions at the bottom surface was selected displacement/rotation, figure (6.7).

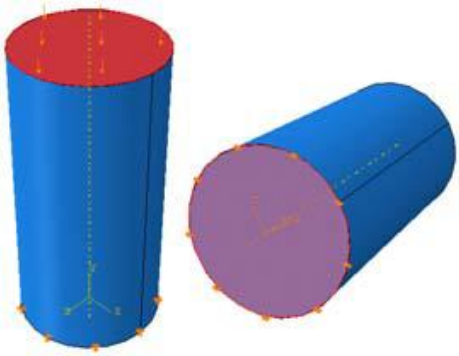

Figure 6.7: Load and boundary conditions of 3D concrete column model

6.5 Finite Element Model Predictions and Discussion

The behavior of plain concrete and geo-polymer concrete beams/columns were studied experimentally in chapter four. The results were compared to analytical calculations in chapter five. Extended Finite Element Method (X-FEM) was used to model the behavior of those elements numerically to confirm these calculations, as well as to provide a valuable supplement to the experimental investigations in this study.

The ABQUS CAE finite element software (ABAQUS CAE 6.9-1) was adopted in this study to simulate the behavior of the experimental beams and columns, and predict the load - displacement response of plain concrete and geo-polymer concrete beams and columns numerically**.**

6.5.1 Numerical Modeling of regular concrete beams (100% Humidity)

2D nonlinear extended finite-element (X-FE) model was developed to study the behavior of concrete beams (figure 6.2). The section type was selected "deformed" and "Maxps Damage' was chosen as the type of damage. The section was meshed by size of = 0.8; the total number of nodes was 400 (figure 6.3); the element type was selected as "plane strain", and the element shape was chosen "quad-dominated-structured'. The Poisson's ratio was assumed as equal to 0.18; the concrete failure ratio was 1.16, and concrete density equal to 0.0867 lb/in3.

By using the WLF equation in chapter 5, and get the shifting of compressive strength vs. time curves for concrete columns (Figure6.8), the compressive strength that used as input data was as following:

$$fr(t)=- 0.0003\ (t^2)+1.5464(t)+4949.5 \qquad (6.7)$$

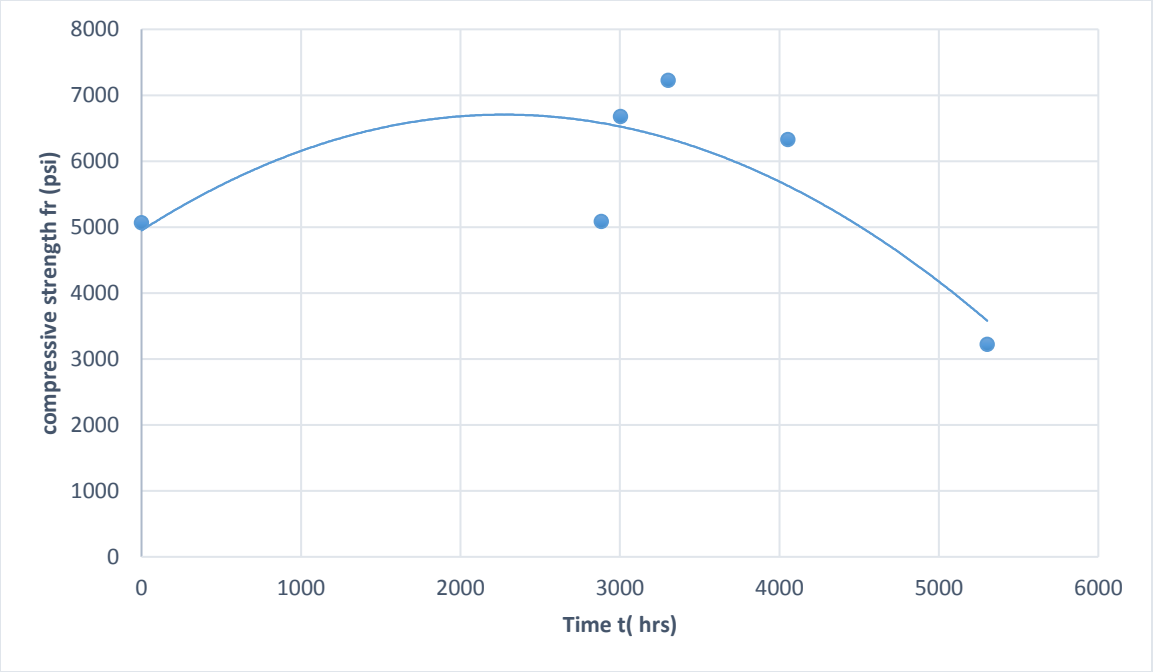

Figure 6.8: Shifting of compressive strength vs. time curves for concrete columns

By substitute t=0 for the control beam, the compressive strength that used as input was equal = 4949.5 psi, and the modulus of elasticity of concrete was 4010.0 ksi

By running the ABQUS-CAE software, the load started increase via steps and the section began deform until failed, figure 6.9 shows the crack propagation.

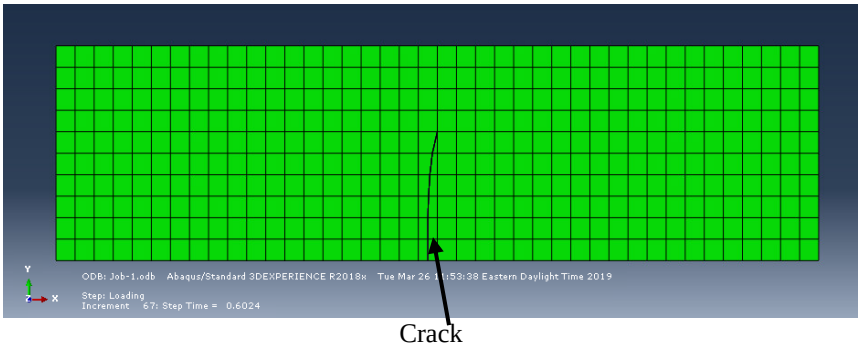

Figure 6.9: Crack propagation of plain concrete beam model

Figure 6.10 explains the typical crack shape of the control beam specimen, (the term CF in the legend means concentrated force). The crack started at the lowest node at mid-span then

propagated gradually to the top of the section, the magnitude of the maximum flexural load was 3216 *lbs*. The mid-span deflection at maximum load was 0.00172″ (the term U_2 in the legend represents the vertical displacement "mid-span deflection", see figure 6.11).

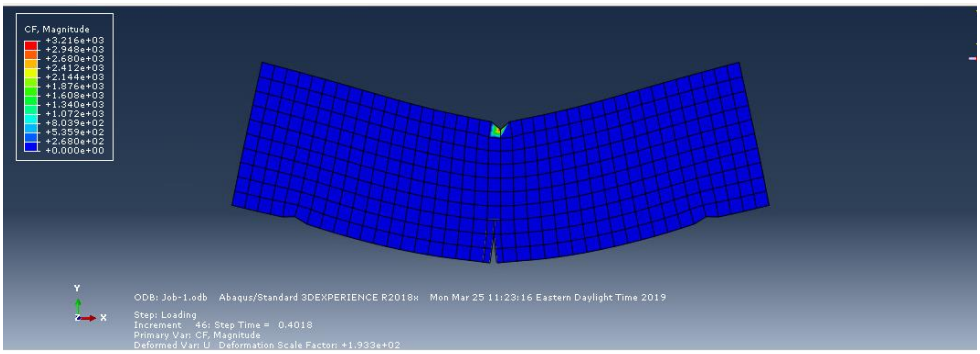

Figure 6.10: regular concrete beam under flexural failure, (H=100% control beam)

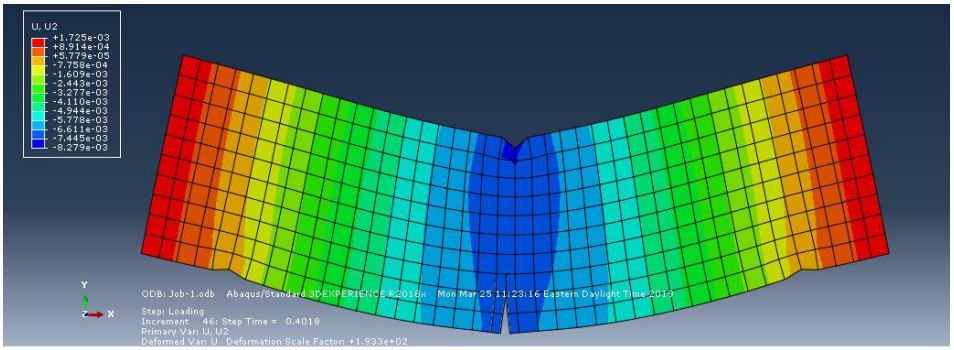

Figure 6.11: Maximum displacement of regular concrete beam (H=100% control beam)

Table 6.2 shows the compressive strength and the modulus of elasticity for each cycle period that used as input data by substitute the cycle period (t) in equation 6.7:

Table 6.2 the compressive strength and the modulus of elasticity for each cycle period that used as input data

Cycle period (t) hrs	Compressive strength (psi) fc'	modulus of elasticity (ksi) 57000√fc'
80	5071	4060
200	5247	4130
500	5648	4284
1250	6414	4565
2500	6941	4749

Table 6.3: Comparison of numerical failure load with experimental for Regular concrete beams 100% Humidity

H %	Cycle	Experimental results (lbs)	Numerical Results (lbs)	Differences
100%	Control beam	3051.1	3216	5.40%
	40cy	3061	3295	7.64%
	100cy	4020	3671	8.68%
	250cy	4350	4521	3.93%
	625cy	3810	5316	39%
	1250cy	1940	5654	190%

The flexural load of regular concrete beam simulation at different environmental conditions of exposure compared to the experimental flexural load results are presented in table 6.3.

Similarly to the experimental work, the magnitudes of flexural strength increases varied with the number of cycles. However, the magnitude of flexure strength kept increasing to reach the highest at 1250cycle.

In the numerical case, it can be due to the change of the input data which were the material properties of the regular concrete. Since the WLF equation was used to determine the properties of the regular concrete as shown in table 6.2, it is very clear that the compressive strength of the regular concrete was increasing after each period of cycle to reach the maximum at 1250 cycle which was reflecting on the numerical results.

The numerical results of flexural for the control beam, 40cy, 100cy, and 250 cycle were about 7.2% different from the experimental results, which means the finite element model has been successful in prediction of regular concrete beam failure load for these cases, however, for the 625 cycle, and 1250cycle, the different was high. A comparison between the experimental test results and the numerical results of the flexural load-number of cycles are plotted in figures (6.12).

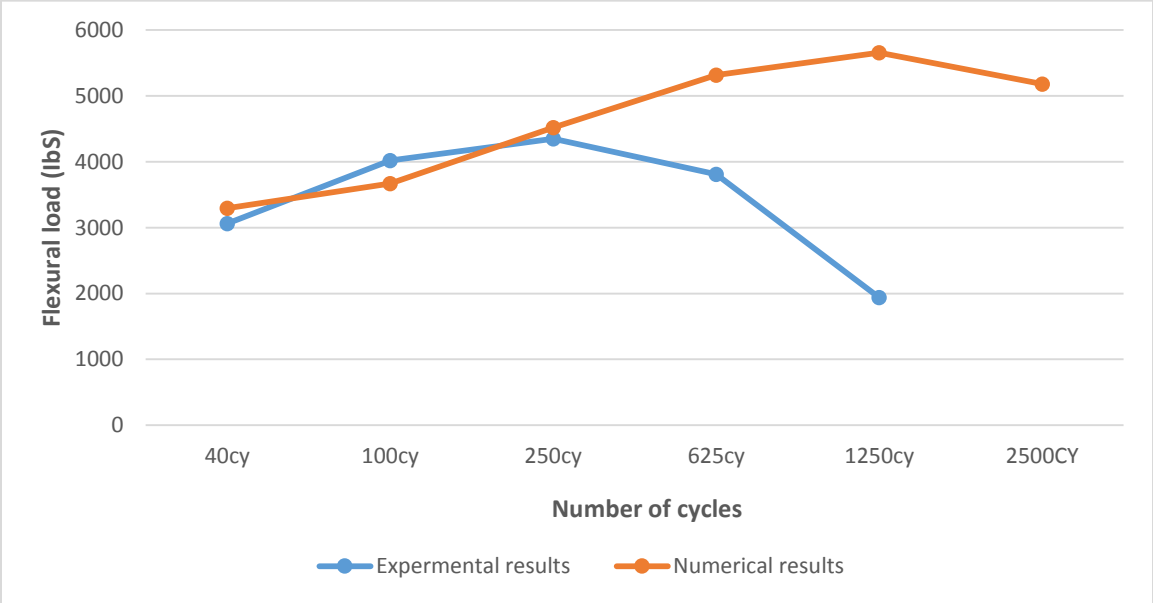

Figure 6.12: Numerical and experimental load/number of cycle curves of regular concrete beams

6.5.2 Numerical Modeling regular Concrete Columns

A three dimensional (3D) nonlinear extended finite-element (X-FE) model was developed to predict the behavior of regular concrete columns. The model was simulated based on the following assumptions. The model space was "3D", "deformable", and "solid". The section type was selected "homogeneous" and "Maxps Damage" was chosen as the type of damage. The section was meshed by size of = 0.2 (see figure 6.13). The element type selected as "3D stress" and the element shape was chosen "quad-dominated-structured". The Poisson's ratio was assumed as equal to 0.18. The concrete failure ratio was 1.16, and concrete density equal to 0.0867 lbs/in^3.

The compressive strength, and the modules of elasticity were from table 6.2.

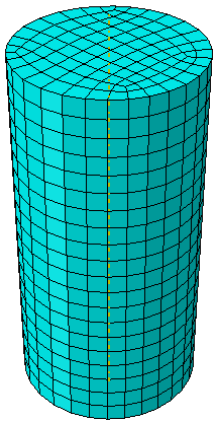

Figure 6.13: Meshing of 3-D regular concrete column model

The numerical results of the compression load for the control column, 40cy, 100cy, and 250 cycle were about 5.9% different from the experimental results, which means the finite element model has been successful in prediction for regular concrete columns failure load for these cases, however, for the 625 cycle, and 1250cycle, the different was also high (table 6.4). A comparison

between the experimental test results and the numerical results of the compression load-number of cycles are plotted in figures (6.14).

Table 6.4: Comparison of numerical failure load with experimental for Regular concrete columns 100% Humidity

H %	Cycle	Experimental results (lbs)	Numerical Results (lbs)	Differences
100%	Control column	35780	37939	6 %
	40cy	35925.5	38315	6.65%
	100cy	47180	50884	7.85%
	250cy	51044.6	52653	3.15%
	625cy	44708	59015	32%
	1250cy	22763.4	56909	150%

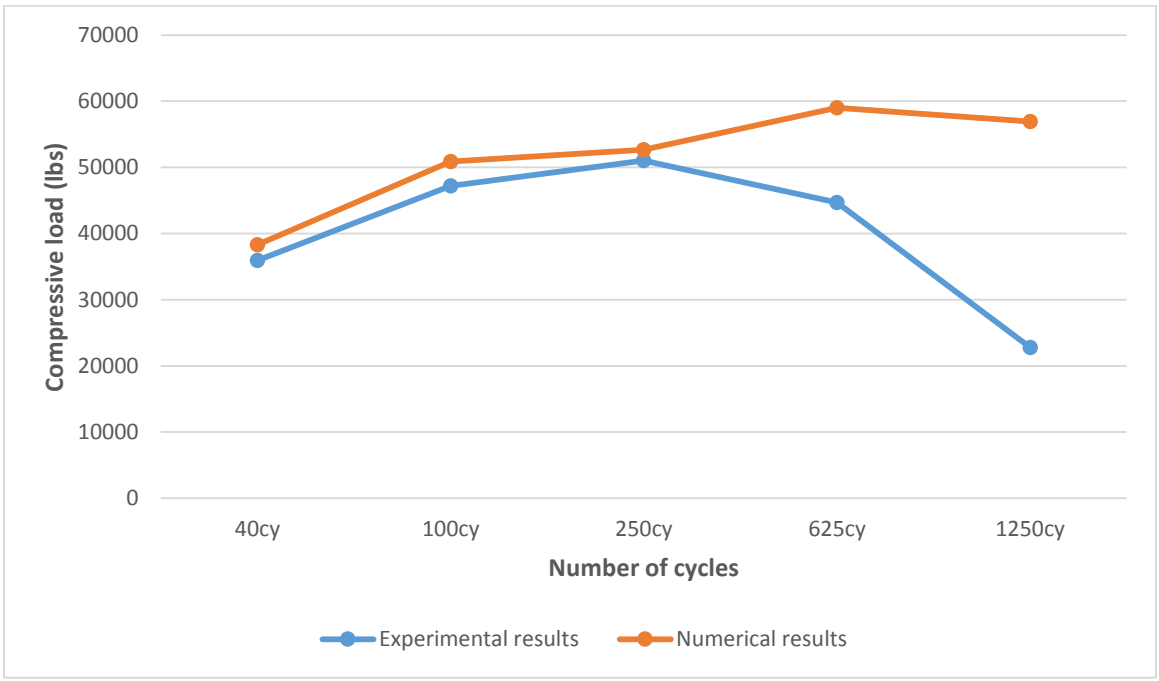

Figure 6.14: Numerical and experimental load/number of cycle curves of regular concrete column

6.5.3 Numerical Modeling of geo-polymer concrete beams (100% Humidity)

The same model that have been applied to regular concrete beam case was applied for the geo-polymer concrete beam as well.

By using the WLF equation in chapter 5, and get the shifting of compressive strength vs. time curves for geo-polymer concrete columns (Figure6.15), the compressive strength that used as input data was as following:

$$fr(t)=- 0.0003 (t^2)+1.6316(t)+4937.8 \quad (6.8)$$

Table 6.5 shows the compressive strength and the modulus of elasticity for each cycle period that used as input data by substitute the cycle period (t) in equation 6.8:

Table 6.5 the compressive strength and the modulus of elasticity for each cycle period that used as input data

Cycle period (t) hrs	Compressive strength (psi) f_c'	modulus of elasticity (ksi) $57000\sqrt{f_c'}$
80	5066	4057
200	5252	4131
500	5679	4295
1250	6509	4599
2500	7141.8	4817

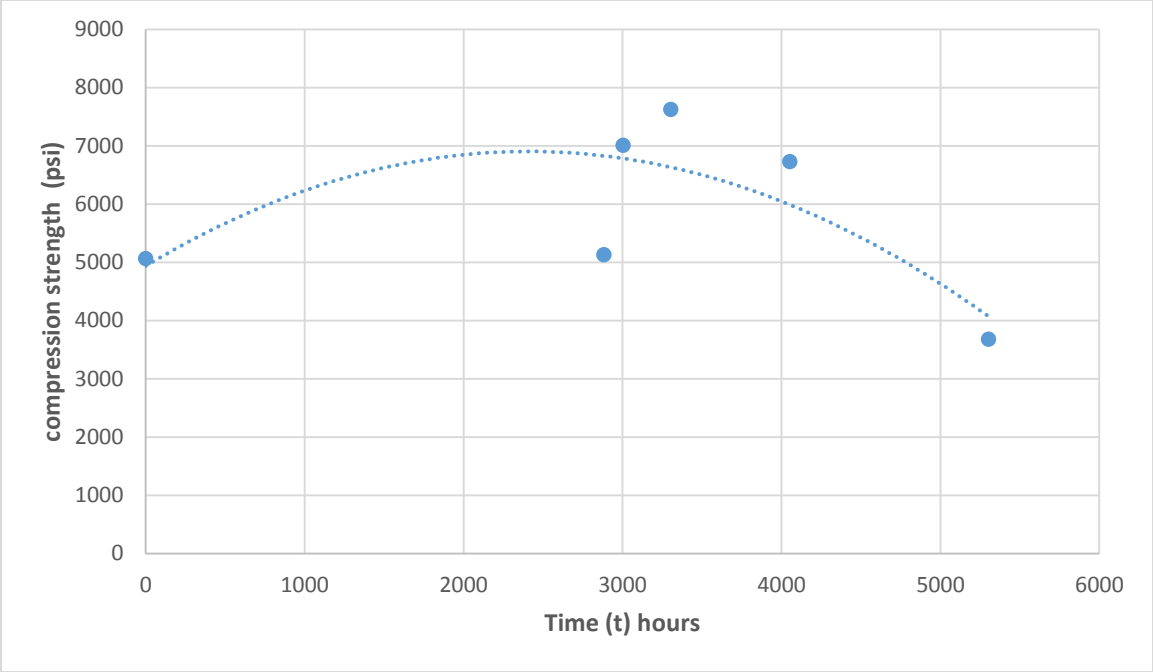

Figure 6.15: Shifting of compressive strength vs. time curves for geo-polymer concrete columns

Similarly to the regular concrete beams, the magnitudes of flexural strength increases varied with the number of cycles. However, the magnitude of flexure strength kept increasing to reach the highest at 1250cycle.

The numerical results of flexural for 40cy, 100cy, and 250 cycle were about 6.41% different from the experimental results, which means the finite element model has been successful in prediction of geo-polymer concrete beam failure load for these cases, however, for the 625 cycle, the different was 41%, and 1250cycle, the different was 170% (table 6.6). A comparison between the experimental test results and the numerical results of the flexural load-number of cycles are plotted in figures (6.16).

Table 6.6: Comparison of numerical failure load with experimental for geo-polymer concrete beams 100% Humidity

H %	Cycle	Experimental results (lbs)	Numerical Results (lbs)	Differences
100%	40cy	3100	3329	7.64%
	100cy	4150	4459	7.45%
	250cy	4520	4708	4.15%
	625cy	3708	5229	41%
	1250cy	2021	5457	170%

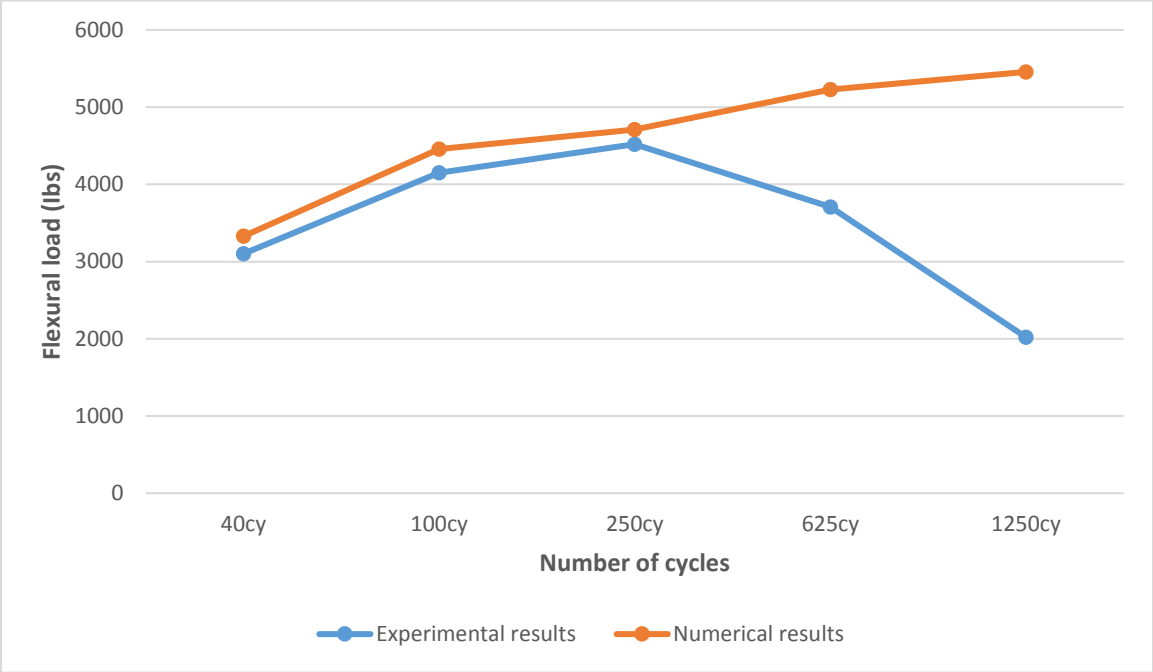

Figure 6.16: Numerical and experimental load/number of cycle curves of geo-polymer concrete beams 100% H

6.5.4 Numerical Modeling of geo-polymer concrete columns (100% Humidity)

The same model that have been applied to regular concrete column case was applied for the geo-polymer concrete columns as well.

Using the same material properties (table 6.5), the results are shown in table 6.7, and the pattern of compressive load and number of cycle curves are shown in (figures 6.17). They indicate that

the numerical model has a good prediction of compressive load compared to the experimental results for the cycle periods (40cy, 100cy, and 250cy). The average variation between numerical experimental results of compressive load for these cases was only 5.39%, however, for the 625cy, the different was 35%, and for 1250cy, the different was 160%.

Table 6.7: Comparison of numerical failure load with experimental for geo-polymer concrete columns 100% H

H %	Cycle	Experimental results (lbs)	Numerical Results (lbs)	Differences
100%	40cy	36243.4	38371	5.87%
	100cy	49511.5	52576	6.19%
	250cy	53870.6	56090	4.12%
	625cy	47534	64171	35%
	1250cy	26013.3	67635	160%

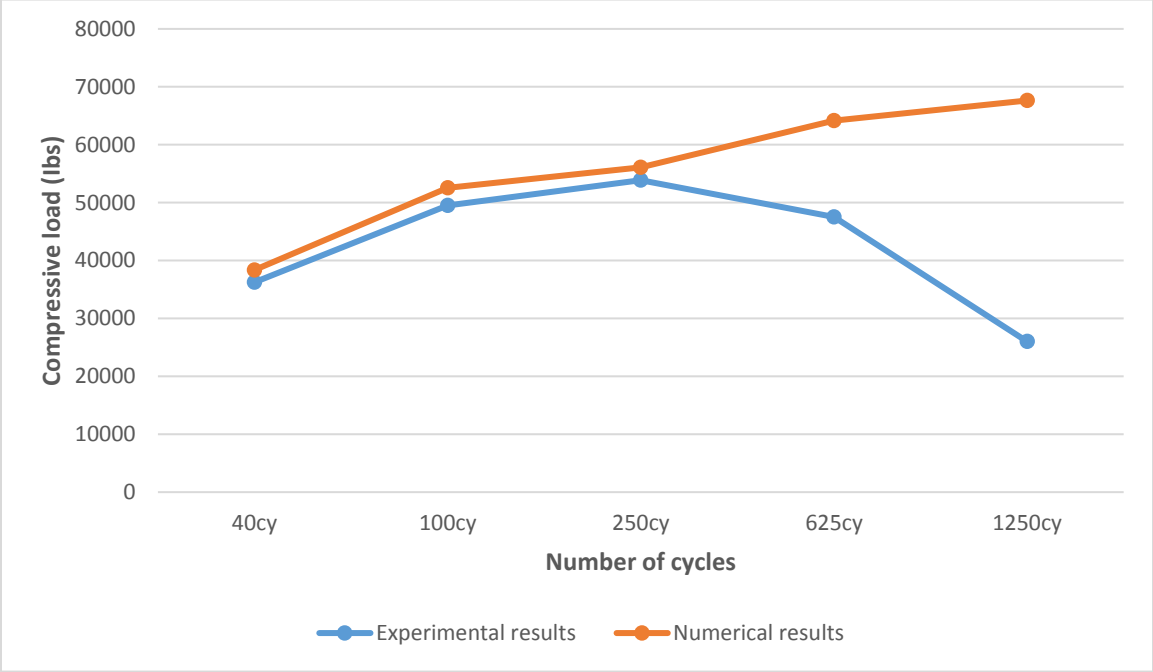

Figure 6.17: Numerical and experimental load/number of cycle curves of geo-polymer concrete column 100%H

6.5.5 Numerical Modeling of regular concrete columns (0% Humidity)

The same model that have been applied to regular concrete column case, and geo-polymer concrete column case (100% Humidity), was applied for regular concrete columns (0% Humidity) as well. By using the WLF equation in chapter 5, and get the shifting of compressive strength vs. time curves for regular concrete columns (0% humidity), (Temp. 45$_o$C, and 70$_o$C) (Figure6.18, and figure 6.19), the compressive strength that used as input data was as following:

For Temp. 45$_o$C: $fr(t)=- 0.0003\ (t^2)+1.4227(t)+4943.5$ (6.9)

For Temp. 70$_o$C: $fr(t)=- 0.0004\ (t^2)+1.623(t)+4936$ (6.10)

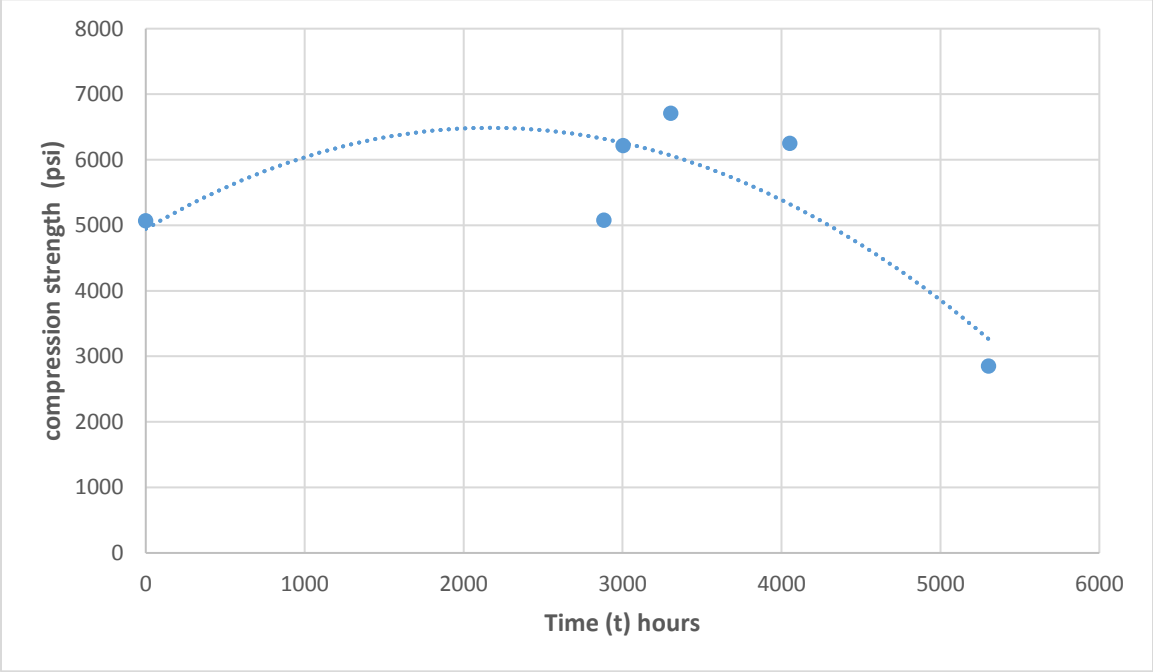

Figure 6.18: Shifting of compressive strength vs. time curves for regular concrete columns (0%humidity, Temp. .45$_o$C)

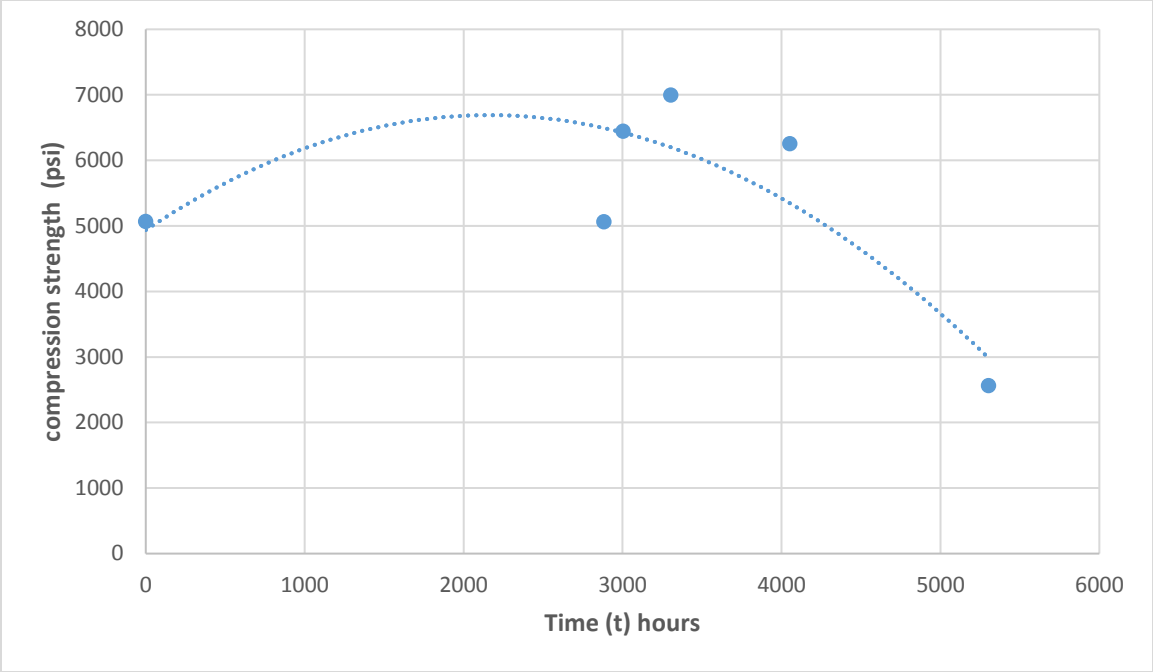

Figure 6.19: Shifting of compressive strength vs. time curves for regular concrete columns (0%humidity, Temp. .70$_o$C)

Table 6.8, and 6.9 show the compressive strength and the modulus of elasticity for each cycle period that used as input data by substitute the cycle period (t) in equation 6.9, and 6.10 respectively

Table 6.8 the compressive strength and the modulus of elasticity for each cycle period that used as input data (0%humidity, Temp. .45$_o$C)

Cycle period (t) hrs	Compressive strength (psi) fc'	modulus of elasticity (ksi) 57000√fc'
80	5055	4053
200	5216	4117
500	5580	4258
1250	6253	4507
2500	6625	4639

Table 6.9: the compressive strength and the modulus of elasticity for each cycle period that used as input data (0%humidity, Temp. .70^{o}C)

Cycle period (t) hrs	Compressive strength (psi) fc'	modulus of elasticity (ksi) 57000√fc'
80	5063	4056
200	5243	4127
500	5648	4284
1250	6340	4539
2500	6494	4593

The results are shown in table 6.10, and the pattern of compressive load and number of cycle curves are shown in (figures 6.20). They indicate that the numerical model has a good prediction of compressive load compared to the experimental results for the cycle periods (40cy, 100cy, and 250cy). The average variation between numerical experimental results of compressive load for these cases was only 12.8%, however, for the 625cy, and 1250cy, the different was high.

Table 6.10: Comparison of numerical failure load with experimental for regular concrete columns 0% H

H %	Temp. *oC*	Time (*Hr*)	Experimental results (lbs)	Numerical Results (lbs)	Differences
0%	45	80	35854.87	38288	6.78%
		200	43923.10	52216	18.8%
		500	47392.72	55112	16.2%
		1250	44156.25	61647	39.6%
		2500	20147.96	62741	211%
	70	80	35741.83	38348	7.3%
		200	45533.92	52486	15.3%
		500	49440.87	55784	12.8%
		1250	44177.44	62505	41.5%
		2500	18095.51	61500	240%

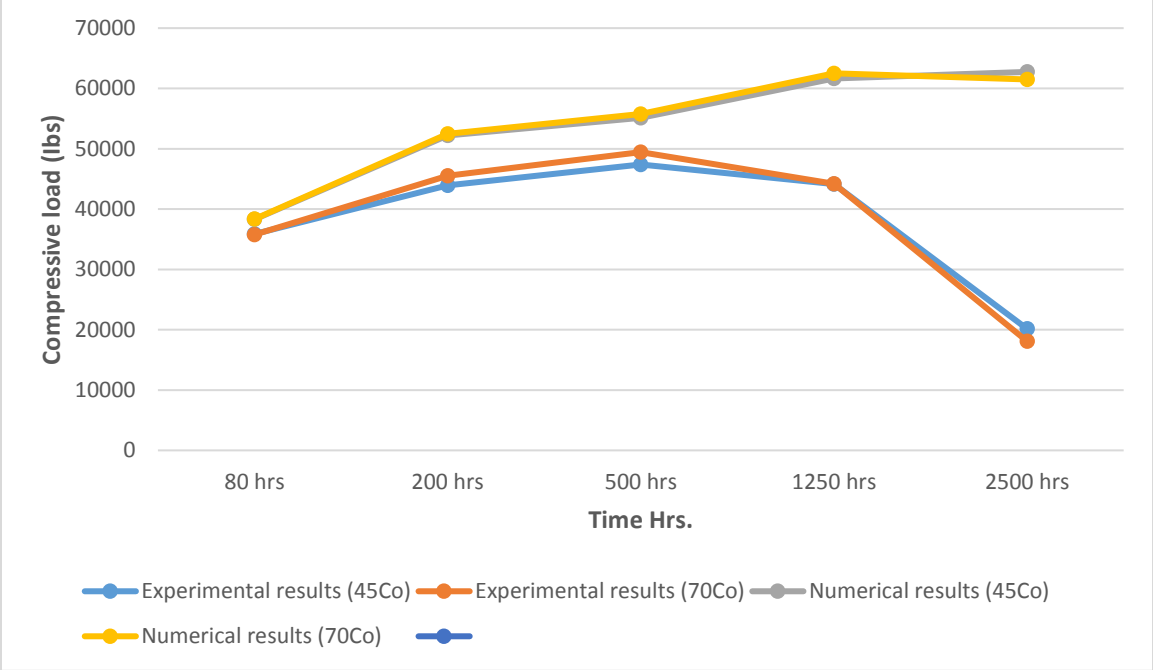

Figure 6.20: Numerical and experimental load/number of cycle curves of regular concrete column 0%H

6.5.6 Numerical Modeling of geo-polymer concrete columns (0% Humidity)

The same model that have been applied to regular concrete column case, and geo-polymer concrete column case (100% Humidity), was applied for geo-polymer concrete columns (0% Humidity) as well. By using the WLF equation in chapter 5, and get the shifting of compressive strength vs. time curves for geo-polymer concrete columns (0% humidity), (Temp. 45$_o$C, and 70$_o$C) (Figure6.21, and figure 6.22), the compressive strength that used as input data was as following:

For Temp. 45$_o$C: $fr(t)=- 0.0003\ (t^2)+1.6462(t)+4937.9$ (6.11)

For Temp. 70$_o$C: $fr(t)=- 0.0003\ (t^2)+1.6149(t)+4948.9$ (6.12)

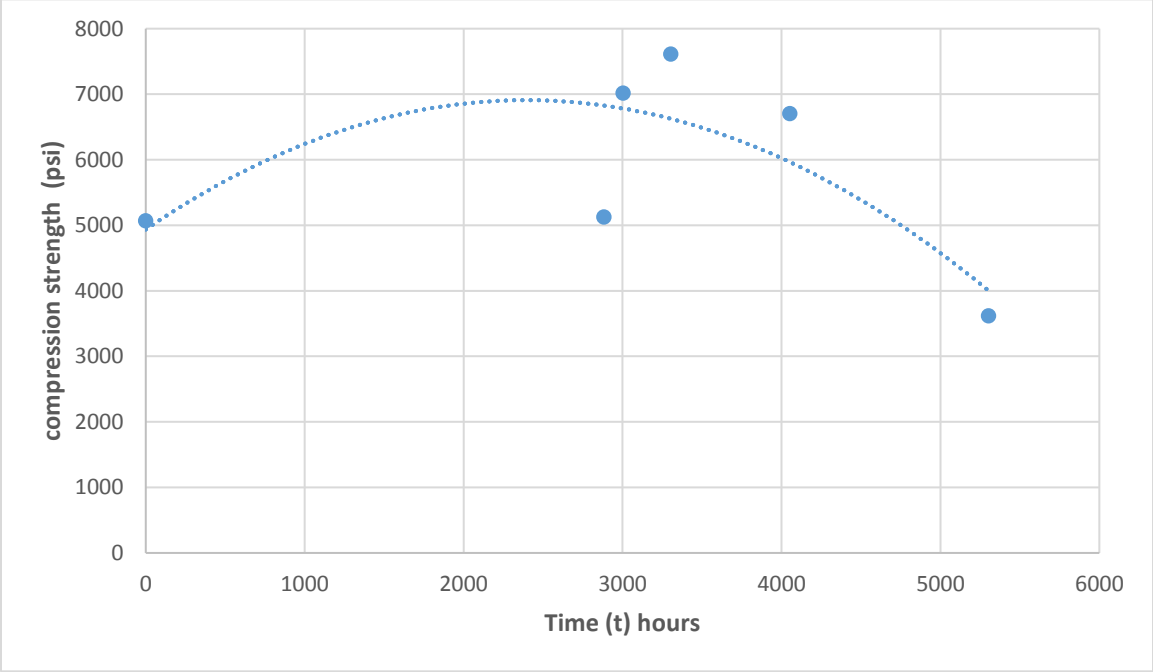

Figure 6.21: Shifting of compressive strength vs. time curves for geo-polymer concrete columns (0%humidity, Temp. .45$_o$C)

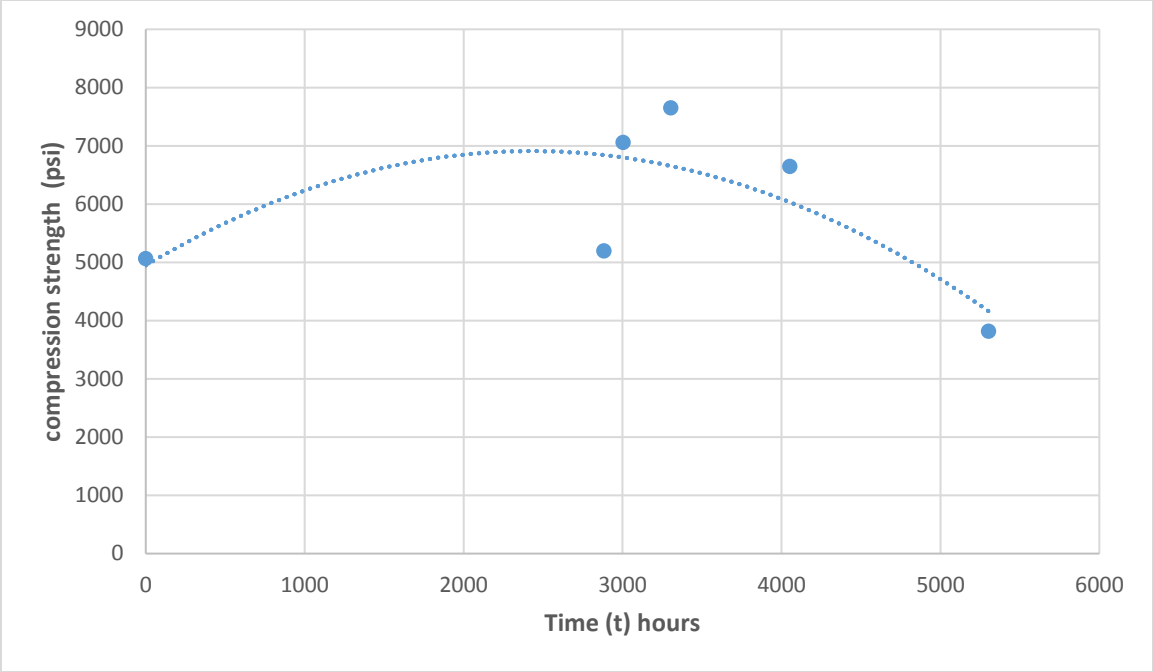

Figure 6.22: Shifting of compressive strength vs. time curves for geo-polymer concrete columns (0%humidity, Temp. .70$_o$C)

Table 6.11, and 6.12 show the compressive strength and the modulus of elasticity for each cycle period that used as input data by substitute the cycle period (t) in equation 6.11, and 6.12 respectively

Table 6.11 the compressive strength and the modulus of elasticity for each cycle period that used as input data (0%humidity, Temp. .45$_o$C)

Cycle period (t) hrs	Compressive strength (psi) fc'	modulus of elasticity (ksi) 57000√fc'
80	5068	4058
200	5255	4132
500	5686	4298
1250	6527	4605
2500	7178	4829

Table 6.12: the compressive strength and the modulus of elasticity for each cycle period that used as input data (0%humidity, Temp. .70$_o$C)

Cycle period (t) hrs	Compressive strength (psi) fc'	modulus of elasticity (ksi) 57000√fc'
80	5076	4061
200	5260	4134
500	5681	4296
1250	6499	4595
2500	7111	4807

The results are shown in table 6.13, and the pattern of compressive load and number of cycle curves are shown in (figures 6.23). They indicate that the numerical model has a good prediction of compressive load compared to the experimental results for the cycle periods (40cy, 100cy, and 250cy). The average variation between numerical experimental results of compressive load for these cases was only 5.11%, however, for the 625cy, and 1250cy, the different was high.

Table 6.13: Comparison of numerical failure load with experimental for geo-polymer concrete columns 0% H

H %	Temp. *oC*	Time (*Hr*)	Experimental results (lbs)	Numerical Results (lbs)	Differences
0%	45	80	36208.12	38386	6.01%
		200	49560.97	52606	6.14%
		500	53778.78	56159	4.42%
		1250	47356.69	64348	35.8%
		2500	25539.97	67978	166%
		80	36702.67	38447	4.75%

	70	200	49878.9	52656	5.56%
		500	54047.25	56110	3.81%
		1250	46946.92	64072	36.4%
		2500	26981.23	67343	149.6%

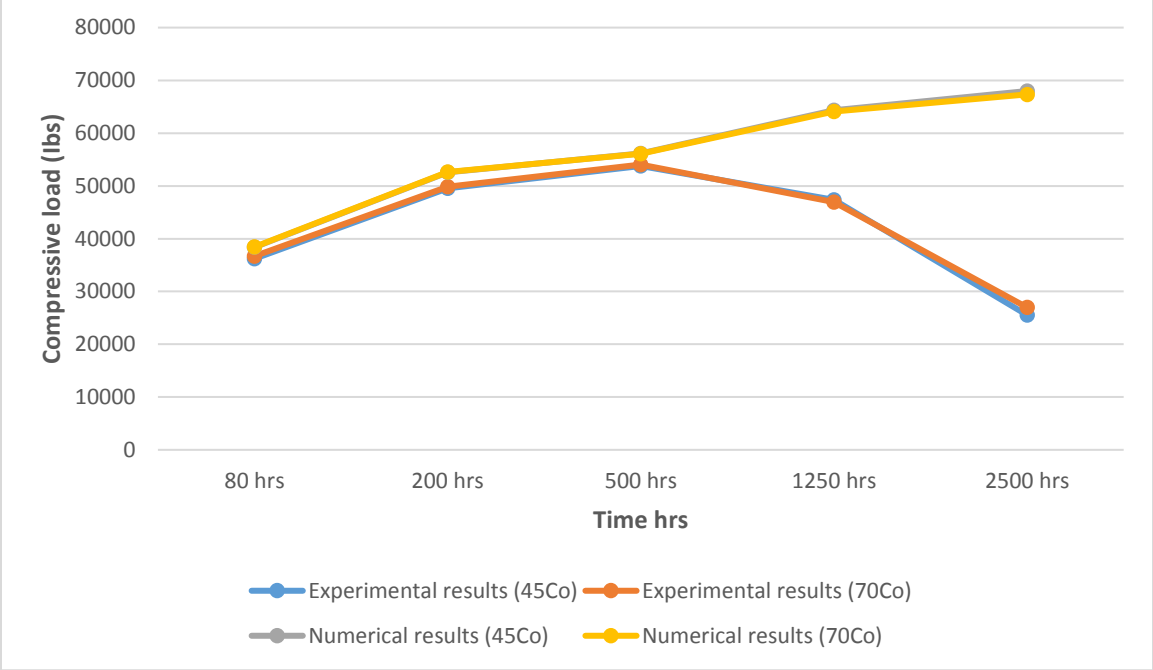

Figure 6.23: Numerical and experimental load/number of cycle curves of geo-polymer concrete column 0%H

CHAPTER 7 CONCLUSIONS AND FUTURE WORK

7.1 Conclusions

The intent of this research was to develop a durability performance of geo-polymer concrete beams and columns that are exposed to different environments. Extensive laboratory tests have been implemented for regular concrete and geo-polymer concrete beams and columns.

The results that have been obtained experimentally, evaluated and compared to the analytical solutions and numerical results. These results concluded to the following:

***Effect of temperature on regular concrete beams and columns*:** the flexural strength of regular concrete beams increased due to subjecting to 100% relative humidity with temperature changing from 25^{o}*C to 100* ^{o}*C*, the magnitudes of flexural strength increases varied with the number of cycles. The strength was the highest after 250 cycles, comparing to 100 cycles, and 40 cycles, then the strength was reduced after 625 cycles.

The compressive strength for regular concrete column specimens that were exposed to 100% relative humidity with temperature changing from 25^{o}*C to 100* ^{o}*C*, improved about 43% after 250 cycles, and about 25% after 625 cycles compared to the control specimen, and similarly to the regular concrete beams, the strength was the highest after 250 cycles, comparing to 100 cycles, and 40 cycles, then the strength was reduced after 625 cycles.

***Effect of temperature on geo-polymer concrete beams and columns*:** the flexural strength of geo-polymer concrete beams increased due to subjecting to 100% relative humidity with temperature changing from 25^{o}*C to 100* ^{o}*C*, the magnitudes of flexural strength increases varied with the number of cycles. The strength was the highest after 250 cycles, comparing to 100 cycles, and 40 cycles, then the strength was reduced after 625 cycles. The increase in the geo-polymer concrete is slightly larger than the increase in the regular concrete case.

The compressive strength for geo-polymer concrete column specimens that were exposed to 100% relative humidity with temperature changing from 25^{o}*C to 100* ^{o}*C*, improved about 50.5% after 250 cycles, and about 33% after 625 cycles compared to the control specimen, and similarly to the geo-polymer concrete beams, the strength was the highest after 250 cycles, comparing to 100 cycles, and 40 cycles, then the strength was reduced after 625 cycles.

In summary, compared to the standard laboratory condition results, temperature changing from 25^{o}*C to 100* ^{o}*C* with 100% relative humidity showed that an improvement in the strength of both regular concrete and geo-polymer concrete beams/columns until 250 cycles. The increase in the geo-polymer concrete is slightly larger than the increase in the regular concrete case.

Effect of relative humidity: 30 plain concrete columns, and 30 geo-polymer concrete columns have been subjected to 0% relative humidity with two fixed temperature (T= 45^{o}C & T=70 ^{o}C). The experimental test results indicate that humidity has some negative influence on the strength of regular concrete columns. 100% relative humidity has more strength than regular concrete columns with 0% relative humidity at the same numbers of cycle, while, geo-polymer concrete columns has no big change in term of strength between 0% relative humidity and 100% humidity. That means, the humidity does not affect the strength of geo-polymer concrete.

Effect of Number of cycles*:* the number of cycles played an essential influence on the materials strength for both regular concrete and geo-polymer concrete. The regular concrete results recorded an improvement in the strength by about 32% after 100 cycles, 43% after 250 cycles, and 25% after 625 cycles, however, the strength will start decreasing after that.

The geo-polymer concrete results recorded as well an improvement in the strength by about 36% after 100 cycles, 48% after 250 cycles, and 22% after 625 cycles, however, the strength will start decreasing after that as well.

In conclusion, the strength of materials improves by aging of exposure (number of cycle) under temperature changing from $25^{o}C$ *to* $100\ ^{o}C$. The strength was the highest after 250 cycles, comparing to 100 cycles, and 40 cycles, then the strength was reduced after 625 cycles.

7.2 Future Work

In this research, the durability performance for both regular concrete and geo-polymer concrete was studied experimentally with exposing both to hygro-thermal laboratory conditions using furnaces and ovens. Future research can be done by exposing them to long term real conditions and compare the results.

Although, it was some safety issues in this research by dealing with chemical material in geo-polymer concrete, future study can be done by studying the most accurate way to perform the geo-polymer concrete safely.

REFERENCES

1. Hwai-Chung Wu, Peijiang Sun. New building materials from fly ash-based lightweight inorganic polymer, International Journal of Construction and Building Materials, No. 1, 21(2007) 211–7.
2. J, D. (1994). High Alkali cement for 21st century Concrete. Concrete Technology past present and future ACI special publication SP 144. Farmington Hills, Michigan.
3. Kapoor, Shruti. (2014). Fly Ash as a Sustainable Material. Retrieved from http://www.researchgate.net/publication/259604793.
4. Panias D., Giannopoulou I. P. (2006). Development Of Inorganic Polymeric Materials Based On Fired Coal Fly Ash. Athens, Greece.
5. J. W. Wang and T.W. Cheng. "Production geo polymer materials by coal fly ash". The 7th International Symposium on East Asian Resources Recycling Technology (2003): 263. Print.
6. FRANTIŠEK ŠKVÁRA, LUBOMÍR KOPECKÝ, JIØÍ NÌMEÈEK, ZDENÌK BITTNAR. (2006). Microstructure of Geo polymer Materials Based on Fly Ash. Department of Glass and Ceramics, Institute of Chemical Technology in Prague, Technická 5, 166 28 Prague, Czech Republic, Department of Structural Mechanics, Czech Technical University in Prague, Thákurova 7, 166 29 Prague, Czech Republic.
7. Hwai-Chung Wu, and Boubacar Diallo.Ductile Compressive Failure Using Hybrid Composite Reinforcement. Department of Civil and Environmental Engineering, Wayne State University, Detroit, MI 48202, USA.
8. Sun P. Fly ash based inorganic polymeric building material. PhD Dissertation. Wayne State University, Detroit, MI; 2005.

9. Ammar Motorwala, Vineet Shah, Ravishankar Kammula, Praveena Nannapaneni, Prof. D. B. Raijiwala. “ALKALI Activated FLY-ASH Based Geopolymer Concrete.” International Journal of Emerging Technology and Advanced Engineering 3 (2013): 159. Print.
10. https://en.wikipedia.org/wiki/Fly_ash.
11. Peijiang Sun, Hwai-Chung Wu. Chemical and freeze–thaw resistance of fly ash-based inorganic mortars, journal homepage: www.elsevier.com/locate/fuel, Fuel 111 (2013) – 740.
12. G. Saravanan, C. A. Jeyasehar and S. Kandasamy. Flyash Based Geopolymer Concrete – A State of the Art Review, Journal of Engineering Science and Technology Review 6 (1) (2013) 26.
13. Ching AU. Behavior of FRP-Confined Concrete. Master of Science, MASSACHUSETTS INSTITUTE OF TECHNOLOGY; 2001.
14. AASHTO. (2012).LRFD guide specifications for design of concrete filled FRP tubes for flexure and axial members, first edition 2012.
15. Bank, Lawrence C., Composites For Construction:Structural Design with FRP Materials,Canada, ISBN: 978-0-471-68126-7, 560 pages, July 2006.
16. Shen, Y., Xu, M., Chandrashekhara, K., and Nanni, A., "Finite Element Analysis of FRP Tube Assemblies for Bridge Decsk", Advanced Composite Materials, October 2001.
17. Elarbi, Abulgasem Mohamed, Durability Performance of FRP Strengthened Concrete Beams and Columns Exposed to Hydrothermal Environment, Dissertation, Submitted to the Graduate School of Wayne State University, Detroit, Michigan, Doctor Of Philosophy 2011.

18. Seible, F. "US Perspective of Advanced Composites Bridge Technology in Europe and Japan," Proceeding of the Second International Conference on Composites in Infrastructure, ICCI'98, Tucson, Arizona, USA, 1998.
19. Engineering, Vol. 120, pp. 464-485. Youn, S. and Chang, S. "Behavior of Composite Bridge Decks Subjected to Static and Fatigue Loading," ACI Structural Journal, Vol. 95, pp. 249-258, 1998.
20. Matthews, F.L.; Davies, G.A.O.; Hitchings, D.; and Soutis, C.' Finite element modeling of composite materials and structures' , Woodhead Publishing Ltd, CRC Press, 2000 - Science - 214 pages
21. P. Duxson, A. Fernandez-Jimenez, J. L. Provis, G. C. Lukey, A. Palomo, J. S. J. Van Deventer: J Mater Sci Vol. 42 (2007), p. 2917-2933
22. W. K. W. Lee and J. S. J. Van Deventer: Cement and Concrete Research Vol. 34 (2004), p.195-206
23. T. Bakharev : Cement and Concrete Research Vol. 35 (2005), p. 1233-1246
24. Thomas, Michael, Optimizing the Use of Fly Ash in Concrete, http://www.cement.org/docs/default-source/fc_concrete_technology/is548-optimizing-the-use-of-fly-ash-concrete.pdf.
25. Peter Duxon , John L.Provis, Grant C.Lukey , Seth W. Mallicoat, Waltraud M. Kriven, Jannie S.J. Van Deventer," Under standing the relationship between geopolymer composition, microstructure and mechanical propertiesColloids and Surfaces "A. Phsicochem. Eng. Aspects 269 (2005) 47-58

26. Balaguru.P, Hammell.J.A, and Foden.A, "Mechanical Characterization and durability Study of Geopolymer Composites". www.geo org.
27. Hardijito.D, Wallah.S.E,. Sumajouw.D.M.J,and Rangan.B.V, "Properties of Geopolymer Concrete with Fly ash as Source Material: Effect of mixture Composition" www.geo org.
28. Van Jaarsveld .J.G.S, Van Deventer J.S.J, Lukey.G.C,"The characterisation of source materials in fly ash- based geopolymers", Materials letters 57 (2003) 1272- 1280
29. Zhang Yunsheng, Sun Wei, Li Zongjin, Zhou Xiangming, Eddie, Chau Chungkong, "Impact properties of geopolymer based extrudates incorporated with fly ash and PVA short fiber".
30. Sofi .M, Van Deventer J.S.J, Mendis .P.A, Lukey. G.C," Engineering properties of inorganic polymer concretes (IPCs)", Cement and Concrete research 37(2007) 251- 257
31. Kaps.Ch, Buchwald.A, "Property controlling influences on the generation of geopolymeric binders based clay".www.geopolymer strength properties
32. Domone.J "A review of the hardened mechanical properties of selfcompacting Concrete",Cement and Concrete composites 29(2007) 1-12
33. Hongling wang ,Haihong Li, Fengyuan Yan, 'Synthesis and mechanical properties of metakaolinite –based geopolymer"r, Colloids and Surfaces A. Phsicochem. Eng. Aspects 268(2005) 6
34. Kraiwood Kiiattikomol, Chai Jaturapipitakkul, Smith Songpiriyakij, Seksun Chutibtim ," A Study of ground coarse fly ashes with different finenesses from various sources as pozzolanic materials", Cement & Concrete Composites 23 (2001) 335-343

35. Faguang Lang , Naiqian Feng , Xinying Lu," An Experimental study on the properties of resistance to diffusion of chloride ions of fly ash and blast furnaceslag cvoncrete'\, , Cement and concrete Research 30 (2000) 989-992.

36. Wong .Y. L., Lam . L, Poon C.S, Zhou. F.P, "Properties of fly ashmodified cement mortar-aggregate interfaces" , Cement and concrete Research 29 (1999) 1905 -1913

37. Chindaprasirt.P, Chareerat . T, Sirivivatnano"Workability and strength of coarse high calcium fly ash geopolymer" , Cement & Concrete Composites 29 (2007) 224-229

38. Swanepoel .J.C, Strydom.C.A, "Utilisation of fly ash in a geopolymeric material", Applied Geochemistry 17 (2002) 1143-1148.

39. Hota V.S. GangaRao, Ph.D., P.E. P.V. Vijay, Ph.D., P.E. ' FEASIBILITY REVIEW OF FRP MATERIALS FOR STRUCTURAL APPLICATIONS', Constructed Facilities Center Dept. of Civil & Env. Engineering College of Engineering and Mineral Resources West Virginia University, Morgantown, WV-26506, November 2010 (Revised).

40. Singiresu, S. RAO, The Finite Element Method in Engineering, Fifth edition, Amsterdam • Boston • Heidelberg • London• New York • Oxford • Paris • San Diego San Francisco • Singapore • Sydney • Tokyo; Butterworth-Heinemann is an imprint of Elsevier; 2011 elsevier Inc.

41. (ACI-318-05) " Building code requirements for structural concrete (ACI 318-05) and Commentary (ACI 318R-05).

42. Bathe, K. J., Finite Element Procedures, Prentice-Hall, Inc., Upper Saddle River, New Jersey, 1996.

43. Adams, V. and Askenazi, A., Building Better Products with Finite Element Analysis, OnWord Press, Santa Fe, New Mexico, 1998.

44. Klamer, E. L. , Hordijk, D. A., and Hermes, M. C.J. 'The influence of temperature on RC beams strengthened with externally bonded CFRP reinforcement'. HERON Vol. 53(2008) No.3.

45. http://theconstructor.org/practical-guide/specific-gravity-of-cement/2239/.

46. Sambhav Gangwal*, Raksha Parolkar, 'STUDIES ON EFFECT OF SEWAGE WATER ON NATURAL CONCRETE AND RECYCLED CONCRETE' INTERNATIONAL JOURNAL OF ENGINEERING SCIENCES & RESEARCH TECHNOLOGY, February, 2015].

47. A. K. Parande MTech, P. L. Ramsamy BTech, S. Ethirajan BTech, C. R. K. Rao PhD and N. Palanisamy PhD,'' Deterioration of reinforced concrete in sewer environments'' Article in Municipal Engineer · January 2006.

48. Masood Tofik Noori; " Hot Weather Concreting" Noor City-Kirkuk Investment Project(Kirkuk-Iraq).

49. Suyun Ham, and Taekeun Oh; "Effect of Mixing and Placing in Hot Weather on Hardened Concrete Properties" (Received January 8, 2013, Accepted April 4, 2013).

50. Tarun R. Naik, AND Shiw S. Singh. "MECHANICAL PROPERTIES OF CONCRETE INFLUENCED BY INCLUSION OF FLY ASH AND TEMPERATURE" Department of Civil Engineering and Mechanics College of Engineering and Applied Science. THE UNIVERSITY OF WISCONSIN – MILWAUKEE (Report No. CBU-1990-10 Septemper 1990).

51. US Environmental Protection Agency'' https://www.epa.gov/climate-indicators/weather-climate''

52. S. E. Wallah and B. V. Rangan, "LOW-CALCIUM FLY ASH-BASED GEOPOLYMER CONCRETE: LONG-TERM PROPERTIES" Research Report GC 2 Faculty of Engineering Curtin University of Technology Perth, Australia 2006.

53. Klieger, Paul, "Effect of Mixing and Curing Temperature on Concrete Strength", ACI Journal, Proc. Vol. 54, June 1958, pp. 1063-1081.

54. Lovewell, C.E., and Washa, G.W., "Proportioning Concrete Mixtures using Fly Ash", ACI Journal, Proc. V. 54, June 1958, pp. 1093-1101.

55. Berry, E.E., and Malhotra, V.M., "Fly Ash for Use in Concrete - A Critical Review", ACI Journal, Proc. V. 77, No. #2, March - April, 1980, pp. 59-73.

56. Lohtia, R. P. , Nautiyal, B. 0 , and Jain, 0. P. , "Creep of Fly Ash Concrete" , ACI Journal, Proc. V. 73, No. 8, Aug., 1976, pp. 469-472.

57. Ghosh, R. S. and Tikalsky, J. , "Creep of Fly Ash Concrete", ACI Journal, Proceedings V. 78, No. 5, September - October, 1981.

58. Lane, R.O., and Best, J. F., "Properties and Use of Fly Ash in Portland Cement", Concrete International, July, 1982, pp. 81-92.

59. Mittelacher, M., "Effect of Hot Weather Conditions on the Strength Performance of Set-Retarded Field Concrete", in "Temperature Effects on Concrete", T. R., Naik, Ed., STP 858, ASTM, Philadelphia, 1985, pp. 88-106.

60. Al-Ani, S.H., and Al-Zaiwary, A.K., "The Effects of Curing Period and Curing Delay on Concrete in Hot Weather", Materials and Structures, Vol. 22, No. 123, May 1988, pp. 205-212.

61. Abbasi, A. F. , and Al-Tayyb, A.J. , "Effect of Hot Weather on Modulus of Rupture and Splitting Tensile Strength of Concrete", Cement and Concrete Research, Vol. 15, 1988, pp. 233-244.

62. Cebeci, O. Z. , "Strength of Concrete in Warm and Dry Environment" , Materials and Structures, RILEM, V. 20, No. 118, July, 1987, pp. 270-272.

63. Ravindrarajah, R.S. and Tam, C.T., "Properties of Concrete Containing Low-Calcium Fly Ash Under Hot and Humid Climate", in "Fly Ash, Silica Fume, Slag and Natural Pozzolan in Concrete", V. M. Malhotra, Ed. , Proceedings of the Third International Conference, Trondheim, Norway, ACI $P-114, ACI, Detroit, 1989, pp. 139-155.

64. Linda Monfardini and Fausto Minelli, "Experimental Study on Full-Scale Beams Made by Reinforced Alkali Activated Concrete Undergoing Flexure" DICATAM—Department of Civil Engineering, Architecture, Environment, Land Planning and Mathematics,University of Brescia, 25123 Brescia, Italy, August 2016.

65. S.Kumaravel, S.Thirugnanasambandam, "FLEXURAL BEHAVIOUR OF GEOPOLYMER CONCRETE BEAMS" Department of Civil and Structural Engg., Annamalai University, Annamalainagar-608 002, Tamilnadu, India, November 2013.

66. Vijaya Rangan, "Geopolymer concrete for environmental protection" The Indian Concrete Journal, April 2014, Vol. 88, Issue 4, pp. 41-48, 50-59.

67. Dr. Abdul Aleem M.I. and Dr. Arumairaj P.D. ," ANALYTICAL MODELING OF GEOPOLYMER CONCRETE WITH MANUFACTURED SAND USING ANSYS" Department of Civil Engineering, Sri Ramakrishna Institute of Technology, Coimbatore, and Department of Civil Engineering, Governement. College of Technology, Coimbator, June 2016.

68. The American Society for Testing and Materials, ASTM, C989-99.

69. Elliot, D. F., Ground Granulated Blast-Furnace Slag for Use in Airfield Pavements, Lone Star Industries, New Orleans, LA.

70. Satpute Manesh B., Wakchaure Madhukar R., Patankar Subhash V "Effect of Duration and Temperature of Curing on Compressive Strength of Geopolymer Concrete" International Journal of Engineering and Innovative Technology (IJEIT) Volume 1, Issue 5, May 2012.

71. Basil S. Al-Shether , Tareq Salih Al-Attar , Zaid A. Hassan "Effect of Curing System on Metakaolin Based Geopolymer Concrete" Journal of Babylon University/Engineering Sciences/ No.(3)/ Vol.(24): 2016.

ABSTRACT

DURABILITY PERFORMANCE OF GEOPOLYMER CONCRETE BEAMS AND COLUMNS EXPOSED TO HYGROTHERMAL ENVIRONMENT

by

NAJEB HASEN SH. SAWSI

May 2020

Advisor: Dr. Hwai-Chaung Wu

Major: Civil and Environmental Engineering (Structural Engineering)

Degree: Doctor of Philosophy

Among the most important advances of research and technological development for viable applications of coal-fired fly ash, the development of new inorganic polymeric materials, named alkali activated cement or "Geopolymers", seems to gain increasing attention during the last twenty years. The present investigation intends to study the effect of hot weather environments (either by changing relative humidity and temperature is kept constant, or by changing temperature but relative humidity is maintained same) on the durability performance of geopolymer concrete beams and columns. The study include the long term influence of moisture, high temperature, and combined hygrothermal conditions on the mechanical properties of geopolymer beams and columns.

An extensive experimental research has been done throughout implement and test several sets of specimens include regular concrete beams and columns, and geo-polymer concrete beams and columns exposed to different environmental conditions.

Also, two and three-dimensional extended finite element method (X-FEM) is developed and implement ted in the ABAQUS-CAE package to predict the behavior of both regular concrete

beams and columns and geo-polymer concrete beams and columns exposed to different environmental conditions.

In addition, analytical calculations for regular concrete and geo-polymer concrete were developed to predict the long-term strength of regular concrete and geo-polymer concrete that exposed to various environmental conditions. William-Landel-Ferry (WLF) equation was employed here to develop the shift factor for regular concrete and geo-polymer concrete exposed to different environmental conditions. The shift factors were determined empirically based on experimental test results.

To confirm the validity of the analysis process and the solution obtained, the flexural load and compressive load were acquired using the analytical calculations compared to experimental results and FE analysis.

Finally, conclusions and suggestions for future study research are presented.

AUTOBIOGRAPHICAL STATEMENT

NAJEB SAWSI

Najeb received his B.Sc. in Civil Engineering in 2005 from the college of engineering in the city of Sabrata, Sabrata-Libya, and his master degree in Civil Engineering "Structural Engineering" in 2010 from Wayne State University, Detroit, USA. Since 2014, he has been studying towards his doctoral degree in Civil Engineering at Wayne State University. His research interests are durability performance of geo-polymer concrete beams and columns exposed to different environmental conditions, finite element modeling, concrete technology, and structures and materials testing.